# LANDSAT SNOW PERSISTENCE AND SNOW REGIME MAPPING FOR ALASKA, AND LICHEN COVER MAPPING FOR YUKON–CHARLEY RIVERS NATIONAL PRESERVE

FINAL REPORT



Prepared for

**United States Geological Survey**
**Alaska Science Center**
4210 University Drive
Anchorage, Alaska 99508

Prepared by

Matthew J. Macander
Christopher S. Swingley

**ABR, Inc.—Environmental Research & Services**
P.O. Box 80410
Fairbanks, Alaska 99708–0410

January 2017

# TABLE OF CONTENTS


LIST OF FIGURES ..... iv

LIST OF TABLES ..... v

ACKNOWLEDGMENTS ..... vi

SECTION 1: SNOW PERSISTENCE MAPPING, ALASKA ..... 1

INTRODUCTION ..... 1

STUDY AREA ..... 1

METHODS ..... 1

Landsat Snow Persistence Mapping ..... 2
SnowMap in Complex Terrain ..... 2
Data Summary by Day of Year ..... 4
Classification of Normal Snow-free Date ..... 5
Final Landsat Snow Persistence Map ..... 5

Validation and Intercomparison of Landsat Snow Persistence Map ..... 6
Internal consistency ..... 6
SNOTEL ..... 6
MODIS Snow Metrics ..... 7

Characterizing Snow Regime from Landsat and MODIS metrics ..... 8

RESULTS AND DISCUSSION ..... 8

Landsat Snow Persistence Mapping ..... 8
SnowMap in Complex Terrain ..... 8
Data Summary by Day of Year ..... 9
Classification of Normal Snow-free Date ..... 10
Final Landsat Snow Persistence Map ..... 10

Validation and Intercomparisons of Landsat Snow Persistence Map ..... 14
Internal consistency ..... 14
SNOTEL ..... 15
MODIS Snow Metrics ..... 16

Annual 30 m Snow Persistence Combining Landsat and MODIS ..... 17

CONCLUSION ..... 18

SECTION 2: LICHEN COVER MAPPING, YUKON–CHARLEY NATIONAL PRESERVE ..... 19

INTRODUCTION ..... 19

STUDY AREA ..... 19

METHODS ..... 20

Plot Data ..... 20
Vegetation Point Intercept (VPI) Data ..... 21
Vegetation Quadrat Data ..... 22
Vegetation Training Data ..... 23

Predictors ..... 23
Environmental Predictors ..... 23
Landsat Imagery ..... 24
DigitalGlobe Imagery ..... 26

Modeling ..... 26
Overlay of Training Data ..... 26
Develop and Evaluate Models ..... 27

RESULTS AND DISCUSSION ..... 28

Plot Data ..... 28
Vegetation Point Intercept (VPI) Data ..... 28
Vegetation Quadrat Data ..... 29
Vegetation Training Data ..... 30

Predictors ..... 31

Modeling ..... 32
Plot-based Lichen Cover Models, 30 m ..... 32
Classification of Lichen Presence/Absence, 30 m ..... 32
Transect-based Lichen Cover Models, 2 m ..... 33
Raster-based Lichen Cover Models, 30 m trained from 2 m ..... 34

CONCLUSIONS ..... 35

REFERENCES ..... 37

## LIST OF FIGURES


Figure 1.1. Landsat snow persistence mapping study area, Alaska.
Figure 1.2. Example of results of SnowMap in Complex Terrain algorithm for single Landsat scenes, Alaska.
Figure 1.3. Count of total snow-covered, snow-free land, and snow-free water observations on May 15, for the period 1999–2015, Alaska. Analysis was based on all available Landsat scenes analyzed using the SnowMap in Complex Terrain algorithm.
Figure 1.4. Time series of snow presence and absence for a single pixel near Fairbanks, Alaska for the period 1999–2015. Logistic regression and binary classification tree results are also plotted.
Figure 1.5. Map of climatological snow-free date from Landsat at 30 m resolution for Alaska, for the 1999–2015 period.
Figure 1.6. Full resolution examples of climatological snow-free date from Landsat at 30 m resolution for Alaska, for the 1999–2015 period.
Figure 1.7. Count of Landsat observations used to determine climatological snow-free date in Alaska, for the 1999–2015 period.
Figure 1.8. Proportion of observations classified as snow for February 1–August 31, 1999–2015, Alaska.
Figure 1.9. Proportion of land observations classified to snow-covered or snow-free status consistent with climatological snow-free date from Landsat, for the period February 1–August 31, 1999–2015, Alaska.
Figure 1.10. Map of Snowpack Telemetry (SNOTEL) sites and count of years with snow persistence data, 2000–2015, Alaska.
Figure 1.11. Climatological snow-free date from Landsat vs. median first snow-free date from SNOTEL, 2000–2015, Alaska.
Figure 1.12. MODIS snow metric last day of longest continuous snow segment, 2001–2015 and median, Alaska.
Figure 1.13. Climatological snow-free date from Landsat (aggregated to 500 m) vs. Median MODIS last day of longest continuous snow segment metric, 2001–2015, Alaska.
Figure 1.14. Difference between Landsat snow-free date (aggregated to 500 m pixels) and median MODIS snow persistence metrics (2001–2015), Alaska.
Figure 1.15. Metrics of snow regime variability based on Landsat and MODIS snow persistence mapping, Alaska.
Figure 1.16. Smoothed annual anomaly in MODIS last day of longest continuous snow segment, Northwestern Alaska, 2001–2015.
Figure 1.17. Annual snow persistence map at 30 m resolution based on MODIS and Landsat snow persistence metrics, Anaktuvuk Pass, Alaska, 2001–2015.
Figure 2.1. Lichen mapping study area, Alaska.
Figure 2.2. Diagram showing the layout of a vegetation monitoring plot, including transects and quadrat placements, for Yukon–Charley Rivers National Preserve, Alaska . These plots are 16 m in diameter and encompass about 200 m².
Figure 2.3. Plot locations and total terricolous macrolichen cover by vegetation point intercept (VPI) and quadrat methods, Yukon–Charley Rivers National Preserve, Alaska.
Figure 2.4. Total terricolous macrolichen cover on vegetation sampling transects by vegetation point intercept method, for 4 plots on the Flat Creek grid, Yukon–Charley Rivers National Preserve, Alaska.

Figure 2.5. Selected spectral and ancillary predictors for cover modeling, Yukon–Charley Rivers National Preserve, Alaska.
Figure 2.6. Observed vs. out-of-bag predictions of vegetation point intercept total terricolous macrolichen cover, 30 m resolution, Yukon–Charley Rivers National Preserve, Alaska. Linear fit line is red, and 1:1 line is black.
Figure 2.7. Map of total terricolous macrolichen cover from vegetation point intercept plots, 30 m resolution, Yukon–Charley Rivers National Preserve, Alaska.
Figure 2.8. Maps of terricolous macrolichen presence and absence at different thresholds of total lichen cover, 30 m resolution, Yukon–Charley Rivers National Preserve, Alaska.
Figure 2.9. Map of total terricolous macrolichen cover from vegetation point intercept transects, 2 m resolution, Yukon–Charley Rivers National Preserve, Alaska.
Figure 2.10. Map of total terricolous macrolichen cover at 30 m resolution, trained from 2 m resolution total lichen cover maps, Yukon–Charley Rivers National Preserve, Alaska.

## LIST OF TABLES

Table 1.1. Summary of tests in SnowMap in Complex Terrain algorithm, and resulting determination of snow status. ..... 40
Table 1.2. Reclassification of reverse split and no split categories from snow–free date analysis, based on proportion of snow observations in the time–series. ..... 41
Table 1.3. Areal summary of climatological snow–free date from Landsat, 1999–2015, Alaska. ..... 42
Table 1.4. Areal summary of percentage of Landsat observations consistently classified by climatological snow-free date from Landsat, 1999–2015, Alaska. ..... 44
Table 1.5. Summary of Snowpack Telemetry stations and snow persistence metrics for the study area, Alaska. ..... 45
Table 2.1. Environmental and spectral predictors at 30 m resolution for lichen cover mapping. Predictors in italics were not used in the final modeling. ..... 48
Table 2.2. Frequency distribution of sample point counts at vegetation point intercept plots, Yukon–Charley Rivers National Preserve, Alaska. ..... 49
Table 2.3. Summary of all lichen hits at vegetation point intercept plots, Yukon–Charley Rivers National Preserve, Alaska. ..... 49
Table 2.4. Summary of lichen position in canopy at vegetation point intercept plots, Yukon–Charley Rivers National Preserve, Alaska. ..... 50
Table 2.5. Summary of terricolous macrolichen cover by genus at quadrat plots, Yukon–Charley Rivers National Preserve, Alaska. ..... 51
Table 2.6. Summary of terricolous macrolichen color groups and dominant genera at quadrat plots, Yukon–Charley Rivers National Preserve, Alaska. ..... 52
Table 2.7 Model performance summary for 30 m resolution terricolous macrolichen cover models based on vegetation plot training data, Yukon–Charley Rivers National Preserve, Alaska. ..... 53

Table 2.8. Classification accuracy of 30 m resolution terricolous macrolichen presence/ absence maps for varying thresholds of lichen cover, based on plot averaged total lichen cover metric from vegetation point intercept transects, Yukon–Charley Rivers National Preserve, Alaska. ..... 54
Table 2.9. Model performance summary for 2 m resolution terricolous macrolichen cover models using Digital Globe imagery, Yukon–Charley Rivers National Preserve, Alaska. ..... 55

## ACKNOWLEDGMENTS

We thank Dave Gustine and Kyle Joly (National Park Service) for proposing this work, and Layne Adams (USGS) for managing the project. Carl Roland (National Park Service) provided the vegetation plot data for Yukon–Charley that was the basis for the lichen mapping. David Selkowitz (USGS) provided the algorithm for the revised cloud mask used in the snow persistence mapping. Gerald V. Frost (ABR), David Swanson and Kyle Joly (National Park Service), and David Douglas (USGS) provided constructive review. This project was funded by the US Geological Survey as a USGS National Park Monitoring Project.

# SECTION 1: SNOW PERSISTENCE MAPPING, ALASKA

## INTRODUCTION

The distribution and abundance of snow are critical factors influencing the distribution, movements, and nutritional ecology of caribou (*Rangifer tarandus*) in Alaska. There is a lack of spatially explicit snow cover data at fine resolution (30 m) over the extensive range. Maps that depict patterns of snow persistence (a proxy for snow depth) are required to improve understanding of the spatial and nutritional ecology of caribou herds in Alaska and adjacent Canada. Landsat-based 30 m snow persistence mapping has been performed for >500,000 km² in northwestern Alaska (Macander et al. 2015) and this mapping has been applied to characterize high-value winter habitat for the Western Arctic caribou herd (Wilson et al. 2014). For the current effort, we developed snow persistence products that will be useful for analyzing caribou habitat selection and informing caribou management practices. These products can support a wide variety of other research and management purposes (e.g., hydrology, landscape change) and are likely to be of interest to multi-disciplinary researchers and land managers. We also developed several metrics to characterize the snow regime of Alaska based on both Landsat and MODIS snow products.

## STUDY AREA

This project was funded to extend the existing 30 m snow persistence mapping (Macander et al. 2015) to cover northeastern Alaska. Recent technical advances allowing more efficient processing of Landsat imagery have enabled us to extend the mapping to cover most of mainland Alaska and a portion of Canada's Yukon Territory (Figure 1.1). The snow persistence study area covers habitat utilized by most Alaska caribou herds, including several interior Alaska herds that were the primary motivation for the work: the Fortymile, Porcupine, Hodzana Hills, White Mountain, and Nelchina caribou herds. The mapping provides data that is relevant to habitat selection for all of those herds.

## METHODS

We characterized snow persistence at 30 m resolution based on an analysis of the Landsat archive, 1999–2015. Within this period, we used all available 30 m resolution

Landsat 5–8 imagery (Thematic Mapper [TM], Enhanced Thematic Mapper+ [ETM+], and Operational Land Imager [OLI]) with collection dates between February 1–August 31. Each image was classified to snow, snow-free, or snow status unknown. Then, we applied a binary classification tree to identify the day of year that best separates the snow-covered season from the snow-free season for each 30 m pixel. We assessed the accuracy of the snow persistence map by comparing the new map product to existing *in situ* snow records and coarser remotely-sensed data products based on imagery from the Moderate Resolution Imaging Spectroradiometer (MODIS) sensor.

## LANDSAT SNOW PERSISTENCE MAPPING

The climatological normal date for the end of the snow cover season is the date that best identifies the transition from snow to snow-free status over a multi-year period. We mapped the climatological normal snow-free date at 30 m resolution for most of Alaska for 1999–2015. We used a dense Landsat time-series, following the general approach of Macander et al. (2015) with several modifications.

### SNOWMAP IN COMPLEX TERRAIN

We developed an algorithm—SnowMap in Complex Terrain—to map the presence or absence of snow in any Landsat TM, ETM+, or OLI scene that has been processed to produce a surface reflectance Climate Data Record. The required inputs are the Landsat reflective bands (calibrated to top-of-atmosphere reflectance), scene metadata (e.g., acquisition date, scene-center sun elevation, azimuth), CFmask cloud mask product (produced as part of the surface reflectance Climate Data Record) (Zhu and Woodcock 2012), and a 30 m resolution DEM. The required Landsat data became available on Google Earth Engine (GEE, a cloud-based platform for the analysis of remote sensing data), in spring 2016. Using GEE, a series of rules were applied to determine the snow status for each pixel in every Landsat scene that was acquired over the study area from February 1–August 31, 1999–2015. The procedure to classify each Landsat pixel to snow, water, snow-free land or unknown is summarized in Table 1.1 and is described in detail below.

Cloud Masking

The CFmask layer was used for initial screening of clouds, cloud shadows, and water. Selkowitz and Forster (2015) observed that CFmask has high commission errors of mapping cloud cover in mountainous regions, especially when snow cover is patchy, and developed a decision tree model to reassess cloud pixels and reclassify some of them as cloud-free. We applied this model across all the scenes in our analysis to review all pixels mapped initially as "cloud" by CFmask and assign them to either a cloud or clear ("released cloud") category.

Shadow Modeling

The mapping of snow properties is greatly complicated by shadows in complex terrain. To address this, we modeled shadows using spectral information, topographic inputs, solar geometry, and CFmask. First, very dark pixels (Green < 0.07 and near-infrared [NIR] < 0.07, Selkowitz and Forster 2015) were flagged as unknown and were excluded. These areas were considered too dark to make reliable determinations of snow-cover status.

Shadowed areas that were not excluded by the dark reflectance test were considered illuminated enough to determine snow status, but they were flagged so that different spectral rules for snow occurrence could be applied (see next section). Two shadow types were flagged: cloud shadows and terrain shadows. Cloud shadows were mapped based on the "cloud shadow" CFmask class, while terrain shadows were mapped by elevation modeling using the Advanced Spaceborne Thermal Emission and Reflection Radiometer (ASTER) GDEM2 digital elevation model, combined with sun geometry from Landsat scene metadata. The GEE hillshadow algorithm (with 250 pixel [7500 m] neighborhood) mapped terrain shadow pixels for each scene.

In addition, the solar incidence angle was calculated for each pixel in each scene using the slope and aspect derived from GDEM2, and the scene-center solar geometry values from the scene metadata:

$$i = \arccos [ \cos \theta \cos e + \sin\theta \sin e \cos(\varphi m - \varphi s) ]$$

where $i$ = solar incidence angle, $\theta$ = solar zenith angle, $e$ = terrain slope, $\varphi m$ = terrain aspect, and $\varphi s$ = solar azimuth.

Pixels with incidence angles >80 degrees were also flagged as terrain shadows, because such pixels have a very low effective sun angle and are likely shadowed due to uneven terrain and/or vegetation (Macander et al. 2015).

Snow Presence / Absence Mapping (with Canopy Adjustment)

Using Landsat imagery calibrated to top-of-atmosphere reflectance, we mapped snow presence/absence based on the SnowMap algorithm (Hall et al., 1995; Hall et al., 2002) with standard thresholds (snow present if Normalized Difference Snow Index [NDSI] > 0.4, Red > 0.1, and NIR > 0.1). In order to better capture snow under tree and shrub canopies, we used an additional spectral metric, the Normalized Difference Vegetation Index (NDVI), to map snow in pixels that fell in a NDVI/NDSI feature space that tends to correspond to snow under canopies (Klein 1998).

In areas flagged as terrain or cloud shadow (except very dark shadow), the 0.4 NDSI threshold was applied to map the presence or absence of snow, but the two additional reflectance thresholds of the SnowMap algorithm were not applied. The NIR and Red reflectance tests improve snow mapping under normal illumination conditions because snow is very bright, but shadowed areas are often dark enough that even snow-covered areas do not exceed the reflectance thresholds (Macander et al. 2015). Pixels in shadow that occurred within the NDVI//NDSI canopy feature space (Klein 1998) were classified as unknown, because the canopy adjustment was not developed for application in shadowed areas.

## DATA SUMMARY BY DAY OF YEAR

We generated a multiband raster layer for each day of year that summarized the count of snow presence and snow absence observations, pooling Landsat data from 1999–2015. The summary rasters were exported at 30 m resolution in the Alaska Albers North American Datum (NAD) 1983 coordinate system, and included bands summarizing the total count of snow, snow-free land, and snow-free water observations for each day of year over the time period. The total count of unknown observations (dark shadow, cloud, or undetermined snow status) was also calculated.

## CLASSIFICATION OF NORMAL SNOW-FREE DATE

The daily summary rasters were ingested into R statistical software (R Core Team 2016) and were broadcast into time-series arrays for each pixel. The arrays contained the snow status (1 = snow, 0 = snow-free land or water) and the Julian date (1–365) of each observation. The time-series for each pixel was then analyzed using a binary classification tree (rpart; Therneau et al. 2015) that was restricted to a single split. This step identified the day of year that best separated the snow-covered and snow-free seasons for each pixel during 1999–2015. Based on the range of Landsat acquisition dates used as model inputs (February 1–August 31), the possible snow-free Julian dates range 32–243. For "non-split" cases that lacked a well-defined split and the pixel was better characterized as a single class (i.e., snow-covered or snow-free all year), the values were coded as -400 (snow) or 400 (snow-free). Some of these represented pure classes (e.g. glaciers and permanent snow fields), while others represented areas that were alternately snow-covered and snow-free, but that lacked a strong seasonal snow regime such that the time-series could be reliably classified into a snow-covered and snow-free season. For the rare "reverse split" pixels where the time-series transitioned from snow-free to snow, the day of year of the transition was coded as a negative value (-32 to -243). Finally, the count of snow, snow-free land, and snow-free water observations in the time-series was also calculated for each pixel.

## FINAL LANDSAT SNOW PERSISTENCE MAP

The final map was produced by reclassifying the non-split and reverse split pixels into classes that described the frequency of snow cover over the time-series (Table 1.2). The algorithm was primarily intended for mapping the snow regime on land and results over water bodies were noisy and difficult to interpret. Therefore, land-only version of the map was produced by using a pre-existing water map to mask pixels mapped as water. The water mask was based on the 30 m water mapping produced for NASA's Arctic Boreal Vulnerability Experiment by Carroll (2016), such that any pixel mapped as water in either 2000 or 2010 was masked from the land-only snow persistence map. The southwestern corner of the study area was not covered by the Carroll (2016) map, so the water mask produced as part of the Hansen et al. (2013) global forest cover change map was used

instead. The final map was stored as a GeoTIFF with the Byte data type, with a color map and raster attribute table.

## VALIDATION AND INTERCOMPARISON OF LANDSAT SNOW PERSISTENCE MAP

### INTERNAL CONSISTENCY

We calculated the proportion of Landsat observations that were correctly classified to snow or snow-free, based on the final map of climatological snow-free date. Observations of snow before the snow-free date, and snow-free observations on or after the snow-free date, were counted as correctly classified. This provides a measure of the internal consistency of the snow persistence map product as well as of the variability of the snow regime for a pixel.

### SNOTEL

We analyzed daily data from Snowpack Telemetry (SNOTEL) sites in Alaska that recorded snow water equivalent (SWE) and/or snow depth. We only considered SNOTEL data from February 1–July 31, 2000–2015, in order to match the period of record and seasonal constraints used in developing the Landsat and MODIS snow persistence products (the seasonal window of the MODIS product was used, though the Landsat seasonal window extended to August 31). The SNOTEL data were reviewed to verify the thresholds for missing data codes. For each station, we only included data from years in which data were missing for fewer than 10% of the days in the February 1–July 31 seasonal period.

The daily SNOTEL data were reclassified to snow-free if snow depth or SWE were ≤0, and to snow otherwise. There were relatively rare occurrences of small negative values for snow depth or SWE (~0.3% of SNOTEL observations between -10.0 and -0.1), suggesting that there were some small calibration errors in the SNOTEL data; these were interpreted as snow absence. There may be a parallel occurrence of small positive values when snow was absent, due to a similar calibration error in the opposite direction, and which could lead to incorrect interpretation of snow presence. Since the occurrence of the negative values was low we assumed that the occurrence of small positive values was also low and would have only a minor effect on the multi-year results.

The first snow-free day and the last snow day were then extracted for each year for each station. In addition, a binary classification tree analysis was run for each year and station to determine the Julian date that best separated the snow-covered and snow-free seasons. For example, in a year that was characterized by continuous snow cover through a particular date in spring, and then remained snow-free through July 31, the last snow day was one day before the first snow-free day and the classification tree result was halfway in between. The spread of these three Julian date metrics was wider at stations with more complex seasonal snow regimes.

The SNOTEL snow metrics for each station were summarized to calculate the median first snow-free date, the median last snow date, and the median split date for 2000–2015. The total number of years with data were assessed for each station, and stations with less than 12 years of data (i.e., <75% of the total years in the 2000–2015 range) were excluded. Then the Landsat snow-free date values were extracted for each pixel that overlapped a SNOTEL location.

## MODIS SNOW METRICS

The MODIS snow metrics data (Lindsay 2015) for 2000–2015 were compiled and summarized to characterize both the central tendencies and interannual variability in snow regime for the study area. There are two metrics that characterize the end of the snow season: (1) the end of the longest continuous snow segment (hereafter, longest CSS end day); and (2) the last snow day (latest date with snow). We calculated three median dates from these time series: (1) the median longest CSS end day; (2) the median last snow day; and (3) the median day from both metrics combined.

To match the 500 m spatial resolution of the MODIS snow data products, the Landsat snow persistence map was aggregated to 510 m resolution, selecting for the median value of snow-free date (ignoring water and pixels without a snow-free date). The proportion of 30 m Landsat pixels with a snow-free date was tabulated for each 510 m pixel, so that the aggregated data could be filtered based on how much of the pixel had a snow-free date for land. No-split pixels (e.g. permanent snowfields) had a coded value with a different

interpretation—snow frequency—rather than the Julian date values used to characterize snow-free date.

## CHARACTERIZING SNOW REGIME FROM LANDSAT AND MODIS METRICS

From the 30 m resolution Landsat map of snow-free date, we selected land pixels that had a snow persistence date (i.e., excluding no-split and reverse split pixels) , and calculated the standard deviation of the snow persistence within each 510 m pixel. This measure of dispersion characterizes the variability of snowmelt within each MODIS pixel and can be used to identify areas where the snow cover has high spatio-temporal heterogeneity.

We examined the MODIS time-series of longest CSS end day and last snow day by reviewing annual maps of the 2 metrics, and annual maps of the departure from the 2000–2015 median for the 2 metrics. The variability of the MODIS snow metrics was assessed in several ways. First, the difference between the median longest CSS end day and the median last snow day was calculated. For regions that are generally characterized by a continuous snowpack through the winter, followed by melt and a snow-free season in late spring or early summer, the difference between the two metrics will be small. On the other hand, regions that are characterized by alternating periods of snow and no snow each winter will have a large offset between the two metrics. Finally, we calculated the standard deviation of each end-of-snow metric over the 2000–2015 time-series to characterize the interannual variability in the snow regime.

# RESULTS AND DISCUSSION

## LANDSAT SNOW PERSISTENCE MAPPING

### SNOWMAP IN COMPLEX TERRAIN

The results for two spring Landsat scenes in the Arctic National Wildlife Refuge (Figure 1.2) illustrate the results of the cloud mask refinement (Selkowitz and Forster 2015) and the snow mapping. The northern portion of both scenes (first row) includes areas that are clearly cloud-free, but that are initially classified as cloud (second row). The revised cloud masks correct this cloud-masking error, with the “released cloud” category representing areas that have been revised to cloud-free (third row). The revised cloud mask will introduce some

commission errors (clouds mapped as "released cloud"). For example, there are "released clouds" interspersed in the cloud banks in the southern half of the 2010-06-08 image (Figure 1.2, left) and while some of this area appears to be translucent cloud edges with ground visible beneath, other areas appear to be shadowed clouds. The revised cloud mask has been demonstrated to improve accuracy in mountainous regions (Selkowitz and Forster 2015) and qualitative inspection of several dozen scenes distributed in diverse regions of Alaska indicate similar improvement and an absence of widespread "released cloud" commission errors. Since mountainous areas often have extremely variable snow distribution, a cloud mask that improves the data quality in those regions is particularly valuable. The final results of the SnowMap in Complex Terrain algorithm are summarized to snow-covered, snow-free and unknown categories (bottom row).

## DATA SUMMARY BY DAY OF YEAR

The SnowMap in Complex Terrain algorithm was applied to all the Landsat scenes in the study area that met the seasonal date criteria, and the results were summarized in one raster for each day of year. The resulting image had four bands for observation counts, tallying the number of snow, snow-free land, snow-free water, and unknown snow status Landsat observations for each pixel. These were the final products generated by Google Earth Engine; the entire study area for the dates February 1–August 31 was processed in about 3 days. The results for May 15 (Figure 1.3), when about half of mainland Alaska is typically snow-free, show one or more observations of snow during 1999–2015 across most of the North Slope and at high elevations throughout the study area. Most of interior Alaska, southcentral Alaska and the Alaska Peninsula had no snow observations on May 15, but did have one or more snow-free land observations. In addition, scattered areas on the North Slope have snow-free land observations on May 15. Some areas, such as the Seward Peninsula, had both snow and snow-free land observations, indicating that the period around May 15 is the time of year when snow cover normally disappears there. Portions of the study area such as the western Kenai Peninsula, Kodiak Island, and far northwest Alaska had no cloud-free observations on May 15, due to cloud cover and/or paucity of Landsat scenes. The area of snow-free water was very limited (Figure 1.3, right panel) because most of the lakes and rivers are covered in ice during mid-May (coastal water is masked in this presentation).

## CLASSIFICATION OF NORMAL SNOW-FREE DATE

The time-series for one pixel near Fairbanks (Figure 1.4) includes all the snow (1) and snow-free (0) observations, by day of year. The overall pattern shows many snow observations through day 120 (April 30) and few after that, and few snow-free observations before day 110 (April 20) and many afterwards. The Julian date range between 120 and 130 has many overlapping snow and snow-free observations, and represents the time of year when snow cover is typically disappearing. There is noise in the time series, with several snow observations later in the spring, as well as a few snow-free observations earlier in the winter. These could be due to unusual conditions (e.g., early melt or midsummer snow events) or algorithm errors. The most common algorithm errors are missed clouds (i.e., clouds not detected by the revised CFMask) being interpreted as snow, and moderately dark areas (often with dense canopy cover) being misinterpreted as snow-free. Given the inherent intra-annual and inter-annual variability in snow cover in Alaska, a robust classification of the time-series into snow-covered and snow-free seasons needs to be resistant to outliers. A logistic fit to the data (Figure 1.4, blue curve) is highly prone to influence from outliers, which in this case are mainly late observations of snow. The binary classification tree (black line) considers all observations, but it does not give extra weight to outliers, unlike a least-squares error-minimizing technique such as logistic regression. Therefore, we used the binary classification tree to identify the climatological snow-free date for the study area, which in the Figure 1.4 example is April 26.

## FINAL LANDSAT SNOW PERSISTENCE MAP

The map of the climatological snow-free date for the study area from Landsat (Figure 1.5) depicts gradients of snow persistence at several different spatial scales. At the scale of the statewide map, the earliest regions of seasonal snow disappearance normally occur in mid-April at low elevations in southwest Alaska and on the Tanana Flats in interior Alaska. Extensive areas melt in late April in the Yukon and Tanana lowlands of interior Alaska, southwest and southcentral Alaska, and the Copper River valley. By mid-May, nearly all the lower elevations south of the Brooks Range are normally snow-free, along with parts of the North Slope. Most remaining snow disappears in late May, except near the Beaufort Sea

coast and at higher elevations. Snow on the Beaufort Sea coast normally disappears in early June, with remaining snow confined to higher elevations and local drifts. Black, white, and gray depict areas that lack a strong seasonal snow regime, either because they are nearly always snow-free (darker), always to nearly always snow-covered (whiter), or else highly variable within and/or across years (grayer). Whites occur in glaciers, snowfields, and some aufeis. Dark gray occurs most extensively along the coasts of the northern Alaska Peninsula, Kodiak Island, and Cook Inlet, where the strong maritime influence and low elevation contribute to an erratic snow regime. For the northern Alaska Peninsula a rain/snow shadow effect is likely also an important factor. "Usually snow-free" and early-melting (March) areas in interior Alaska lowlands and uplands appear to be frequently associated with dense spruce forests, and these likely represent areas where the snow cover is present during winter but is not visible, even with the canopy adjustment. These tend to occur on south-facing and/or windy areas where conditions may be unfavorable to holding snow on canopy branches. Overall these areas are of limited extent in interior Alaska. Note that while the map is presented with colors representing a range of 10–15 days, the underlying data have daily resolution.

The area summary for the study (Table 1.3) shows that more than 1.7 million $km^2$ were mapped, with over 1.5 million $km^2$ on land. Most of the no-split area with snow frequency < 50% was over water. For land, 79.3% of the study area had a climatological snow-free date between April 21 and May 31, with the peak (26.0%) in the May 11–20 period. 8.8% of land had a snow-free date in June, and only 0.9% in July or August. 2.0% of land had no pattern and <50% snow frequency, and 5.6% had a snow-free date of April 20 or earlier (of which only 1.1% had a snow-free date of April 10 or earlier). 3.4% of land had no pattern and >50% snow frequency, with 3.1% at >=90% or higher snow frequency and 2.3% at >=98% snow frequency.

Local- to regional-scale gradients in snow persistence are evident in smaller-scale subsets of the climatological snow-free date map (Figure 1.6). In the eastern Brooks Range (panel a), permanent snowfields occur adjacent to a dynamic arctic mountain snow landscape, with extensive scours on south-facing slopes and complex drifting patterns on north-facing slopes. In addition, some late-melting aufeis is evident in the valley bottom.

Note that although aufeis patches are often captured, their high interannual variability in extent is a confounding factor in this analysis, which pools all 1999–2015 observations.

The Utukok Uplands (Figure 1.6, panel b) is a tundra environment with rolling hills and incised drainages. Snow persistence is mostly homogeneous, with the exception of some scoured ridges and drifts that persist in valley bottoms and terrain breaks. Snow capture by tall shrubs may contribute to the local drifting.

At Barrow (Figure 1.6, panel c), the longest-lasting snow occurs on lakes, which are masked out in this presentation. Here, there is some early snowmelt along the coast. Snow persists longer in natural and artificial terrain breaks, including drainages, drained lake basins, and roads. The longest-lasting snow on land is adjacent to a snow fence that protects the town.

At several Brooks Range sites, including a lower elevation eastern Brooks Range site (Figure 1.6, panel d), the DeLong Mountains (panel e), and Anaktuvuk Pass (panel g), there are strong linkages between terrain roughness and the variability in snow persistence. There are strong snow persistence gradients where terrain is more rugged, and more subtle to absent gradients in gentler terrain. Along the Beaufort Sea coast (Figure 1.6, panel f), snow drifts are evident along bluffs and in drainages.

The remaining sites depicted are further south, in interior and southwest Alaska. Near the village of Tanana (Figure 1.6, panel h), there is a large area that usually lacks snow southwest of the Tanana River. Here, the braided river has extensive silt bars that appear to be highly wind-scoured during the winter, and that redistribute silt downwind to the southwest as well. It would be useful to inquire with village residents to determine whether this area is in fact frequently snow-free during the winter, or if wind-transported silt on the snow surface may be interfering with the snow mapping. The diagonal stripes evident here are not real patterns, but are spatial artifacts related to the scan-line corrector malfunction on Landsat 7 and the resultant differences in input data. Artifacts related to the scan-line corrector malfunction are widespread but mostly small (≤3 days), and are most obvious in areas with a homogeneous snow regime.

The Andreafsky Hills near the Yukon River Delta (Figure 1.6, panel i) show a strongly wind-affected snow regime, with scoured high elevations melting much earlier than low-lying valleys. In contrast, the Yukon Uplands (Figure 1.6, panel j) mostly show longer snow persistence at high elevations, and earlier melt in the valleys. There is also much earlier melt on southwest-facing slopes, which is likely a consequence of higher solar insolation.

On the Yukon-Kuskokwim Delta, there is high variability related to terrain at Cape Romanzof (Figure 1.6, panel k), with early snow disappearance at low elevations along the southwest coast and long-lasting snow in the rugged uplands. There may be some permanent snow patches in some terrain traps. Finally, the Nulato Hills (Figure 1.6, panel l) has strong scouring on southern and eastern slopes, with drifting on western and northern slopes and in valley bottoms.

The map of the sample size of cloud-free observations of snow status (Figure 1.7) provides information on how much data were available to assess snow persistence. The wedges in the map are due to the increasing overlap of Landsat paths at high latitudes. The orbital characteristics of Landsat satellites provide areas of additional overlap in the north, and gaps with less overlap in the south. There is also a paucity of data for the Alaska Peninsula and Kodiak Island, most likely due to persistent cloud cover. The highest data density is in a portion of northeast Alaska, which likely has less frequent cloud cover than other areas in Alaska. There are also fewer data available at higher elevations, likely related to cloud formation that occurs when air rises and cools when moving over mountains.

There is an abrupt decline in the count of observations in the far west of the study area (Figure 1.7). The surface reflectance Landsat product has not yet been produced for the westernmost Landsat paths in Alaska, and so was not available for this analysis. As a result there are portions of the study area with no data. The northwestern Alaska snow persistence map (Macander et al. 2015), which did not use the CFMask product as an input, could be used to fill this gap. Northwest Alaska, southwest Alaska and the Aleutians are beyond the station mask of the ground receiving stations in Fairbanks, and so have less data coverage since the data had to be saved and downlinked later.

We calculated the snow frequency based on all the Landsat observations (Figure 1.8). The patterns are very similar to the snow-free date map (Figure 1.5), and these data were used to populate that map in cases where the classification tree did not identify a snow-free date (Table 1.2). Snow frequency classes were assigned instead of a snow-free date in these cases with "no split" or "reverse split" in the classification tree (5.4% of the land in the study area, with detailed areas in Table 1.3).There is a strong south-north gradient with a higher snow proportion in the north, as well an elevation gradient with snow frequency increasing with elevation. In areas that lack a single transition from snow to snow-free (i.e. they commonly alternate between periods of snow and snow-free within a single year), the snow frequency metric may be a better metric than the snow-free date. The metric could be further improved by calculating snow frequency by month or week, and then averaging, to avoid bias caused by seasonal variations in cloudiness and data availability.

## VALIDATION AND INTERCOMPARISONS OF LANDSAT SNOW PERSISTENCE MAP

### INTERNAL CONSISTENCY

For each pixel, we calculated the percentage of Landsat observations that had a snow status that conformed to the climatological snow-free date (Table 1.4). Results for both the full study area and for land pixels are presented. The snow mapping algorithm is optimized for land and so those results are the most robust. Overall, >35% of the land in the study area had a snow status classification consistency of ≥95%, and >95% of the land in the study area had a snow status classification consistency of ≥85%. The highest classification consistency are in permanent snowfields and near the Arctic coast (Figure 1.9). The classification consistencies below 85% are mainly in southern coastal areas and over large portions of southwest Alaska and the Alaska Peninsula. These regions are characterized by intermittent snow cover in many winters and may be snow-free at any time of year. Many montane areas are also characterized by lower classification consistency, for example on the southern slopes of the Alaska Range and Brooks Range. Ephemeral snow may also be common on these sites in late spring and summer.

SNOTEL

We summarized data for all the SNOTEL sites in the study area that collected some snow depth or SWE data during 2000–2015 (Table 1.5). All values <-0.5 (for SWE) and <-10 (for snow depth) were interpreted as missing data, and all other values ≤0 were interpreted as snow absence. There were 64 sites total, and 24 sites had data available in at least 12 of the 16 years (Table 1.5, Figure 1.10). The data summary for all sites is presented in Table 1.5; however, only sites with at least 12 years of data are used for the comparison to the Landsat snow-free date.

The median values for the 3 SNOTEL metrics are in agreement at the 24 sites with 12 or more years of data (Table 1.5). They are within 1 day of each other at 22 of the sites, which is the best that can be achieved because in a simple snow cover time-series the last snow day is by definition the day before the first snow-free date. At 2 sites (McNeil Canyon and Summit Creek), the range of dates for the 3 metrics is 4–5 days, suggesting that an intermittent snow regime with alternating periods of snow presence and absence in late winter and spring is common there. Although the SNOTEL sites are distributed across the study area (Figure 1.10), the sites with 12 or more years of data are concentrated in interior and southcentral Alaska.

A plot of the climatological snow-free date from Landsat versus the median first snow-free date from SNOTEL (Figure 1.11) shows good overall agreement between Landsat and SNOTEL snow persistence metrics, with an adjusted *r*-squared of 0.82. There is a bias evident such that Landsat snow-free dates tend to be earlier than SNOTEL dates. There are also several outliers with large disagreements between the Landsat and SNOTEL dates. Some of the discrepancy for the outliers may be explained by imprecise locations of the SNOTEL stations (some station locations available from the SNOTEL website have truncated coordinates). We did use locations provided by Peter Kirchner, NPS, who has compiled the best available locations from various sources. The overall bias with the Landsat results being earlier than the SNOTEL record could be related to the resolution (30 m pixels are much larger than SNOTEL sensors), over-story vegetation, and/or the thresholds used for snow detection in the Landsat algorithm.

## MODIS SNOW METRICS

The longest CSS end day MODIS snow metric (Figure 1.12) shows the general pattern of snow persistence as well as the inter-annual variability. The variability is most pronounced in southwest Alaska, where bare ground can occur in late winter due to low snowfall and/or warm weather.

The median value for the MODIS longest CSS end day snow metric was calculated (Figure 1.12, bottom right) and compared to the aggregated Landsat snow-free date (Figure 1.13). There is good agreement between the two snow persistence metrics, with a correlation of 0.79, mean absolute error of +/-4.5 days and a bias of -3.2 days, with the MODIS snow-free date slightly earlier. The scatterplot shows good agreement with the 1:1 line (black), except for a secondary cluster of pixels where the MODIS longest CSS end day is much earlier than the Landsat snow-free date. This secondary cluster represents areas where midwinter snowmelt events occur regularly, and the last day of the longest CSS is often followed by additional periods of snow cover, so the metric does not represent the overall snow persistence very well. These areas are mainly in southwest and south-central Alaska, The last snow day MODIS snow metric better represents the overall snow persistence for southwest Alaska and similar areas, since midwinter snow-free periods are more common. However, the last snow day can be in early- to mid-summer in some years due to short-lived summer snow events that occur before August 1, and therefore can be a misleading snow persistence metric (especially in northern Alaska).

A difference map of the Landsat and MODIS snow persistence metrics demonstrates the areas where the two MODIS metrics agree and disagree with the Landsat snow persistence (Figure 1.14). The left panel, comparing Landsat to the median MODIS longest CSS end day, shows that the two metrics agree within 4 days for most of the state, but there are several regions where the Landsat metric is 5 or more days later than the MODIS metric. These are primarily in southwest and southcentral Alaska, and in montane areas particularly on south-facing slopes at intermediate elevation. The right panel compares the Landsat snow-free date with the MODIS last snow day metric. The areas where Landsat is earlier are much less extensive than for the MODIS longest CSS end day, and are primarily evident in southwest and southcentral Alaska. There are more widespread areas where Landsat is later than

MODIS, however, especially in the interior. The center panel of Figure 1.14 extracted a median value from a combined stack of the two MODIS metrics, and is effective at representing the central tendency of the end of the snow season even in regions with differing snow regimes. Overall, the differences between Landsat and MODIS are smallest for this combined metric.

We analyzed the Landsat and MODIS metrics to characterize snow regimes based on snow persistence patterns (Figure 1.15). First, we assessed the local variability of snow persistence by calculating the standard deviation of the 30-m snow-free date within each 510 m pixel (left panel). This local spatial variability shows areas where snow is highly heterogeneous at the scale of MODIS pixels (500 m) and where the information from the 30 m Landsat scale is most valuable. The local spatial variability is highest in rugged terrain.

The middle panel of Figure 1.15 shows the difference between the median values of the two MODIS snow metrics, longest CSS end day and last snow day. The difference is generally low where the snow regime is characterized by a continuous period of winter snow directly followed by snow-free conditions for the spring and summer, and high in areas where multiple periods of snow cover tend to occur during the late winter, spring and summer. There is a difference of ≤7 days for most of the study area, but also some extensive areas with a >21 day difference (and relatively small area with an 8–21 day difference). The northern Alaska Peninsula and south-facing mountain areas exhibit the largest differences between the two metrics.

We evaluated the interannual variability of snow persistence by calculating the standard deviation of the MODIS longest CSS end day metric for 2000–2015. This measure of the snow season length does not consider snow onset date, but is a useful metric of variability in the persistence of snow in spring. Variability is lowest on the North Slope and highest in southwest and southcentral Alaska and along coastlines of the Gulf of Alaska. There is also high variability on south-facing mountain slopes.

## ANNUAL 30 M SNOW PERSISTENCE COMBINING LANDSAT AND MODIS

There is important variability in snow cover at the 30 m scale of the Landsat map, but the interannual variability is also important. Therefore, we calculated the annual anomaly

compared to median snow persistence at 500 m resolution for each year in the MODIS record (Figure 1.16). Then, we applied that as an adjustment to the climatological normal snow-free date, to estimate the annual snow persistence at the Landsat scale. Figure 1.17 provides an example of the results for the vicinity of Anaktuvuk Pass, central Brooks Range. This product is provided as a proof of concept. Validation and refinement of these annual 30 m maps would be a useful subject of future research.

## CONCLUSION

We calculated the climatological average snow persistence for most of Alaska using all the Landsat scenes available for February 1–August 31, 1999–2015. Using Google Earth Engine, we developed an algorithm that considered cloud cover, terrain and cloud shadows, and the SnowMap spectral tests to assess the snow status of each pixel in the record. We summarized the snow status for each pixel by day of year, and then applied a binary classification tree to determine the day of year that best separated the snow-covered and snow-free seasons during 1999–2015. The results were broadly consistent with SNOTEL *in situ* measurements and MODIS snow metrics for most of the study area. Areas where agreement was poorer generally correspond to locations with an intermittent snow regime, most likely due to midwinter melt events or frequent episodes of late spring and summer snow.

The results capture fine-scale patterns in many areas that cannot be resolved by coarser resolution satellite data products. This new map, covering most of the state of Alaska, will be useful for characterizing snow patterns for habitat availability and suitability studies for caribou and other wildlife. There are also applications for hydrology and surface energy balance. Work is ongoing to relate the snow persistence patterns to snow depth and snow water equivalent.

# SECTION 2: LICHEN COVER MAPPING, YUKON–CHARLEY NATIONAL PRESERVE

## INTRODUCTION

The distribution and abundance of forage lichen are critical factors influencing the movements, distribution, and nutritional ecology of caribou in Alaska. Forage lichens are mainly light-colored genera, primarily *Cladonia, Cladina, Cetraria,* and *Flavocetraria* spp. They are terricolous (i.e. occurring on the ground, not in trees) macrolichens (i.e. fruticose or foliose growth forms, not crustose). The Fortymile caribou herd has been increasing since the 1970s but recent evidence suggests the herd has reached or exceeded its carrying capacity, leading to declining body condition and recruitment, as well as overgrazing of upland habitat within Yukon–Charley Rivers National Preserve (YUCH) (Boertje et al. 2012). The herd's range is expansive, stretching from the White Mountains into Canada and covers most of YUCH. Little is known about the spatial distribution of potential overgrazing effects, due to the lack of spatially explicit habitat characteristics over the extensive range. In an effort to better understand the spatial and nutritional ecology of Fortymile caribou, maps that depict patterns of lichen abundance are required. The lichen cover products will be useful for analyzing caribou habitat selection and caribou management. They have applications in other disciplines including vegetation science and landscape change, and may be used by a variety of researchers and other land managers operating in the region.

## STUDY AREA

The lichen mapping study area is limited to YUCH (Figure 2.1), where systematically collected vegetation data are available from a network of Long-Term Ecological Monitoring (LTEM) plots maintained by the National Park Service. YUCH is therefore the inference domain of these ground data. The LTEM dataset available for this study includes measurements of vegetation cover and structure collected at 528 systematically located plots located within the LTEM grids (Figure 2.1). The study area was defined by applying a 3 mile buffer to the YUCH boundary, so that information would be available in areas immediately adjacent to the preserve.

# METHODS

## PLOT DATA

The Central Alaska Network (CAKN) has a vegetation monitoring program in YUCH which is described in a detailed protocol document (Roland et al. 2004). The LTEM vegetation program involves systematic sampling of grids that include up to 25 plots each. The sampling of YUCH was only partially completed at the time of this study. Carl Roland, NPS botanist, provided three data tables summarizing the data from the vegetation monitoring program at YUCH. These tables covered data collected and summarized in YUCH through spring 2016. The data tables included:

YUCH_plot_locs, a Microsoft Access database table that includes a comprehensive list of 528 plots with a plot center location (decimal degrees in the North American 1983 horizontal datum) and field sampling date;

YUCH_transect_records, a Microsoft Access database table that includes all vegetation and ground hits recorded at each point on the sample transects at each plot (see Figure 2.2). The vascular plant data were aggregated to growth form (e.g. Tree, Dwarf Shrub, etc.);

YUCH_Lichen_cover_by_genus.xlsx, a spreadsheet with genus-level summaries of lichen cover from the quadrats at a subset of the plots.

The vegetation monitoring plots are circular with a diameter of 16 m (Figure 2.2). There is a 16 m transect oriented east-west, and two 6 m transects oriented north-south (the 6 m transects skip the portion of the line within 2 m of the plot center). Transects are sampled at 30–50 cm intervals and vegetation hits are recorded within 10 vertical strata. Details of the VPI protocol are provided in Roland et al. 2004. Nonvascular plants are recorded only as Lichen or Moss on the vegetation point-intercept (VPI) transects (i.e., no attempt is made to identify them). The only lichens recorded are terricolous macrolichens (i.e. no crustose or arboreal lichens). Lichens typically occur only in the lowest vertical strata, but the data from other strata were considered to assess the frequency with which ground lichens were overtopped by other vegetation.

There are 4 quadrats aligned adjacent to the transects, each covering 1 m² total, and each includes a nested 0.25 m² quadrat. We received data that had aggregated the cover for all the quadrats at the plot. Nonvascular species are recorded if they are on a list of ~57 nonvascular taxa "that are common, abundant, and widespread in their distribution among CAKN parklands" (Roland et al. 2004). They are also vouchered with collections if the field identification is not certain. In addition, any nonvascular taxon exceeding 4% cover on a quadrat is recorded and vouchered. At the time the field data were delivered for this study, processing of the vouchers was incomplete, and so genus-level data were provided based on the provisional field identifications.

VEGETATION POINT INTERCEPT (VPI) DATA

First, the vegetation data were reviewed to identify lichen hits that occurred directly above rock hits. These were identified as most likely crustose lichen hits that were mistakenly recorded in the field by new crews still learning the sampling protocol. These would normally be removed during the comprehensive Quality Assurance/Quality Control (QA/QC) that is completed when sampling of a parkland is completed. Since we were working with provisional data we performed this recommended correction (Carl Roland, personal communication).

Second, we assessed the occurrence of lichen with and without overtopping layers. Points with lichen in the ground stratum (0–9 cm) and vegetation hits in higher vertical strata were identified. In addition, lichen hits that occurred with other vegetation hits in the same stratum (0–9 cm) were identified. Vascular plant, standing dead, and litter hits that occurred in the ground stratum were assumed to overtop the lichen, while moss and soil hits that occurred in the ground stratum were assumed to lie beneath the lichen.

Third, we generated summaries of lichen cover (percentage of points where lichen was present) and top lichen cover (percentage of points where lichen was present and was not overtopped). We summarized the VPI data for the full YUCH dataset by plot, and by transect. For the plot summary, we split the 16 m east-west transects into two 8 m transects. This resulted in four transects per plot: north and south of plot center (6 m each); and east and west of plot center (8 m each).

## VEGETATION QUADRAT DATA

We received a provisional summary of lichen cover from 275 plots, which aggregated cover across the 4 1 $m^2$ quadrats at each plot. Lichen cover was reported by genus, based on the provisional field identifications. After discussion with Carl Roland, we added an additional 39 plots to the quadrat dataset that were intended to be included in the provisional summary but were inadvertently excluded because they lacked any lichen.

### Lichen Genera and Color Groups

We summarized the quadrat data by color using nested color groups developed by Emily Holt (University of Northern Colorado) and Peter Nelson (University of Maine at Fort Kent). The color groups include light lichens (grey, yellow, white, and orange) and dark lichens (black, brown, green, and green-grey). Examples of light and dark lichens can be seen on the report cover. Details on the color groupings of lichen genera are provided below in the results.

The genus-level taxonomic precision of the quadrat data meant that more than one color group was associated with many of the lichen taxa. We aggregated the quadrat data to describe the overall cover of each lichen genus in the full YUCH dataset, and then summarized cover by the fine (8 category) and coarse (2 category) color groups. In addition, there were multiple (mixed) categories for taxa that included more than one color group at the two levels. For example, field identifications of the genus *Cladina*—which includes numerous important caribou forage species—were aggregated to a mixed (gray, white, and yellow) fine color group, and to the light coarse color group.

The genus and color group data from the vegetation quadrats were summarized for the entire dataset, to characterize the relative importance of the different groups in the lichen cover across YUCH. The coarse color group data were also summarized by plot, so that the total lichen cover recorded on the VPI transects could be partitioned among the light, dark, and multiple (mixed) color categories.

### VEGETATION TRAINING DATA

For training raster-based models, the vegetation transect and quadrat data summaries were evaluated both independently (VPI only, quadrat only) and combined (VPI cover scaled by quadrat color fractions). In addition, training data were developed at two levels: plot and transect (4 transects per plot).

Four transect lines were generated in GIS for each of the plots. These lines were later used to extract raster values from high-resolution imagery. The vegetation transects were laid out in the field using a compass with no declination set (i.e. magnetic north-south, and magnetic east-west) (Roland et al. 2004). We used the "oce" library (Kelley and Richards 2016) in the R statistical package to determine the appropriate declination at the time each plot was laid out. Then, we used the ArcGIS "Bearing Distance to Line" tool to calculate 8 m geodesic lines for each transect. The lines started at the plot center and were oriented to the 4 cardinal compass directions, adjusted for declination at the date the plot was established. We masked out the inner 2 m of the north-south transect per the plot layout (Figure 2.2).

A set of lichen cover summaries was then generated for each plot and each transect (4 per plot) from the VPI and quadrat data. These included summaries based only on the VPI data (with no color groups), summaries based only on the quadrat data (cover by coarse color group and total), and summaries based on the total lichen cover from the VPI data weighted by the color groups from the quadrat data.

## PREDICTORS

A set of environmental and Landsat predictors was developed for the study area. The complete 30 m predictor set is listed in Table 2.1 and is described below.

### ENVIRONMENTAL PREDICTORS

#### Tree Canopy Cover

Lichens often co-occur with low to intermediate levels of tree cover (e.g., lichen woodlands). Trees affect the ability of satellites to detect ground lichens, so we obtained forest cover data for the year 2000 from the forest cover loss analysis of Hansen et al. (2013). The "Tree canopy cover for year 2000 (treecover2000)" and "Global forest cover loss 2000–

2014 (loss)" map layers were downloaded from the Global Forest Change website (http://earthenginepartners.appspot.com/science-2013-global-forest/download_v1.2.html). The layers were re-projected to Alaska Albers (NAD 1983) at 30 m resolution to match the Landsat composites. A year 2015 tree canopy layer was estimated by setting the tree canopy cover to zero for any areas mapped as "forest loss" over the 2000–2014 period; we set the tree canopy cover to zero because the vast majority of "forest loss" areas mapped by Hansen et al. (2013) in YUCH pertain to stand-replacing wildfires.

Elevation and Slope

The 2 arc-second National Elevation Dataset (NED) Digital Elevation Model (DEM) data were downloaded and re-projected to Alaska Albers NAD 1983 at 30 m resolution. Slope, in degrees, was calculated from the elevation data using geospatial tools in ArcMap.

## LANDSAT IMAGERY

We developed Landsat composites from Landsat 8 imagery collected in 2013–2016. Composites were produced from Landsat Surface Reflectance products and were generated using Google Earth Engine. Composites are useful because they can be used to map areas larger than a single Landsat scene, and do not require a single cloud-free acquisition. In addition, composites can utilize data from different seasonal windows to characterize reflectance at different stages of the growing season.

We developed composites for spring (selecting for observations after snowmelt but, ideally, before vegetation green-up), midsummer, and fall. Each composite includes the reflective bands and supplemental bands providing the year and day of year of the source scene for each pixel. A "maximum NDVI" compositing rule is frequently used to generate composites, but we observed that using this rule with the Landsat Surface Reflectance product tended to include cloud shadows that were missed by the automated cloud mask. Instead of maximum NDVI, we used a percentile of either near-infrared (NIR) reflectance (for midsummer) or near-infrared plus blue reflectance (for spring and fall), since including the blue band tended to select against partially snow-covered pixels. For the spring composite, we considered observations from April 1–July 31, 2013–2016, and for each pixel selected the observation at the 20th percentile of NIR reflectance plus blue reflectance. This

technique was effective at avoiding both snow and greened-up vegetation. The late end date (July 31) was selected for the spring composite because late-lying snow is common at high elevations in YUCH.

For the summer composite, we selected the observation with the median (50th percentile) NIR from the stack of observations that acquired from June 15–September 15, 2013–2016. Finally, for the fall composite, we selected the observation with the median NIR reflectance plus blue reflectance from September 1–October 15, 2013–2016. This helped to avoid early snow in the fall composite.

Spectral metrics can be useful to reduce the effect of illumination and terrain shadowing, and provide better contrast for vegetation and other features. We included a set of indices based on the Landsat surface reflectance composites for the three seasonal windows:

- NDVI (Normalized Difference Vegetation Index, Rouse et al. 1974):
    - (Red - NIR) / (Red + NIR)
- NDMI (Normalized Difference Moisture Index, Goodwin et al. 2008):
    - (NIR - SWIR1) / (NIR + SWIR1)
- NDWI (Normalized Difference Water Index, McFeeters 1996):
    - (Green - NIR) / (Green + NIR)
- NDSI (Normalized Difference Snow Index [Hall et al. 1995] is also the converse of the Normalized Difference Lichen Index [Falldorf et al. 2014]):
    - (Green - SWIR1) / (Green + SWIR1)
- NBR (Normalized Burn Ratio, Key and Benson 1999):
    - (SWIR2 - Red) / (SWIR2 +Red)
- EVI2 (Enhanced Vegetation Index 2, Jiang et al. 2008):
    - (2.5 x [NIR - Red]) / (NIR + [2.4 x Red] + 1)
- NDBI (Normalized Difference Blue Index). An increase in reflectance from 400-450 nm is diagnostic for some lichens (Rees et al. 2016). We contrasted the

"coastal" blue band available in Landsat 8 and WorldView-2/3 with the traditional blue band to exploit this:

- (Blue - Coastal) / (Blue + Coastal)

Finally, we included the magnitude of the difference between the spring and midsummer reflectance and metrics.

### DIGITALGLOBE IMAGERY

The vegetation plots are 16 m diameter (201 m²), which is less than one quarter of a 30 m Landsat pixel (900 m²). Mapping based on Landsat imagery assumes that the lichen cover in the plot is representative of the full pixel. However, lichen cover and other vegetation can be extremely heterogeneous. Therefore, we also explored methods to train lichen cover models based on ~2 m resolution multispectral DigitalGlobe (DG) imagery (WorldView-2 and WorldView-3) available under the NextView license. Suitable DG scenes overlapping the vegetation grids were identified and analyzed on the Arctic Boreal Vulnerability Experiment (ABoVE) Science Cloud maintained by NASA. The scenes were ortho-rectified based on the Rational Polynomial Coefficients metadata and the 30 m DEM, and were calibrated to top of atmosphere reflectance, using python scripts provided by the Polar Geospatial Data Center at the University of Minnesota.

## MODELING

### OVERLAY OF TRAINING DATA

We applied random forest data-mining models in R to predict lichen cover from the training data, remote sensing imagery, and environmental predictors. We chose random forest to model lichen cover because it is effective at capturing relationships between a large set of co-varying predictors (Breiman 2001). First, the predictor values were extracted for each plot (Landsat) or transect (2 m resolution DG images). For the plots, a weighted value was extracted from each 30 m raster predictor (Table 2.1) from the pixel(s) within 8 m of the plot center. This was a single pixel for plots near the center of a 30 m pixel, and multiple pixels for plots within 8 m of the pixel edge. For the transects, the mean value of all the 2 m

pixels intersected by the 6–8 m transect line was extracted for each band of the 2 m resolution DG image.

## DEVELOP AND EVALUATE MODELS

### Plot-based Lichen Cover Models, 30 m

A suite of models were developed based on the plot training data and the 30 m predictors (Landsat composites, metrics, and environmental predictors). Five measures of lichen cover were modeled:

1. total lichen cover from VPI;
2. top lichen cover from VPI;
3. total lichen cover from quadrats;
4. lichen cover by color group from quadrats; and
5. lichen cover by color group from VPI weighted by quadrat data.

### Classification of Lichen Cover Thresholds, 30 m

For the total lichen cover from VPI modeling, we also assessed the performance of lichen presence/absence models with the threshold set at various levels of lichen cover, ranging from 0–50%. Because lichen is often overtopped by other vegetation, it is difficult to detect at low cover values. We explored using different thresholds to classify absent/low lichen cover versus moderate/high lichen cover.

### Transect-based Lichen Cover Models, 2 m

We developed and evaluated models of total lichen cover from VPI for selected 2 m resolution DG image subsets, trained on the transect summaries that overlapped the imagery. DG images cover limited areas and reflectance values between different images are generally not comparable due to differences in atmosphere, sun angle, and the view angle of the satellite. Therefore the models from the DG images were local and could not be extrapolated from one DG image to another. We included transects from 1–2 grids in each model, with up to 25 plots per grid and 4 transects per plot.

Raster-based Lichen Cover Models, 30 m trained from 2 m

We aggregated the results of the 2 m lichen cover models to 30 m and combined them into a single layer. Then, a subset of the aggregated 30 m pixel values were extracted, and were used to model lichen cover over the entire study area using the 30 m predictors. This provided data at a more appropriate scale for training the Landsat models (full 30 m pixels rather than 16 m diameter circular plots), and also a higher sample size for training the model.

## RESULTS AND DISCUSSION

### PLOT DATA

#### VEGETATION POINT INTERCEPT (VPI) DATA

The VPI data were summarized for 528 plots in YUCH. The number of points per plot (Table 2.2) varied depending on the point spacing, which was usually 50 cm but was sometimes 30 cm or 40 cm. 10 of the plots had unusual point counts, either because only the east-west 16 m transects were sampled (2 plots), or because 1–3 points were inadvertently skipped (8 plots). The variation in point density across plots and minor discrepancies in sample point numbers do not affect the plot cover summaries, because all of these are normalized by the number of points at each plot.

Vegetation cover was measured at a total of 35,193 sample points in the VPI dataset. Summaries of lichen hits in the original dataset indicate that a total of 6,853 lichen hits were recorded, and lichen hits were recorded at 6,782 points (Table 2.3). The small difference occurred because multiple lichen hits were recorded at a few points; we collapsed these multiple hits for our analysis. The QA/QC step of removing lichen hits that occurred above rock hits (most likely crustose lichen hits that should not have been recorded per the measurement protocol) resulted in 5,172 points with terricolous foliose or fruticose lichen, indicating that the overall cover of lichen across YUCH is about 14.7%. This filtered set of points with terricolous macrolichens (i.e., foliose or fruticose lichens) is what is referred to as "lichen" in all subsequent analyses.

We reviewed the vertical position of these lichen hits (Table 2.4) to assess the potential visibility of lichen to direct observation from above (i.e., an overpassing satellite). The vegetation dataset recorded a vertical stratum for each hit, but it did not identify the order of hits when more than one hit occurred in the same stratum. Therefore, there were some cases in which lichen and non-lichen hits occurred in the same vertical layer (almost always the 0–9 cm ground layer). In such cases, we assumed that the lichen occurred below vascular plants, standing dead vegetation, and litter hits, but above moss and soil hits. Of the 5,172 points with lichen, 1,177 (3.3% of YUCH sample points) had lichen as the top hit (i.e., without overtopping vegetation). 3,995 points (11.4% of YUCH sample points) had lichen that was overtopped by vascular plants, standing dead vegetation, or litter.

## VEGETATION QUADRAT DATA

We analyzed quadrat cover data from 313 plots. We were provided with quadrat cover data for 275 of these plots, covering 20 of the sampling grids, and added 39 additional plots at the same grids where we could assume that lichen was absent (Carl Roland, pers. comm.). All of these plots also had VPI data, but there were an additional 215 plots with VPI data that did not have nonvascular cover data for quadrats, either because the data were not collected or had not yet been fully reviewed by the park staff.

### Lichen Genera and Color Groups

The mean lichen cover by genus (Table 2.5 and 2.6) is stratified by coarse color group and lists the most abundant lichens at the top. The dominant genera are *Cladina, Peltigera,* and *Cladonia,* which each average >1% cover overall. Combined, these 3 genera represent over 60% of the lichen cover in YUCH. These genera are each represented by species belonging to 3–4 different fine color groups, which means that these genus-level data are of very limited use for characterizing fine color groups. However, two of the genera (*Cladina* and *Cladonia*) pertain entirely to the light coarse color group, and also include numerous preferred caribou forage species. Though gray lichens are intermediate between the light and dark coarse color groups, and have been considered "dark" in some previous work [Nelson 2013], we considered gray *Cladina* and *Cladonia* lichens to group with light lichens for this

work. Otherwise, 2 of the 3 most common lichen genera would not resolve even to the light and dark coarse color groups.

Of the remaining 9 lichen genera with >0.1% mean cover, *Flavocetraria* and *Cetraria* include lichen forage species. *Cetraria* includes both yellow and brown species, and so cannot be definitively categorized into a light or dark group. It is also the only genus of any abundance that cannot be placed into a single coarse color group.

Although the percent cover on the landscape of by lichen genera is fairly low based on the quadrat data (maximum mean cover for a genus is 1.7%), lichens can be locally abundant, as is seen in the maximum cover. Several genera occur with cover >20% at individual plots, and *Stereocaulon* is recorded with 43.7% cover at one plot.

## VEGETATION TRAINING DATA

### Comparison of VPI and Quadrat Lichen Cover Data

Based on quadrat data, the overall mean cover of lichen in YUCH is 7.5%. This compares to a mean lichen cover of 12.5% based on the VPI data at the same 313 plots. This suggests that for the purpose of training remote sensing models, there is a bias between the two methods used to measure lichen cover in the field (ocular estimates for the quadrats, and point intercept for the VPI transects). The point-intercept method may estimate higher lichen cover than the ocular method, because the sample "point" is actually a small circle and therefore lichen cover may be somewhat overestimated especially for fruticose species with a threadlike growth form (e.g., *Bryocaulon*). For the purpose of training models based on remote sensing imagery with 2–30 m resolution, we expected that the much larger spatial footprint of the 4x6–8 m VPI transects (compared to the 4x1 m quadrats) would be an advantage, especially where the lichen cover is heterogeneous and the composition of the quadrats may not be representative of the overall lichen cover in the plot.

### Vegetation Training Datasets

The complete VPI training dataset was compiled based on all 528 plots (Figure 2.3, top). Since quadrat data were not available for all plots, total lichen cover was the only cover metric available for the full dataset. The plots are well distributed across YUCH. Most of the high lichen cover plots are located in rugged terrain and away from the Yukon River.

A total of 313 plots were available to develop training data based on quadrat cover alone (Figure 2.3, bottom), as well as VPI cover data scaled by coarse color groups recorded at the quadrats. 3 color groups of lichen were identified from the genus-level quadrat data (Table 2.5 and 2.6): light lichens (mainly *Cladonia, Cladina, Flavocetraria*, and *Stereocaulon*); dark lichens (mainly *Peltigera, Umbilicaria,* and *Melanelia*); and mixed light/dark lichen genera (mainly *Cetraria*). For mapping purposes, we considered total lichen (all genera or terricolous macrolichens); light lichen; and light/mixed lichen. The light/mixed category was considered because *Cetraria* spp. can be light-colored and are common forage lichens; we did not map the dark color group because this group includes few forage species. We calculated the total lichen cover, light lichen cover, and light/mixed lichen cover for each of the 313 plots based on quadrat data alone, and for VPI lichen cover scaled by quadrat color group. The total lichen cover from quadrats in Figure 2.3 (bottom) is mostly low along the Yukon River, with few plots >10% cover. Similar to the VPI data, most of the high-lichen cover plots based on quadrat data are in the mountains. The plots with quadrat data are more concentrated along the river, however, with sparser data in the uplands and mountains.

An example of VPI transects overlaid on high-resolution satellite imagery for 4 plots in the Flat Creek grid (Figure 2.4) shows the relative size of the transects and the fine-scale detail of the imagery. The heterogeneity of VPI lichen cover is also apparent at some plots, such as at FLAT_CR12.

**PREDICTORS**

Selected 30 m predictors are presented in Figure 2.5. The northern half of the study area is dominated by the Yukon River and adjacent lowlands, with relatively low elevations and extensive forest cover. The southern portion of the study area is dominated by rocky mountains, with forest cover low or absent.

The spring Landsat composite appears to provide a good depiction of the landscape without snow but with minimal green-up of deciduous plants. This is the phenological period during which lichens may be most visible and the solar elevation is high (thus minimizing the shadow cast by vegetation and rough terrain). The midsummer composite represents the peak of the growing season when vascular plant cover is highest. The seasonal difference in

vascular cover is also seen in the NDVI metrics for the spring and summer composite. The fall composite depicts the time when plant senescence is widespread, and this may be useful for distinguishing plants by their fall colors. However, snow contamination at high elevations, and extensive terrain shadowing, can make the fall imagery less reliable for modeling lichen cover.

## MODELING

### PLOT-BASED LICHEN COVER MODELS, 30 M

The performance summary for 30 m random forest models predicting terricolous macrolichen cover (Table 2.7) shows that the best-performing *in situ* model based on the amount of variance explained is based on VPI total lichen cover (29.7%). However, this model also has the highest root mean square error (RMSE) and Mean Absolute Error (MAE). The VPI top lichen cover model predicts only 9.1% of the variance. Models based on quadrat cover alone have low performance, particularly when partitioned into color groups (1.3% and 3.1% of variance explained for quadrat light and light/multiple lichen cover, respectively). The models based on VPI data scaled by quadrat cover explain less variance than total VPI cover (9.1% and 15.1% for light and light/multiple color groups).

A scatterplot of observed VPI total terricolous macrolichen cover versus the out-of-bag (cross-validated) predictions (Figure 2.6) shows a noisy relationship with a lot of scatter. There is a tendency towards overestimation of lichen cover for low lichen cover plots, and underestimation at high lichen cover plots. The maximum predicted lichen cover is about 42%, while there are many plots with >60% lichen cover based on VPI data.

A map of total terricolous macrolichen cover based on the VPI data (Figure 2.7) shows low lichen cover for most of the lower elevations along the Yukon River, and intermediate lichen cover in foothills, high lichen cover at some higher elevations, but low lichen cover at the highest elevations. There are some hotspots of higher lichen cover at lower elevations.

### CLASSIFICATION OF LICHEN PRESENCE/ABSENCE, 30 M

We evaluated lichen "presence/absence" models using different cover thresholds to define lichen absence, ranging from 0 to 50% (Table 2.8, Figure 2.8 bottom). At the lowest

threshold (0%), 144 of 528 plots are in the "lichen absent" category, while at the 50% threshold, 497 plots were in that category. We applied random forest models to predict lichen presence/absence at each threshold. While the overall out-of-bag classification error was lowest at the 50% threshold (at 6.1%), this was not a useful result since all 528 plots were predicted to be lichen-free at that threshold. The average error rate of false lichen detections and false lichen-free detections is a more useful summary metric, and this error rate is smallest for the lichen presence/absence threshold of 3% (23.2% mean classification error). The mean classification error rates for thresholds from 2–10% range only 23.2–26.7%, with false lichen detections more common at the lower threshold and false non-lichen detections more common at the higher threshold.

Maps of lichen presence/absence for various thresholds (Figure 2.8) show that at the lowest threshold (1%), lichens are predicted to be absent mainly along the Yukon River. At thresholds of 3–9%, increasing proportions of the Yukon River valley and the highest elevations are also predicted to be lichen-free. At a threshold of 15% cover, most of the Yukon valley lowlands are predicted to be lichen-free, and at 30% only isolated high elevation sites are predicted to have lichens.

### TRANSECT-BASED LICHEN COVER MODELS, 2 M

The overall explanatory power of the best Landsat-based models trained with *in situ* plot data was 29.7% (Table 2.7). This is likely due to the scale mismatch between the 16 m diameter plots and the 30x30 m Landsat pixels. Therefore, we assessed finer scale models that were trained by overlaying individual VPI transects (4 per plot) over 2 m resolution multispectral WorldView-2 and WorldView-3 imagery. We performed this exploratory analysis for five image subsets, with one subset covering two LTEM grids, and four covering a single grid (Table 2.9). Results were best for the subsets covering two grids (Ben Creek and Chester Creek), with 24.5% of variance in total terricolous lichen cover explained. The Hanna Creek, Flat Creek, and Funnel Creek subsets each had >14% of the variance explained. Lower Crescent Creek, however, had a result indicating that a negative amount of the variance was explained; this model was discarded. The image acquisition dates for the 4 models that were selected ranged from 12 May to 13 July (late spring to midsummer), while

the Lower Crescent Creek image was acquired in late summer on 26 August (Table 2.9). The lower sun angle and increased shadows in late summer may help explain the poor performance of the latter model.

Maps of the four subsets (Figure 2.9) show large gradients in lichen cover, with substantial areas mapped with lichen cover >50% (unlike the *in situ* plot-trained Landsat model, Figure 2.7). The high lichen areas also appear reasonable based on photo-interpretation of the DG imagery. With the exception of the Ben Creek and Chester Creek model, no lichen-free areas are predicted. This could potentially be addressed by adding photo-interpreted lichen-free areas, such as waterbodies and river barrens, to the training dataset.

We ortho-rectified the 2 m resolution DG images using only the ephemeris and a 30 m DEM (based on the 2 arc-second NED). Even with a high resolution, high quality, current DEM, the ephemeris would only provide a horizontal position accuracy of 5–10 m. With the NED DEM we used, the positional error of the imagery was even greater. Even a 5 m horizontal position error is large relative to the VPI transects, which are only 6–8 m long. We expect that the model performance could be improved substantially by refining the match between the VPI transects and the 2 m resolution DG imagery. This could be accomplished by improving absolute horizontal accuracy (e.g., using a better DEM and high-quality ground-control points) or the relative horizontal accuracy (e.g., matching features on the imagery to plot photos). In addition, the models were trained using only the eight reflective bands of a single image. Using multiple images (e.g., spring and summer), spectral metrics, and environmental predictors could improve the models further.

### RASTER-BASED LICHEN COVER MODELS, 30 M TRAINED FROM 2 M

We aggregated the 2 m resolution DG models to 30 m resolution and calculated the mean lichen cover for each 30 m super-pixel. We then used a subset of the aggregated data to train a new 30 m resolution model for the study area using the same 30 m predictors that were used for the *in situ* trained models (Table 2.1). A subset was used for computational reasons to constrain the volume of training data. The data excluded from this subset could be used for validation, though in this case we used out-of-bag cross-validation instead. The

model based on the aggregated 2 m data explained 64.4% of the variance in the training data (out-of-bag cross-validated predictions), with lower RMSE and MAE than the other total lichen cover models (Table 2.7). While these error metrics do not include errors from the 2 m models, they do demonstrate that upscaling data from 2 m to 30 m tends to maintain model performance and accuracy.

The map of total terricolous lichen cover based on up-scaled 2 m resolution DG imagery (Figure 2.10) maps more lichen hotspots close to the Yukon River compared to the *in situ* trained map (Figure 2.7). The mountainous southern portion of YUCH has relatively homogeneous, moderately high lichen cover. However, none of the four training subsets were located in this region, and it is likely that results could be improved by adding additional subsets of 2 m lichen cover maps.

## CONCLUSIONS

We assessed the terricolous macrolichen cover for Yukon-Charley Rivers National Preserve based on a subset of the long-term vegetation data collected as part of the NPS Inventory and Monitoring program. Terricolous macrolichen was present at 14.7% of 35,193 vegetation point intercept (VPI) sample points that were measured at 528 plots (Table 2.4). Lichen was overtopped at 11.4% of the points and occurred without overtopping vegetation or litter at only 3.3% of points (Table 2.4). At 313 plots where lichen cover data were available for both VPI transects and quadrats, terricolous macrolichen cover averaged 12.5% (VPI cover estimate) and 7.5% (quadrat ocular cover estimate). 3 lichen genera had overall mean cover >1% (Table 2.5), including 2 light-colored genera that include numerous caribou forage species (*Cladina* and *Cladonia*), and one dark non-forage genus (*Peltigera*).

We assessed 30 m resolution lichen cover models using several metrics of lichen cover (VPI cover, quadrat cover/color, and VPI cover scaled by quadrat color). The best model explained 29.7% of lichen total cover variance based on cross-validated out-of-bag predictions and was based on VPI data alone, without scaling from quadrat data.

We assessed the performance of lichen presence/absence models at different thresholds of total VPI terricolous macrolichen cover. Overall the best balance of lichen and non-lichen

detection was at 3% lichen cover, and the average error was similar for thresholds in the range 2–10%.

There is a pronounced scale mismatch between the 16 m diameter LTEM plots and the 30 m resolution Landsat imagery. Therefore we explored using 2 m resolution DG imagery to develop high-resolution lichen cover maps, based on lichen cover from individual VPI transects (4 per plot). The initial results were promising, with the best 2 m model explaining 24.5% of the variance for 2 LTEM grids. We expect that results could be improved further by improving the geolocation match of the vegetation transects and the 2 m imagery, and by including additional image dates, spectral metrics, and environmental predictors in the 2 m models.

Finally, we demonstrated that results from 2 m models covering selected subsets can be aggregated to 30 m resolution and then used to train 30 m models covering the entire study area. The approach of using *in situ* plot data to train 2 m resolution models, then using aggregated 2 m resolution data to train 30 m models, is likely the best method in the long-term to fully exploit the YUCH vegetation plot data given the scale mismatch between the vegetation plots and Landsat pixels.

We produced two 30 m lichen cover maps for the study area. One trained 30 m predictors based on VPI data at 29 LTEM grids (Figure 2.7); and the second trained 2 m predictors based on VPI data at a total of 5 LTEM grids, then aggregated the 2 m maps to train 30 m predictors (Figure 2.10). We recommend that the first map (Figure 2.7) be used for wildlife and botanical studies for two reasons. First, the geographical distribution of plots was much broader with the first map. Second, the accuracy of the 2 m maps was reduced by the geolocation uncertainly between the sample transects and the 2 m imagery. Ideally, a large set of independent ground data would provide the best information to identify which of the two lichen cover maps is the most accurate.

## REFERENCES


Boertje, R., C. L. Gardner, K. A. Kellie, & B. D. Taras. 2012. Fortymile caribou herd: increasing numbers, declining nutrition and expanding range. Alaska Department of Fish and Game, Wildlife Technical Bulletin 14, ADFG/DWC/WTB-2012-14. Juneau, Alaska.

Breiman, L., 2001. Random forests. Machine learning, 45(1), pp.5-32.

Carroll, M., Wooten, M., DiMiceli, C., Sohlberg, R. and Kelly, M., 2016. Quantifying Surface Water Dynamics at 30 Meter Spatial Resolution in the North American High Northern Latitudes 1991–2011. Remote Sensing, 8(8), p.622.

Falldorf, T., O. Strand, M. Panzacchi, and H. Tømmervik. 2014. Estimating lichen volume and reindeer winter pasture quality from Landsat imagery. Remote Sensing of Environment, 140, pp.573-579.

Goodwin, N.R., Coops, N.C., Wulder, M.A., Gillanders, S., Schroeder, T.A. and Nelson, T., 2008. Estimation of insect infestation dynamics using a temporal sequence of Landsat data. Remote sensing of environment, 112(9), pp.3680-3689.

Hall, D.K., Riggs, G.A. and Salomonson, V.V., 1995. Development of methods for mapping global snow cover using moderate resolution imaging spectroradiometer data. Remote sensing of Environment, 54(2), pp.127-140.

Hall, D.K., Riggs, G.A., Salomonson, V.V., DiGirolamo, N.E. and Bayr, K.J., 2002. MODIS snow-cover products. Remote sensing of Environment, 83(1), pp.181-194.

Hansen, M.C., Potapov, P.V., Moore, R., Hancher, M., Turubanova, S.A., Tyukavina, A., Thau, D., Stehman, S.V., Goetz, S.J., Loveland, T.R. and Kommareddy, A., 2013. High-resolution global maps of 21st-century forest cover change. Science, 342(6160), pp.850-853.

Jiang, Z., Huete, A. R., Didan, K., & Miura, T. 2008. Development of a two-band Enhanced Vegetation Index without a blue band. Remote Sensing of Environment, 112(10), 3833–3845.

Kelley, D. and Richards, C. 2016. oce: Analysis of Oceanographic Data. R package version 0.9-20. https://CRAN.R-project.org/package=oce

Key, C.H. and Benson, N.C., 1999. The Normalized Burn Ratio (NBR): A Landsat TM radiometric measure of burn severity. US Dept. Interior, Northern Rocky Mountain Sci. Center, Bozeman, MT.

Klein, A.G., Hall, D.K. and Riggs, G.A., 1998. Improving snow cover mapping in forests through the use of a canopy reflectance model. Hydrological Processes, 12(10), pp.1723-1744.

Lindsay, C., Zhu, J., Miller, A.E., Kirchner, P. and Wilson, T.L., 2015. Deriving snow cover metrics for Alaska from MODIS. Remote Sensing, 7(10), pp.12961-12985.

Macander, M. J., C. S. Swingley, K. Joly, and M. K. Raynolds. 2015. Landsat-based snow persistence map for northwest Alaska. Remote Sensing of Environment 163: 23–31. http://dx.doi.org/10.1016/j.rse.2015.02.028

McFeeters, S.K.. 1996. The use of the Normalized Difference Water Index (NDWI) in the delineation of open water features. International Journal of Remote Sensing, 17(7), pp.1425-1432.

Nelson, P. R., C. Roland, M. J. Macander, and B. McCune. 2013. Detecting continuous lichen abundance for mapping winter caribou forage at landscape spatial scales. Remote Sensing of Environment, 137, 43–54.

R Core Team. 2016. R: A language and environment for statistical computing. R Foundation for Statistical Computing, Vienna, Austria. URL https://www.R-project.org/.

Rees, G., Tutubalina, O., Zimin, M., and Golubeva, E.. 2016. Statistical characteristics of subarctic vegetation on the basis of ground hyperspectral measurements. Presentation at 14th Circumpolar Remote Sensing Symposium, Homer, Alaska. September 2016.

Roland, C.., Karen Oakley, Edward M. Debevec, and Patricia Loomis. 2004. Monitoring vegetation structure and composition at multiple spatial scales in the Central Alaska Network. Version 1.00 (November 1, 2004). Prepared for Central Alaska Network Monitoring Program, National Park Service, U.S. Department of the Interior. 50 pp.

Rouse, J.W, Haas, R.H., Scheel, J.A., and Deering, D.W. 1974. Monitoring Vegetation Systems in the Great Plains with ERTS. Proceedings, 3rd Earth Resource Technology Satellite (ERTS) Symposium, vol. 1, p. 48-62.

Selkowitz, D.J. and Forster, R.R., 2015. An automated approach for mapping persistent ice and snow cover over high latitude regions. Remote Sensing, 8(1), p.16.

Therneau, T., Atkinson, B.and Ripley, B. 2015. rpart: Recursive Partitioning and Regression Trees. R package version 4.1-10. https://CRAN.R-project.org/package=rpart

Wilson, R. R., D. D. Gustine, and K. Joly. 2014. Evaluating potential effects of an industrial road on winter habitat of caribou in north-central Alaska. Arctic, 67, 472–482.

Zhu, Z. and Woodcock, C.E., 2012. Object-based cloud and cloud shadow detection in Landsat imagery. Remote Sensing of Environment, 118, pp.83-94.

Table 1.1. Summary of tests in SnowMap in Complex Terrain algorithm, and resulting determination of snow status.

| Test Order | Interpretation | Snow Status | Test |
|---|---|---|---|
| 1 | Fill Value / NoData | Unknown | CFMask = Fill |
| 2 | CFMask Cloud and Revised Cloud | Unknown | CFMask = Cloud and Selkowitz and Forster (2015) = Cloud |
| 3 | Very Dark | Unknown | Green and Near–infrared TOAR < 0.07 |
| 4 | CFMask Water | Snow–free Water | CFMask = Water |
| 5 | No Terrain Shadow or Cloud Shadow | | GEE Hillshadow = Shadow OR Incidence Angle > 80 OR CFMask = Cloud Shadow |
| 5a | SnowMap = Snow | Snow | NDSI > 0.4 AND Green TOAR > 0.10 AND Near–infrared TOAR > 0.11 |
| 5b | Klein Canopy Snow = Snow | Snow | NDVI/NDSI spectral feature space polygon (Klein 1998) |
| 5c | Otherwise | Snow–free Land | |
| 6 | Terrain Shadow or Cloud Shadow | | |
| 6a | Shadow SnowMap = Snow | Snow | NDSI > 0.4 |
| 6b | Klein Canopy Snow = Snow | Unknown | NDVI/NDSI spectral feature space polygon (Klein 1998) |
| 6c | Otherwise | Snow–free Land | |

Table 1.2. Reclassification of reverse split and no split categories from snow–free date analysis, based on proportion of snow observations in the time–series.

| Frequency of Snow Observations | Raster Value |
|---|---|
| 0.0% snow frequency | 10 |
| 0.1–9.9% snow frequency | 11 |
| 10.0–19.9% snow frequency | 12 |
| 20.0–29.9% snow frequency | 13 |
| 30.0–39.9% snow frequency | 14 |
| 40.0–49.9% snow frequency | 15 |
| 50.0–74.9% snow frequency | 245 |
| 75.0–89.9% snow frequency | 246 |
| 90.0–94.9% snow frequency | 247 |
| 95.0–97.9% snow frequency | 248 |
| 98.0–99.9% snow frequency | 249 |
| 100% snow frequency | 250 |

Table 1.3. Areal summary of climatological snow–free date from Landsat, 1999–2015, Alaska.

| Climatological Snow–free Date Class | Raster Values | Pixels, Land | Pixels, Study Area | Area, Land (sq. km) | Area, Study Area (sq. km) | Percentage of Land |
|---|---|---|---|---|---|---|
| Water | 1 | 245,461,659 | 0 | 220,915 | 0 | |
| No pattern, 0.0% snow frequency | 10 | 227,439 | 469,542 | 205 | 423 | 0.01% |
| No pattern, 0.1– 9.9% snow frequency | 11 | 4,330,748 | 50,865,910 | 3,898 | 45,779 | 0.26% |
| No pattern, 10.0–19.9% snow frequency | 12 | 22,794,099 | 69,461,837 | 20,515 | 62,516 | 1.36% |
| No pattern, 20.0–29.9% snow frequency | 13 | 5,075,038 | 12,323,178 | 4,568 | 11,091 | 0.30% |
| No pattern, 30.0–39.9% snow frequency | 14 | 100,211 | 695,878 | 90 | 626 | 0.01% |
| No pattern, 40.0–49.9% snow frequency | 15 | 5,717 | 36,547 | 5 | 33 | 0.00% |
| Feb 1–March 10 | 32–69 | 1,451,994 | 8,910,226 | 1,307 | 8,019 | 0.09% |
| March 11–20 | 70–79 | 1,048,593 | 2,102,927 | 944 | 1,893 | 0.06% |
| March 21–31 | 80–90 | 5,215,469 | 7,673,967 | 4,694 | 6,907 | 0.31% |
| April 1–10 | 91–100 | 10,180,371 | 13,184,632 | 9,162 | 11,866 | 0.61% |
| April 11–20 | 101–110 | 75,651,384 | 81,154,078 | 68,086 | 73,039 | 4.53% |
| April 21–30 | 111–120 | 276,689,396 | 286,216,901 | 249,020 | 257,595 | 16.56% |
| May 1–10 | 121–130 | 313,691,413 | 330,718,519 | 282,322 | 297,647 | 18.77% |
| May 11–20 | 131–140 | 434,018,107 | 455,327,104 | 390,616 | 409,794 | 25.97% |
| May 21–31 | 141–151 | 299,822,900 | 323,151,909 | 269,841 | 290,837 | 17.94% |
| June 1–10 | 152–161 | 103,973,443 | 121,650,998 | 93,576 | 109,486 | 6.22% |
| June 11–20 | 162–171 | 29,238,941 | 44,973,056 | 26,315 | 40,476 | 1.75% |
| June 21–30 | 172–181 | 14,434,745 | 26,679,070 | 12,991 | 24,011 | 0.86% |
| July 1–15 | 182–196 | 11,316,631 | 18,087,562 | 10,185 | 16,279 | 0.68% |
| July 16–31 | 197–212 | 3,196,666 | 3,602,783 | 2,877 | 3,243 | 0.19% |
| August 1–15 | 213–227 | 1,210,561 | 1,236,567 | 1,090 | 1,113 | 0.07% |
| August 16–31 | 228–242 | 894,332 | 950,538 | 805 | 855 | 0.05% |
| No pattern, 50.0–74.9% snow frequency | 245 | 333,642 | 607,080 | 300 | 546 | 0.02% |
| No pattern, 75.0–89.9% snow frequency | 246 | 3,731,410 | 3,962,775 | 3,358 | 3,566 | 0.22% |
| No pattern, 90.0–94.9% snow frequency | 247 | 6,045,866 | 6,064,435 | 5,441 | 5,458 | 0.36% |

Table 1.3. Continued.

| Climatological Snow–free Date Class | Raster Values | Pixels, Land | Pixels, Study Area | Area, Land (sq. km) | Area, Study Area (sq. km) | Percentage of Land |
|---|---|---|---|---|---|---|
| No pattern, 95.0–97.9% snow frequency | 248 | 8,021,062 | 8,022,871 | 7,219 | 7,221 | 0.48% |
| No pattern, 98.0–99.9% snow frequency | 249 | 22,443,425 | 22,443,713 | 20,199 | 20,199 | 1.34% |
| No pattern, 100% snow frequency | 250 | 15,846,868 | 15,877,527 | 14,262 | 14,290 | 0.95% |
| Total | | 1,670,990,471 | 1,916,452,130 | 1,503,891 | 1,724,807 | 100.00% |

Table 1.4. Areal summary of percentage of Landsat observations consistently classified by climatological snow-free date from Landsat, 1999–2015, Alaska.

| Proportion of Observations with Consistent Snow Status | Land Pixels | All Pixels | Land Area (sq. km) | All Area (sq. km) | Percent of Total Land | Percent of Total Study Area |
|---|---|---|---|---|---|---|
| 50.0–75.0% | 3,238,167 | 12,912,533 | 2,914 | 11,621 | 0.2% | 0.7% |
| 75.1–80.0% | 14,681,708 | 34,402,091 | 13,214 | 30,962 | 0.9% | 1.8% |
| 80.1–85.0% | 64,382,926 | 97,904,080 | 57,945 | 88,114 | 3.9% | 5.1% |
| 85.1–90.0% | 200,154,310 | 269,501,174 | 180,139 | 242,551 | 12.0% | 14.1% |
| 90.1–95.0% | 808,145,226 | 910,005,573 | 727,331 | 819,005 | 48.4% | 47.5% |
| 95.0–97.5% | 492,563,239 | 502,583,736 | 443,307 | 452,325 | 29.5% | 26.2% |
| 97.5–100.0% | 87,824,895 | 89,142,943 | 79,042 | 80,229 | 5.3% | 4.7% |
| | 1,670,990,471 | 1,916,452,130 | 1,503,891 | 1,724,807 | 100.0% | 100.0% |

Table 1.5. Summary of Snowpack Telemetry (SNOTEL) stations and snow persistence metrics for the study area, Alaska.

| Station Name | Station ID | Years with Data, 2000–2015 | Climatological Snow-free Date from Landsat, 1999–2015[a] | SNOTEL Median First Snow-free Date, 2000–2015[b] | SNOTEL Median Last Snow Day, 2000–2015[c] | SNOTEL Median Split Date, 2000-2015[d] | Start Year | Elevation (m) | Latitude | Longitude |
|---|---|---|---|---|---|---|---|---|---|---|
| Bettles Field | 1182 | 16 | 9 May | 14 May | 13 May | 14 May | 1981 | 640 | 66.9167 | -151.5333 |
| Coldfoot | 958 | 16 | 6 May | 13 May | 12 May | 13 May | 1995 | 1040 | 67.2533 | -150.183 |
| Cooper Lake | 959 | 16 | 21 Apr | 19 May | 18 May | 19 May | 1982 | 1200 | 60.3903 | -149.6936 |
| Fairbanks F.O. | 1174 | 15 | 13 Apr | 28 Apr | 27 Apr | 27 Apr | 1983 | 450 | 64.85 | -147.8 |
| Grandview | 956 | 16 | 8 Jun | 16 Jun | 15 Jun | 15 Jun | 1984 | 1100 | 60.6083 | -149.0631 |
| Granite Creek | 963 | 16 | 20 Apr | 24 Apr | 24 Apr | 24 Apr | 1988 | 1240 | 63.9438 | -145.3999 |
| Grouse Creek Divide | 964 | 16 | 28 May | 15 May | 14 May | 15 May | 1989 | 700 | 60.2597 | -149.3423 |
| Independence Mine | 1091 | 12 | 9 Jun | 28 May | 27 May | 27 May | 1998 | 3550 | 61.7912 | -149.2797 |
| Indian Pass | 946 | 16 | 30 May | 2 Jun | 1 Jun | 1 Jun | 1980 | 2350 | 61.0677 | -149.4795 |
| Kenai Moose Pens | 966 | 16 | 12 Apr | 26 Apr | 26 Apr | 26 Apr | 1984 | 300 | 60.727 | -150.4752 |
| Little Chena Ridge | 947 | 15 | 27 Apr | 1 May | 30 Apr | 30 Apr | 1982 | 2000 | 65.1242 | -146.7339 |
| Long Lake | 1001 | 16 | Water | 7 Jun | 7 Jun | 7 Jun | 1967 | 850 | 58.186 | -133.8322 |
| McNeil Canyon | 1003 | 16 | 27 Apr | 5 May | 10 May | 10 May | 1987 | 1320 | 59.7443 | -151.2513 |
| Monument Creek | 949 | 16 | 27 Apr | 30 Apr | 29 Apr | 29 Apr | 1981 | 1850 | 65.0783 | -145.8707 |
| Moraine | 1035 | 13 | 20 Apr | 7 May | 6 May | 6 May | 2002 | 2100 | 61.3773 | -148.9992 |
| Mt. Alyeska | 1103 | 16 | 7 Jun | 4 Jun | 3 Jun | 4 Jun | 1973 | 1540 | 60.9598 | -149.0862 |
| Mt. Ryan | 948 | 15 | 6 May | 6 May | 5 May | 5 May | 1982 | 2800 | 65.2511 | -146.1513 |
| Munson Ridge | 950 | 16 | 10 May | 22 May | 21 May | 22 May | 1981 | 3100 | 64.8503 | -146.2095 |
| Port Graham | 987 | 14 | 23 Apr | 3 May | 2 May | 2 May | 2001 | 300 | 59.3507 | -151.8477 |
| Summit Creek | 955 | 16 | 29 Apr | 10 May | 13 May | 14 May | 1990 | 1400 | 60.6171 | -149.5313 |
| Susitna Valley High | 967 | 16 | 28 Apr | 5 May | 4 May | 4 May | 1988 | 375 | 62.1333 | -150.0417 |
| Teuchet Creek | 951 | 16 | 19 Apr | 28 Apr | 27 Apr | 28 Apr | 1982 | 1640 | 64.9458 | -145.5167 |
| Turnagain Pass | 954 | 16 | 22 Jun | 16 Jun | 17 Jun | 18 Jun | 1983 | 1880 | 60.7804 | -149.1833 |
| Upper Chena | 952 | 13 | 11 May | 14 May | 15 May | 13 May | 1984 | 2850 | 65.1 | -144.9332 |
| Upper Tsaina River | 1055 | 12 | 18 May | 21 May | 20 May | 21 May | 2004 | 1750 | 61.1911 | -145.6481 |
| Alexander Lake | 1267 | 1 | 3 May | 9 Apr | 19 Apr | 8 Apr | 2014 | 160 | 61.7497 | -150.8897 |
| American Creek | 1189 | 4 | 25 Apr | 8 May | 7 May | 8 May | 2011 | 1050 | 64.7897 | -141.2338 |

Table 1.5. Continued.

| Station Name | Station ID | Years with Data, 2000–2015 | Climatological Snow-free Date from Landsat, 1999–2015[a] | SNOTEL Median First Snow-free Date, 2000–2015[b] | SNOTEL Median Last Snow Day, 2000–2015[c] | SNOTEL Median Split Date, 2000-2015[d] | Start Year | Elevation (m) | Latitude | Longitude |
|---|---|---|---|---|---|---|---|---|---|---|
| Anchor River Divide | 1062 | 11 | 6 May | 16 May | 22 May | 15 May | 1981 | 1653 | 59.8597 | -151.315 |
| Anchorage Hillside | 1070 | 10 | 5 May | 16 May | 15 May | 16 May | 2005 | 2080 | 61.1148 | -149.6668 |
| Atigun Pass | 957 | 7 | 9 Jun | 9 Jun | 9 Jun | 8 Jun | 1982 | 4800 | 68.1298 | -149.4782 |
| Checkers Creek | 2213 | 1 | 17 May | 29 Apr | 28 Apr | 28 Apr | 2014 | 326 | 65.403 | -164.711 |
| Chisana | 1093 | 7 | 2 May | 7 May | 6 May | 6 May | 2008 | 3320 | 62.069 | -142.049 |
| Eagle Summit | 960 | 10 | 13 May | 11 May | 10 May | 11 May | 1998 | 3650 | 65.4859 | -145.4121 |
| Exit Glacier | 1092 | 4 | 25 Apr | 12 May | 11 May | 12 May | 2011 | 400 | 60.1903 | -149.6212 |
| Fielding Lake | 1268 | 1 | 15 May | 16 May | 15 May | 15 May | 2014 | 3000 | 63.2027 | -145.6305 |
| Fort Yukon | 961 | 9 | 25 Apr | 28 Apr | 29 Apr | 27 Apr | 1994 | 430 | 66.5705 | -145.2455 |
| Gobblers Knob | 962 | 7 | 12 May | 25 Apr | 6 May | 25 Apr | 1997 | 2030 | 66.745 | -150.6675 |
| Horsepasture Pass | 1264 | 1 | 22 May | 9 May | 8 May | 8 May | 2014 | 4300 | 62.1345 | -147.625 |
| Hozatka Lake | 2210 | 1 | 7 May | 4 May | 3 May | 3 May | 2014 | 206 | 65.198 | -156.635 |
| Imnaviat Creek | 968 | 4 | 24 May | 5 Jun | 4 Jun | 4 Jun | 1981 | 3050 | 68.6168 | -149.3002 |
| Johnson's Camp | 1036 | 7 | 17 May | 13 May | 12 May | 12 May | 2002 | 25 | 64.5646 | -164.2926 |
| Kachemak Creek | 1063 | 8 | 25 May | 26 May | 25 May | 26 May | 2004 | 1660 | 59.7289 | -150.6611 |
| Kanaryagak Camp | 2208 | 2 | 10 May | 24 Apr | 23 Apr | 23 Apr | 2013 | 13 | 61.3588 | -165.1204 |
| Kantishna | 1072 | 8 | 28 Apr | 4 May | 3 May | 4 May | 2006 | 1550 | 63.5417 | -150.994 |
| Kelly Station | 1175 | 4 | 12 May | 10 May | 9 May | 9 May | 1992 | 310 | 67.9333 | -162.2833 |
| Lower Mulchatna | 1233 | 2 | 6 Apr | 20 Feb | 18 Apr | 18 Apr | 2012 | 320 | 59.82 | -156.9906 |
| May Creek | 1096 | 8 | 23 Apr | 30 Apr | 30 Apr | 30 Apr | 2007 | 1610 | 61.3478 | -142.7097 |
| McNeil River Camp | 1191 | 3 | 22 May | 4 May | 13 May | 3 May | 2011 | 25 | 59.0833 | -154.2754 |
| Middle Fork Bradley | 1064 | 8 | 8 Jun | 2 Jun | 1 Jun | 2 Jun | 1991 | 2300 | 59.7768 | -150.7573 |
| Monahan Flat | 1094 | 7 | 11 May | 22 May | 21 May | 21 May | 1984 | 2710 | 63.3053 | -147.6463 |
| Moore Creek Bridge | 1176 | 6 | Water | 30 May | 29 May | 30 May | 1990 | 2250 | 59.5878 | -135.2105 |
| Mt. Eyak | 1073 | 10 | 28 Apr | 31 May | 30 May | 31 May | 2005 | 1405 | 60.55 | -145.745 |
| Nuka Glacier | 1037 | 8 | 8 Jun | 28 May | 6 Jun | 27 May | 1991 | 1250 | 59.6987 | -150.7097 |
| Pargon Creek | 986 | 6 | 16 May | 13 May | 12 May | 12 May | 2001 | 100 | 64.9935 | -163.1032 |

Table 1.5. Continued.

| Station Name | Station ID | Years with Data, 2000–2015 | Climatological Snow-free Date from Landsat, 1999–2015[a] | SNOTEL Median First Snow-free Date, 2000–2015[b] | SNOTEL Median Last Snow Day, 2000–2015[c] | SNOTEL Median Split Date, 2000-2015[d] | Start Year | Elevation (m) | Latitude | Longitude |
|---|---|---|---|---|---|---|---|---|---|---|
| Prudhoe Bay | 1177 | 3 | 4 Jun | 31 May | 30 May | 30 May | 2004 | 30 | 70.2667 | -148.5667 |
| Rhoads Creek | 1178 | 4 | 16 Apr | 17 Apr | 16 Apr | 16 Apr | 1988 | 1225 | 63.931 | -145.3333 |
| Rocky Point | 973 | 8 | 4 May | 17 May | 16 May | 17 May | 2001 | 250 | 64.5348 | -163.4214 |
| Sagwon | 1183 | 4 | 18 May | 20 May | 19 May | 19 May | 1983 | 1000 | 69.4242 | -148.6925 |
| Sugarloaf Mountain | 1095 | 8 | 25 May | 21 May | 20 May | 20 May | 2007 | 550 | 61.081 | -146.2995 |
| Telaquana Lake | 1266 | 1 | 21 Apr | 22 Mar | 18 Apr | 21 Mar | 2014 | 1275 | 60.9824 | -153.9177 |
| Tok | 2080 | 1 | 20 Apr | 27 Apr | 26 Apr | 26 Apr | 2003 | 1630 | 63.3532 | -142.9816 |
| Tokositna Valley | 1089 | 9 | 14 May | 18 May | 17 May | 17 May | 2007 | 850 | 62.63 | -150.7762 |
| Upper Nome Creek | 1090 | 9 | 6 May | 4 May | 11 May | 3 May | 2007 | 2520 | 65.3671 | -146.592 |
| Weary Lake | 1234 | 3 | 10 May | 21 Feb | 1 Jul | 11 May | 2012 | 100 | 59.1342 | -159.0928 |

a. The Landsat analysis described in this report.

b. In each year with SNOTEL data, the first date in the 1 February–31 August range with no snow was identified. The median value from all years with data in the 2000–2015 range is reported here.

c. In each year with SNOTEL data, the last date in the 1 February–31 August range with snow was identified. The median value from all years with data in the 2000–2015 range is reported here.

d. In each year with SNOTEL data, a binary classification tree was applied to identify the date that best separated the snow-covered and snow-free season for the 1 February–31 August range. The median value from all years with data in the 2000–2015 range is reported here.

Table 2.1. Environmental and spectral predictors at 30 m resolution for lichen cover mapping. Predictors in italics were not used in the final modeling.

| |
|---|
| **Environmental Predictors**<br>• Elevation (m)<br>• Slope (degrees)<br>• 2015 Tree Cover |
| **Spectral Predictors**<br>• Spring Landsat Reflectance (Blue, Green Red, Near-infrared, Short-wave infrared 1, Short-wave infrared 2)<br>• Spring Landsat Indices (NDVI, NDMI, NDWI, NDSI, NBR, EVI2, NDBI)<br>• Midsummer Landsat Reflectance (Blue, Green Red, Near-infrared, Short-wave infrared 1, Short-wave infrared 2)<br>• Midsummer Landsat Indices (NDVI, NDMI, NDWI, NDSI, NBR, EVI2, NDBI)<br>• *Fall Landsat Reflectance (Blue, Green Red, Near-infrared, Short-wave infrared 1, Short-wave infrared 2)*<br>• *Fall Landsat Indices (NDVI, NDMI, NDWI, NDSI, NBR, EVI2, NDBI)*<br>• Difference between Midsummer and Spring Reflectances<br>• Difference between Midsummer and Spring Indices |

Table 2.2. Frequency distribution of sample point counts at vegetation point intercept plots, Yukon–Charley Rivers National Preserve, Alaska.

| Number of Vegetation Point Intercept (VPI) points per plot | Point Spacing (cm) | Count of Plots |
|---|---|---|
| 40 | 40 | 2 |
| 58 | 50 | 3 |
| 59 | 50 | 336 |
| 69 | 40 | 2 |
| 71 | 40 | 3 |
| 72 | 40 | 99 |
| 92 | 30 | 83 |

Table 2.3. Summary of all lichen hits at vegetation point intercept plots, Yukon–Charley Rivers National Preserve, Alaska.

| Description | Count | Cover (%) |
|---|---|---|
| Total number of sample points | 35,193 | 100.0 |
| Count of lichen hits | 6,853 | |
| Points with lichen hits | 6,782 | 19.3 |
| Count of foliose/fruticose lichen hits (not over rock) | 5,222 | |
| Points with foliose/fruticose lichen hits (not over rock) | 5,172 | 14.7 |

Table 2.4. Summary of lichen position in canopy at vegetation point intercept plots, Yukon–Charley Rivers National Preserve, Alaska.

| Description | Count | Cover (%) |
|---|---|---|
| Total number of sample points | 35,193 | 100.0 |
| Points with foliose/fruticose lichen hits (not over rock) | 5,172 | 14.7 |
| Lichen alone, with no other hits | 537 | 1.5 |
| Lichen overtopped, hits in higher strata | 1,713 | 4.9 |
| Lichen with hits in same strata | 2,922 | 8.3 |
| Lichen with vascular plant, standing dead, or litter (overtopped) | 2,282 | 6.5 |
| Lichen with only moss or soil (not overtopped) | 640 | 1.8 |
| Top hit is not lichen, but lichen present at point | 3,995 | 11.4 |
| Top hit is lichen | 1,177 | 3.3 |

Table 2.5. Summary of terricolous macrolichen cover by genus at quadrat plots, Yukon–Charley Rivers National Preserve, Alaska.

| Lichen Genus | Mean Cover (%) | Maximum Cover (%) | Proportion of Total Quadrat Lichen Cover | Lichen Colors | Coarse Color Group |
|---|---|---|---|---|---|
| Cladina | 1.68 | 21.75 | 22.3 | gray, white, yellow | light |
| Peltigera | 1.58 | 24.81 | 21.0 | brown, gray, greengray | dark |
| Cladonia | 1.27 | 19.38 | 16.9 | gray, greengray, white, yellow | light |
| Flavocetraria | 0.53 | 9.75 | 7.0 | yellow | light |
| Umbilicaria | 0.39 | 24.25 | 5.1 | brown, gray | dark |
| Cetraria | 0.34 | 10.25 | 4.5 | brown, yellow | multiple |
| Melanelia | 0.30 | 9.13 | 4.0 | brown | dark |
| Stereocaulon | 0.27 | 43.75 | 3.6 | white | light |
| Sphaerophorus | 0.16 | 22.00 | 2.2 | white | light |
| Arctoparmelia | 0.12 | 7.75 | 1.6 | yellow | light |
| Allantoparmelia | 0.12 | 24.50 | 1.6 | black | dark |
| Masonhalea | 0.10 | 5.00 | 1.4 | brown | dark |
| Pseudephebe | 0.09 | 5.75 | 1.2 | brown | dark |
| Parmelia | 0.09 | 2.81 | 1.2 | white | light |
| Vulpicida | 0.08 | 3.75 | 1.0 | yellow | light |
| Dactylina | 0.06 | 4.75 | 0.9 | white, yellow | light |
| Asahinea | 0.06 | 3.50 | 0.8 | gray, yellow | light |
| Xanthoparmelia | 0.05 | 8.50 | 0.7 | yellow | light |
| Nephroma | 0.04 | 3.50 | 0.5 | brown, yellow | multiple |
| Parmeliopsis | 0.04 | 6.50 | 0.5 | white, yellow | light |
| Hypogymnia | 0.03 | 1.50 | 0.4 | brown, white | multiple |
| Bryocaulon | 0.03 | 4.00 | 0.4 | brown | dark |
| Thamnolia | 0.03 | 4.00 | 0.3 | white | light |
| Alectoria | 0.02 | 1.25 | 0.3 | brown, yellow | multiple |
| Icmadophila | 0.01 | 1.75 | 0.1 | green | dark |
| Collema | 0.01 | 1.63 | 0.1 | black | dark |
| Tuckermannopsis | 0.01 | 0.44 | 0.1 | brown | dark |
| Leptogium | 0.00 | 0.56 | 0.1 | black | dark |
| Imshaugia | 0.00 | 0.50 | 0.0 | white | light |
| Psorula | 0.00 | 0.25 | 0.0 | all | multiple |
| Physcia | 0.00 | 0.19 | 0.0 | gray | light |
| Spilonema | 0.00 | 0.19 | 0.0 | black | dark |
| Brodoa | 0.00 | 0.31 | 0.0 | gray | light |
| Phaeophyscia | 0.00 | 0.13 | 0.0 | gray | light |
| Catapyrenium | 0.00 | 0.25 | 0.0 | brown | dark |
| Physconia | 0.00 | 0.19 | 0.0 | gray | light |
| Xanthoria | 0.00 | 0.19 | 0.0 | orange | light |
| Lobaria | 0.00 | 0.06 | 0.0 | brown, gray, green | dark |
| Omphalina | 0.00 | 0.06 | 0.0 | green | dark |
| Psoroma | 0.00 | 0.06 | 0.0 | brown | dark |
| Solorina | 0.00 | 0.06 | 0.0 | greengray | dark |
| Bryoria | 0.00 | 0.06 | 0.0 | brown | dark |
| Fuscopannaria | 0.00 | 0.06 | 0.0 | brown | dark |
| Grand Total | 7.52 | | | | |

Table 2.6. Summary of terricolous macrolichen color groups and dominant genera at quadrat plots, Yukon–Charley Rivers National Preserve, Alaska.

| Lichen Genus | Mean Cover (%) | Lichen Colors | Coarse Color Group |
|---|---|---|---|
| Peltigera | 1.58 | brown, gray, greengray | dark |
| Umbilicaria | 0.39 | brown, gray | dark |
| Melanelia | 0.30 | brown | dark |
| Allantoparmelia | 0.12 | black | dark |
| Masonhalea | 0.10 | brown | dark |
| Other Dark Color Lichen Genera | 0.16 | | dark |
| | | | |
| Cladina | 1.68 | gray, white, yellow | light |
| Cladonia | 1.27 | gray, greengray, white, yellow | light |
| Flavocetraria | 0.53 | yellow | light |
| Stereocaulon | 0.27 | white | light |
| Sphaerophorus | 0.16 | white | light |
| Arctoparmelia | 0.12 | yellow | light |
| Other Light Color Lichen Genera | 0.42 | | light |
| | | | |
| Cetraria | 0.34 | brown, yellow | multiple |
| Other Multiple Color Genera | 0.10 | | multiple |
| | | | |
| Total Dark Color Lichen Genera | 2.64 | | |
| Total Light Color Lichen Genera | 4.45 | | |
| Total Multiple Color Lichen Genera | 0.43 | | |
| | | | |
| Grand Total | 7.52 | | |

Table 2.7 Model performance summary for 30 m resolution terricolous macrolichen cover models based on vegetation plot training data, Yukon–Charley Rivers National Preserve, Alaska.

| Response | VPI Data | Quadrat Data | n | Cross-validated R-squared | Root Mean Square Error | Mean Absolute Error |
|---|---|---|---|---|---|---|
| Total lichen cover, VPI | Cover | n/a | 528 | 0.297 | 14.2 | 10.2 |
| Top lichen cover, VPI | Top cover | n/a | 528 | 0.091 | 5.8 | 3.4 |
| Light lichen cover, VPI scaled | Cover | Scale VPI cover | 313 | 0.151 | 11.0 | 7.4 |
| Light and mixed lichen cover, VPI scaled | Cover | Scale VPI cover | 313 | 0.198 | 11.7 | 7.9 |
| Total lichen cover, Quadrat | n/a | Cover | 313 | 0.125 | 9.0 | 9.2 |
| Light lichen cover, Quadrat | n/a | Cover | 313 | 0.013 | 7.0 | 4.6 |
| Light and mixed lichen cover, Quadrat | n/a | Cover | 313 | 0.031 | 7.3 | 4.8 |
| Total lichen cover from aggregated 2 m models | Cover for 2 m models | n/a | 6730 | 0.644 | 5.2 | 3.6 |

Table 2.8. Classification accuracy of 30 m resolution terricolous macrolichen presence/absence maps for varying thresholds of lichen cover, based on plot averaged total lichen cover metric from vegetation point intercept (VPI) transects, Yukon–Charley Rivers National Preserve, Alaska.

| Lichen Presence/ Absence Threshold (%) | Count of Non-lichen Plots | Count of Lichen Plots | OOB False Lichen Detection Rate (%) | OOB False Non-lichen Detection Rate (%) | Mean OOB False Detection Rate (%) | Overall OOB Error Rate (%) |
|---|---|---|---|---|---|---|
| 0 | 144 | 384 | 52.8 | 8.6 | 30.7 | 20.6 |
| 1 | 156 | 372 | 52.6 | 11.3 | 31.9 | 23.5 |
| 2 | 200 | 328 | 34.0 | 17.1 | 25.5 | 23.5 |
| 3 | 234 | 294 | 26.9 | 19.4 | 23.2 | 22.7 |
| 4 | 237 | 291 | 26.6 | 21.0 | 23.8 | 23.5 |
| 5 | 260 | 268 | 25.4 | 24.3 | 24.8 | 24.8 |
| 6 | 264 | 264 | 26.1 | 27.3 | 26.7 | 26.7 |
| 7 | 281 | 247 | 24.9 | 28.3 | 26.6 | 26.5 |
| 8 | 302 | 226 | 19.9 | 29.6 | 24.8 | 24.1 |
| 9 | 306 | 222 | 17.6 | 31.5 | 24.6 | 23.5 |
| 10 | 319 | 209 | 17.9 | 33.0 | 25.4 | 23.9 |
| 15 | 356 | 172 | 11.2 | 44.8 | 28.0 | 22.2 |
| 20 | 396 | 132 | 4.5 | 57.6 | 31.1 | 17.8 |
| 30 | 450 | 78 | 2.2 | 82.1 | 42.1 | 14.0 |
| 40 | 479 | 49 | 1.0 | 98.0 | 49.5 | 10.0 |
| 50 | 497 | 31 | 0.2 | 100.0 | 50.1 | 6.1 |

Table 2.9. Model performance summary for 2 m resolution terricolous macrolichen cover models using Digital Globe imagery, Yukon–Charley Rivers National Preserve, Alaska.

| Response | Sensor | Date | n | Cross-validated R-squared | Root Mean Square Error | Mean Absolute Error |
|---|---|---|---|---|---|---|
| Ben Creek and Chester Creek | WV2 | 6/22/2013 | 116 | 0.245 | 9.7 | 7.4 |
| Hanna Creek | WV2 | 7/13/2016 | 56 | 0.145 | 18.3 | 13.7 |
| Flat Creek | WV3 | 5/12/2016 | 80 | 0.217 | 24.5 | 21.0 |
| Funnel Creek | WV3 | 6/24/2016 | 92 | 0.168 | 20.8 | 16.1 |
| Lower Crescent Creek | WV2 | 8/26/2013 | 100 | -0.034 | 21.9 | 17.3 |

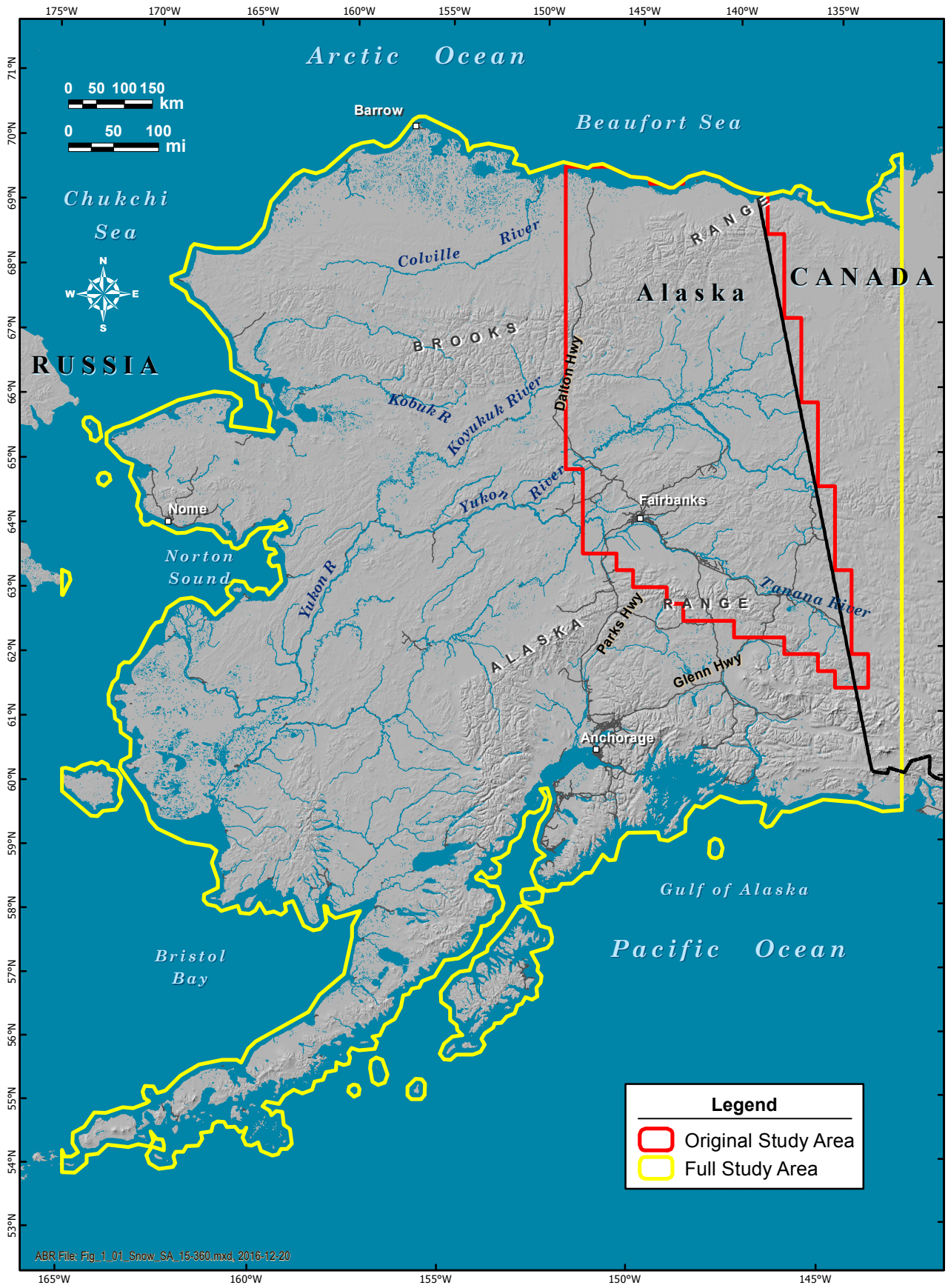



Figure 1.1 Landsat snow persistence mapping study area, Alaska.

Landsat 5 TM, 2010-06-08 (P71R11)

Landsat 8 OLI, 2015-05-07 (p69r12)

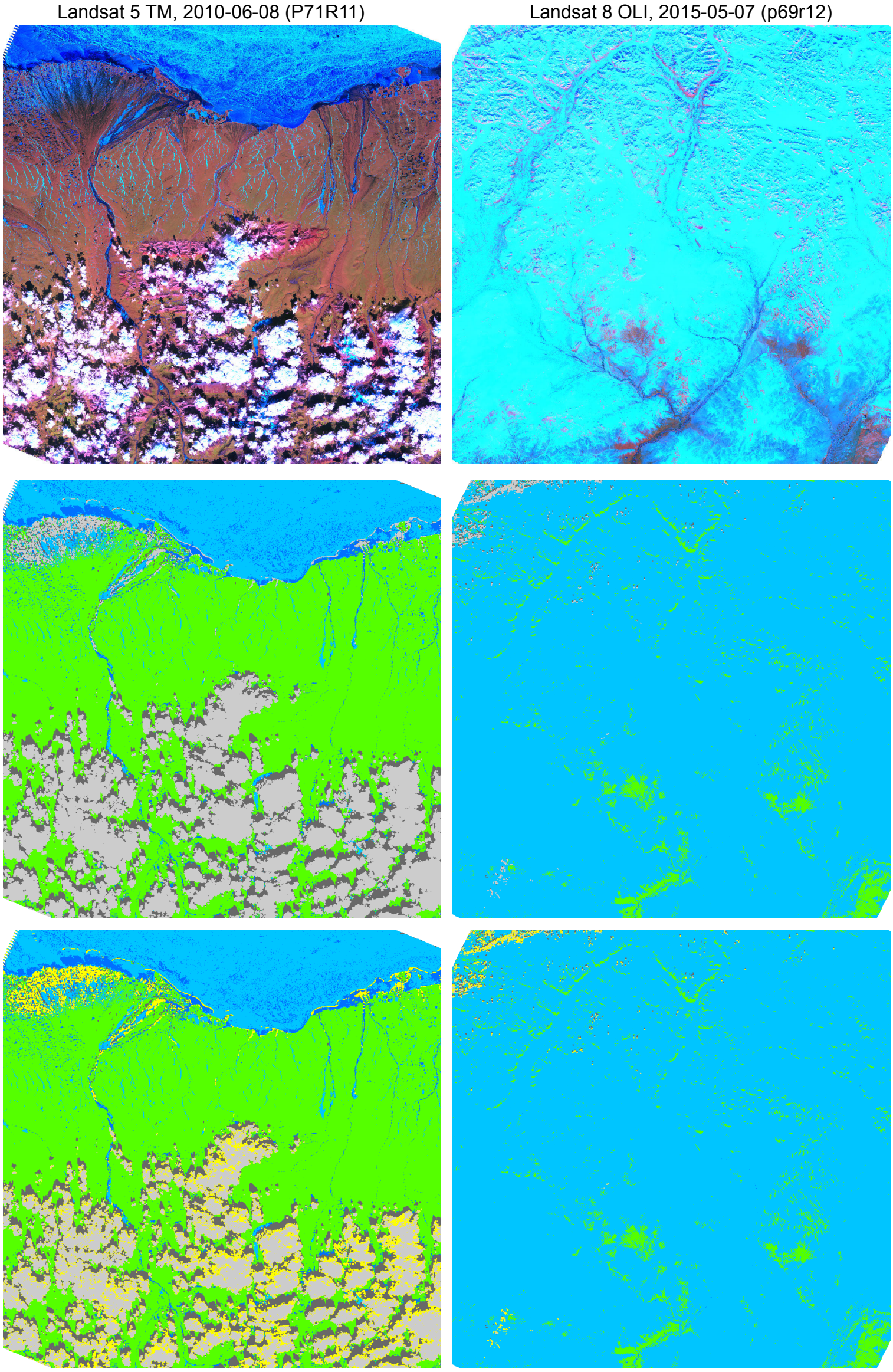


**Figure 1.2 Examples of results of SnowMap in Complex Terrain algorithm for single Landsat scenes, Alaska.**

N
W E
S

Approximate Scale = 1,500,000

0 15 30 45 Miles

0 25 50 Kilometers

**CFMask**

- 0 = Snow-free Land
- 1 = Water
- 2 = Cloud Shadow
- 3 = Snow
- 4 = Cloud

**Revised CFMask**

- 0 = Snow-free Land
- 1 = Water
- 2 = Cloud Shadow
- 3 = Snow
- 4 = Cloud
- 6 = Released Cloud

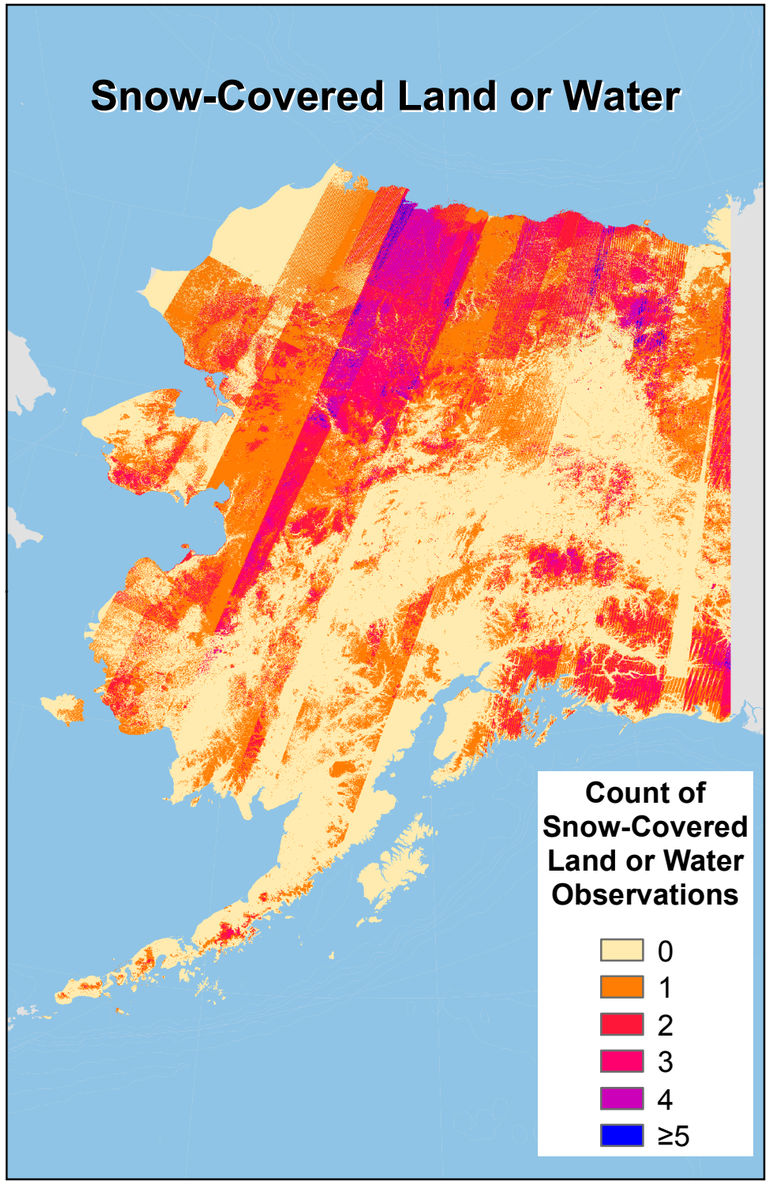
**SnowMap in Complex Terrain**

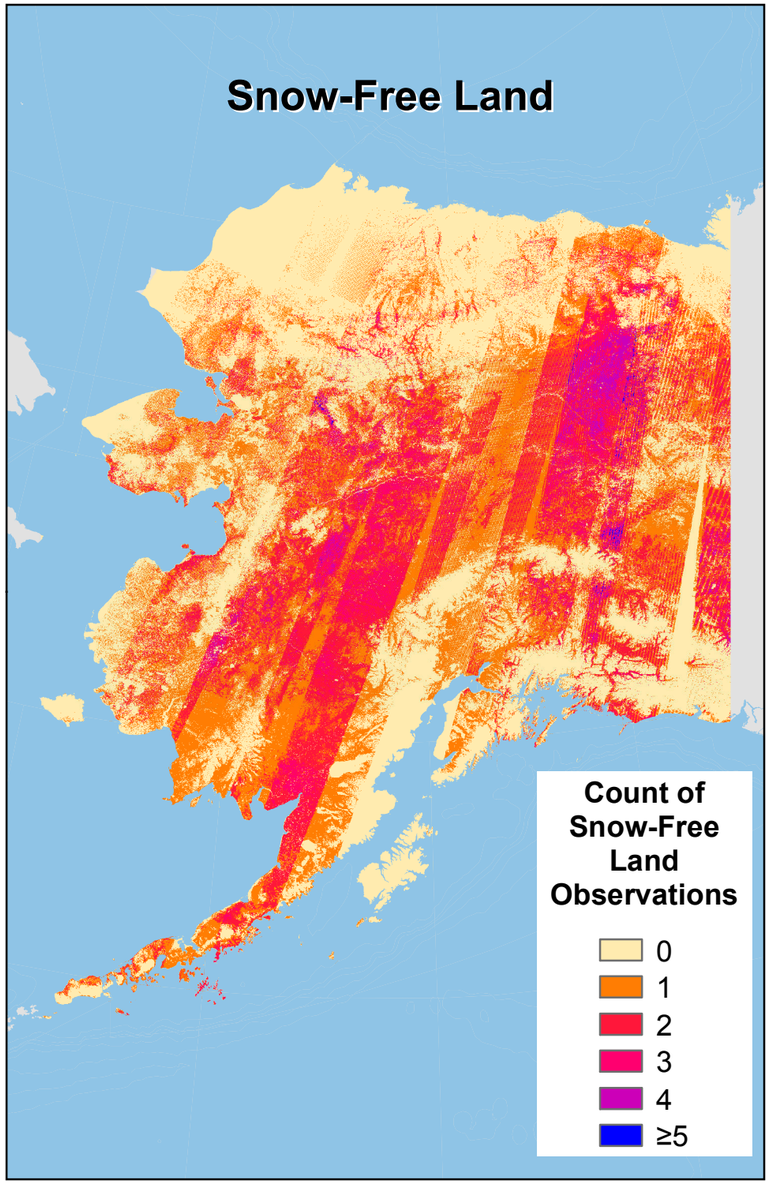
**Snow**
- Snow
- Shadowed Snow
- Snow Under Canopy

**Snow-free**
- Snow-free Land
- Snow-free Land, Shadowed
- Open Water

**Unknown**
- Cloud
- Very Dark
- Unknown (Shadowed Snow under Canopy)
- Image edge or gap

ABR file: Fig_1_02_SMICT_Examples_8panel_15-360.mxd; 19 Dec 2016







Water outside study area
Land outside study area

N
W E
S

0 100 200 300 400 Miles
0 200 400 600 Kilometers

**Figure 1.3. Count of total snow-covered and snow-free observations on May 15, for the period 1999–2015, Alaska. Analysis was based on all available Landsat scenes analyzed using the SnowMap in Complex Terrain algorithm.**

ABR file: Fig_1_03_SMICT_Summary_Counts_May15_15-360.mxd; 19 Dec 2016

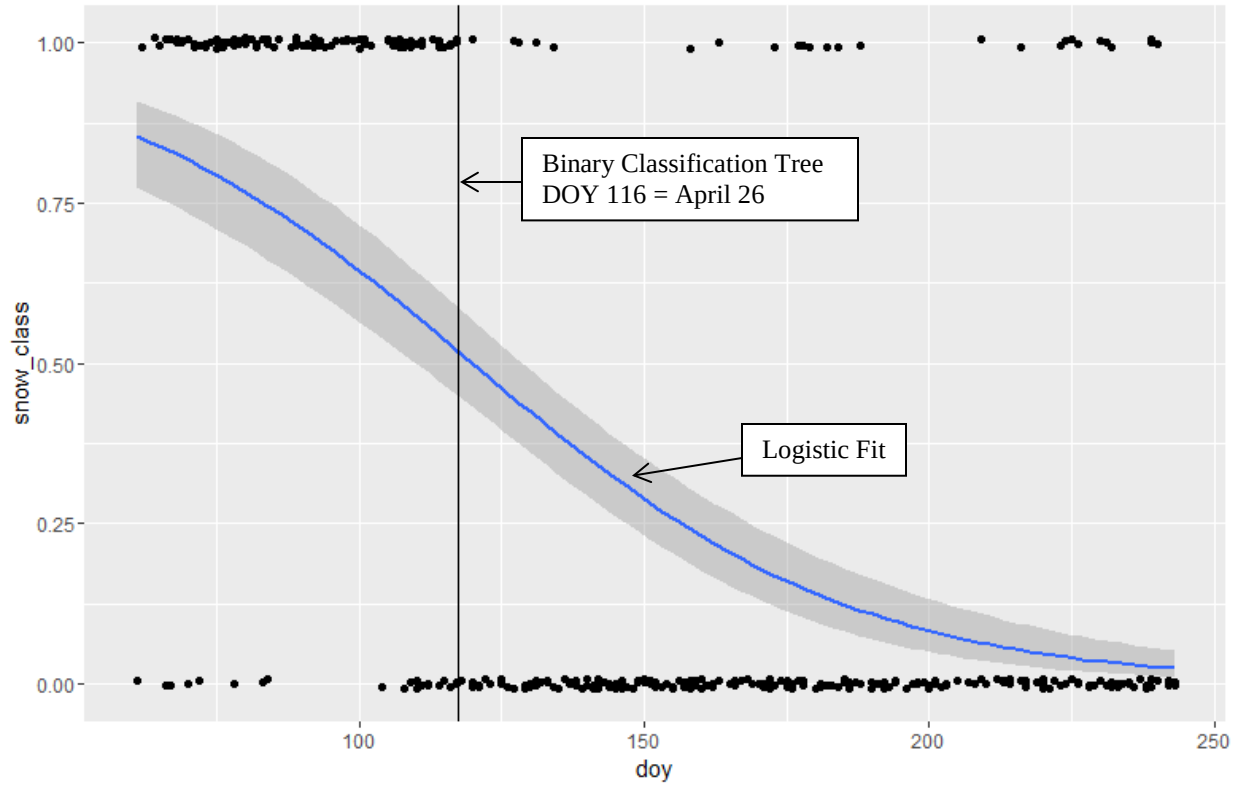



Figure 1.4. Time series of snow presence and absence for a single pixel near Fairbanks, Alaska for the period 1999–2015. Logistic regression and binary classification tree results are also plotted.

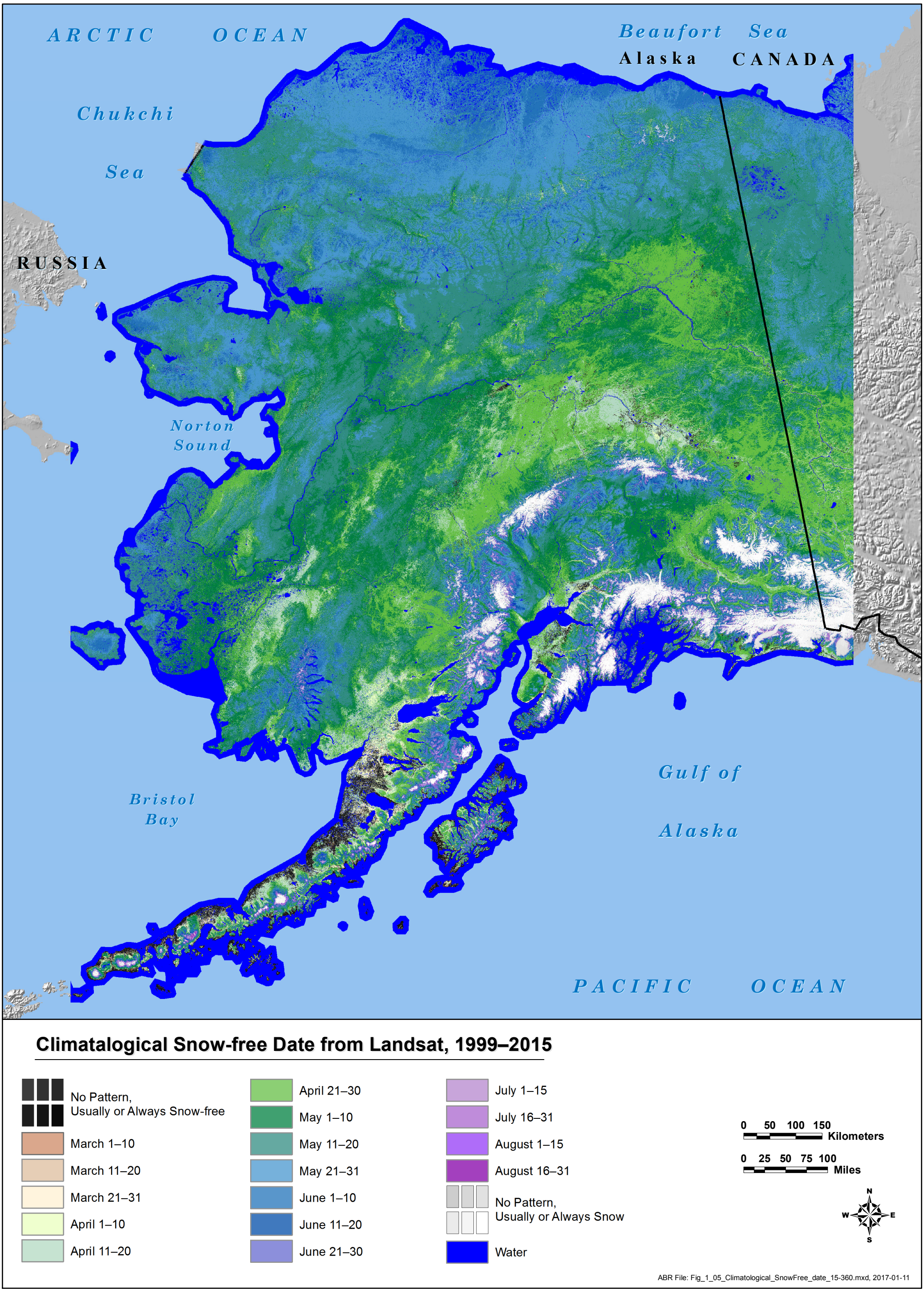



**Figure 1.5. Map of climatalogical snow-free date from Landsat at 30 m resolution for Alaska, for the 1999–2015 period.**

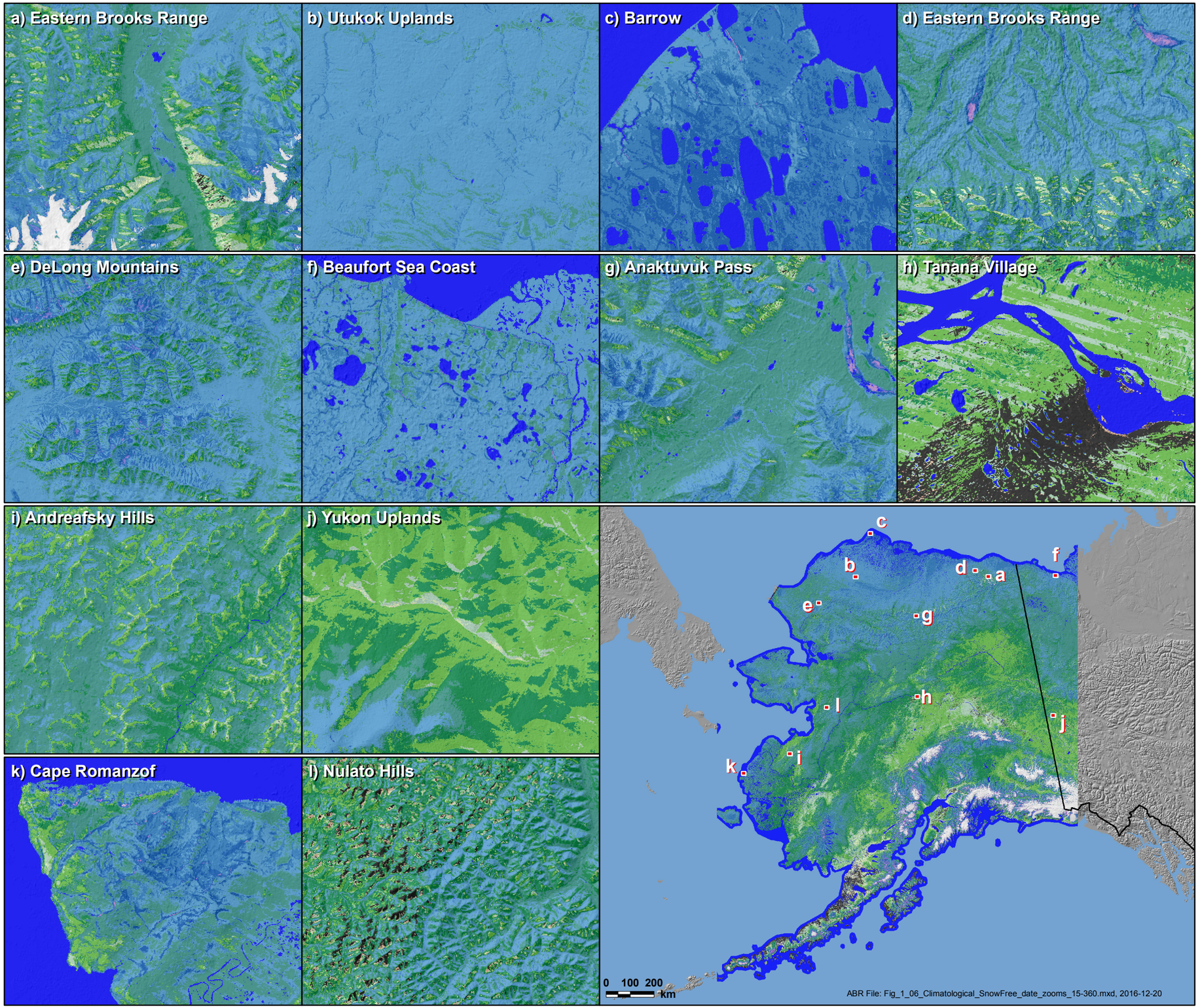



**Figure 1.6. Full resolution examples of climatalogical snow-free date from Landsat at 30 m resolution for Alaska, for the 1999–2015 period.**

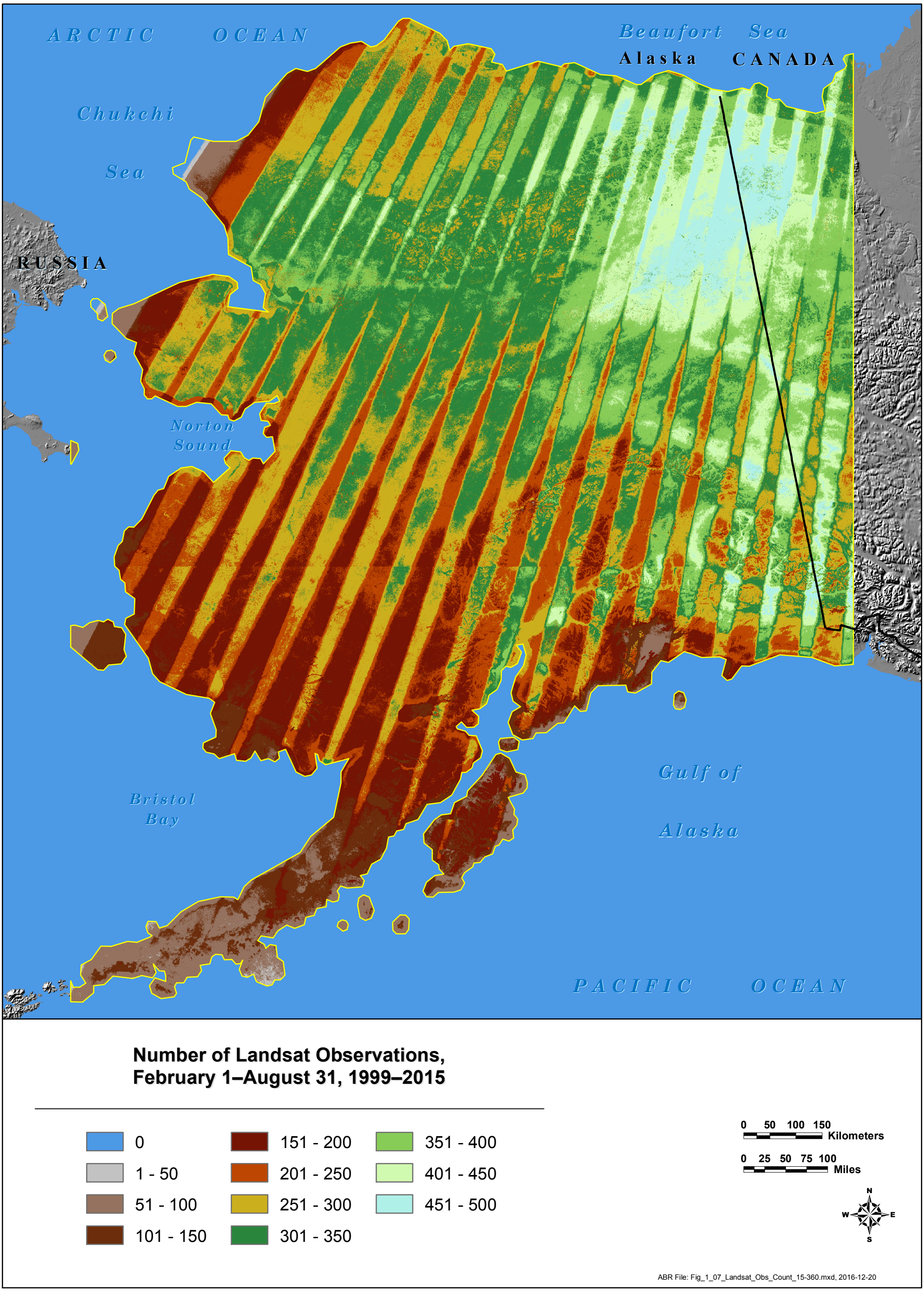



**Figure 1.7. Count of Landsat observations used to determine climatalogical snow-free date in Alaska, for the 1999–2015 period.**

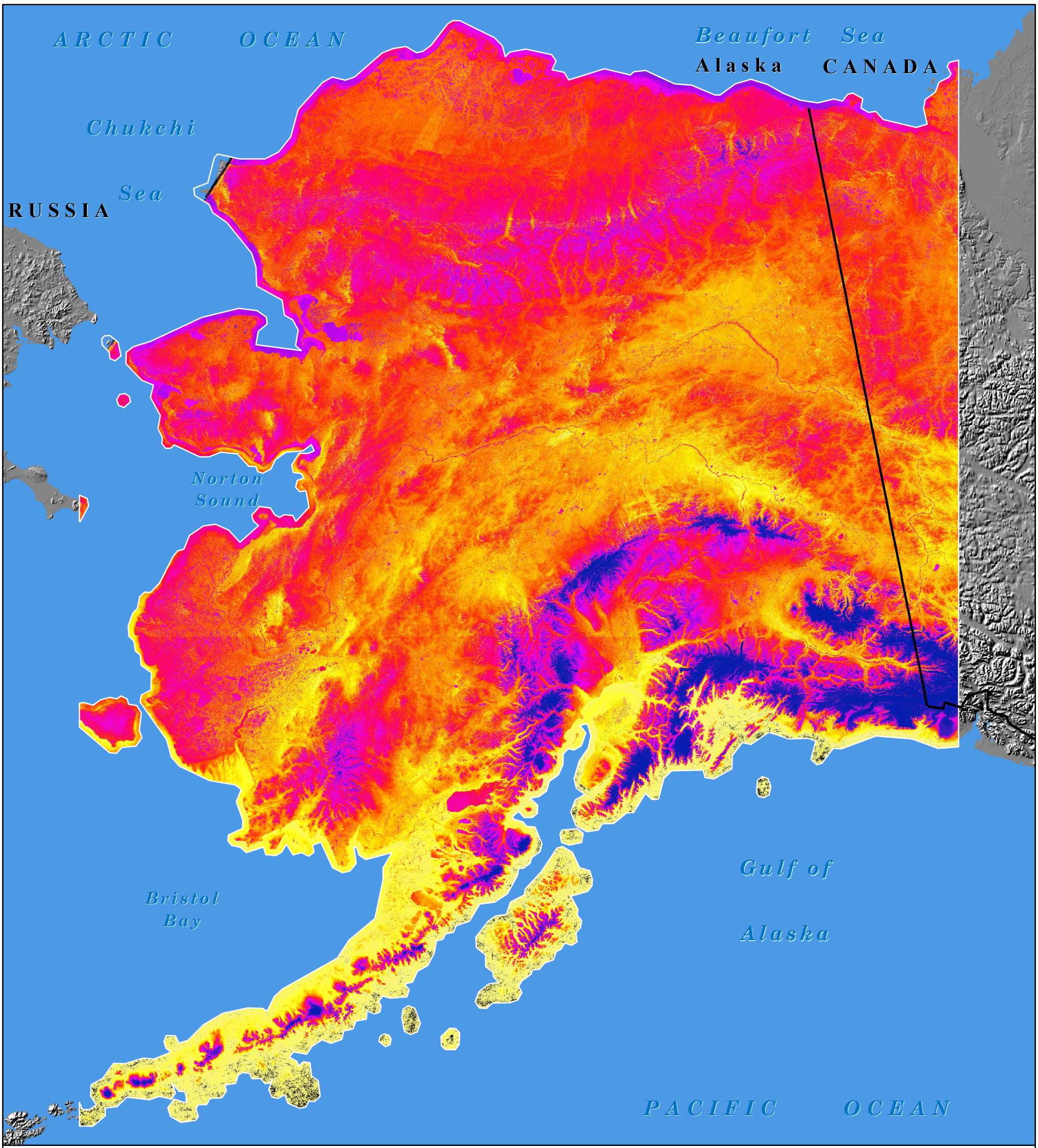



**Figure 1.8. Proportion of observations classified as snow for February 1–August 31, 1999–2015, Alaska.**

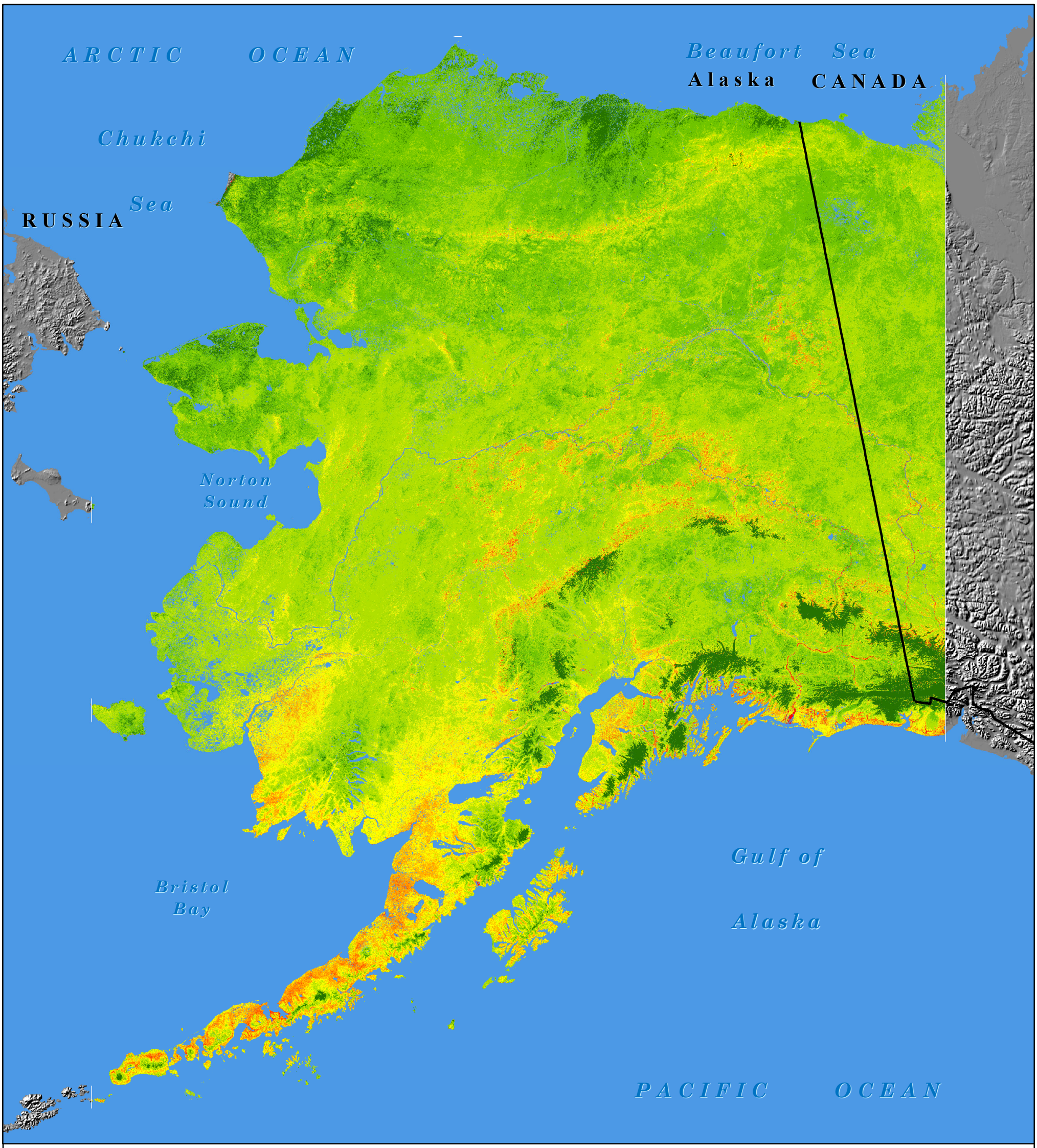



**Figure 1.9. Proportion of land observations correctly classified to snow-covered or snow-free status based on climatological snow-free date from Landsat, for the period February 1–August 31, 1999–2015, Alaska.**

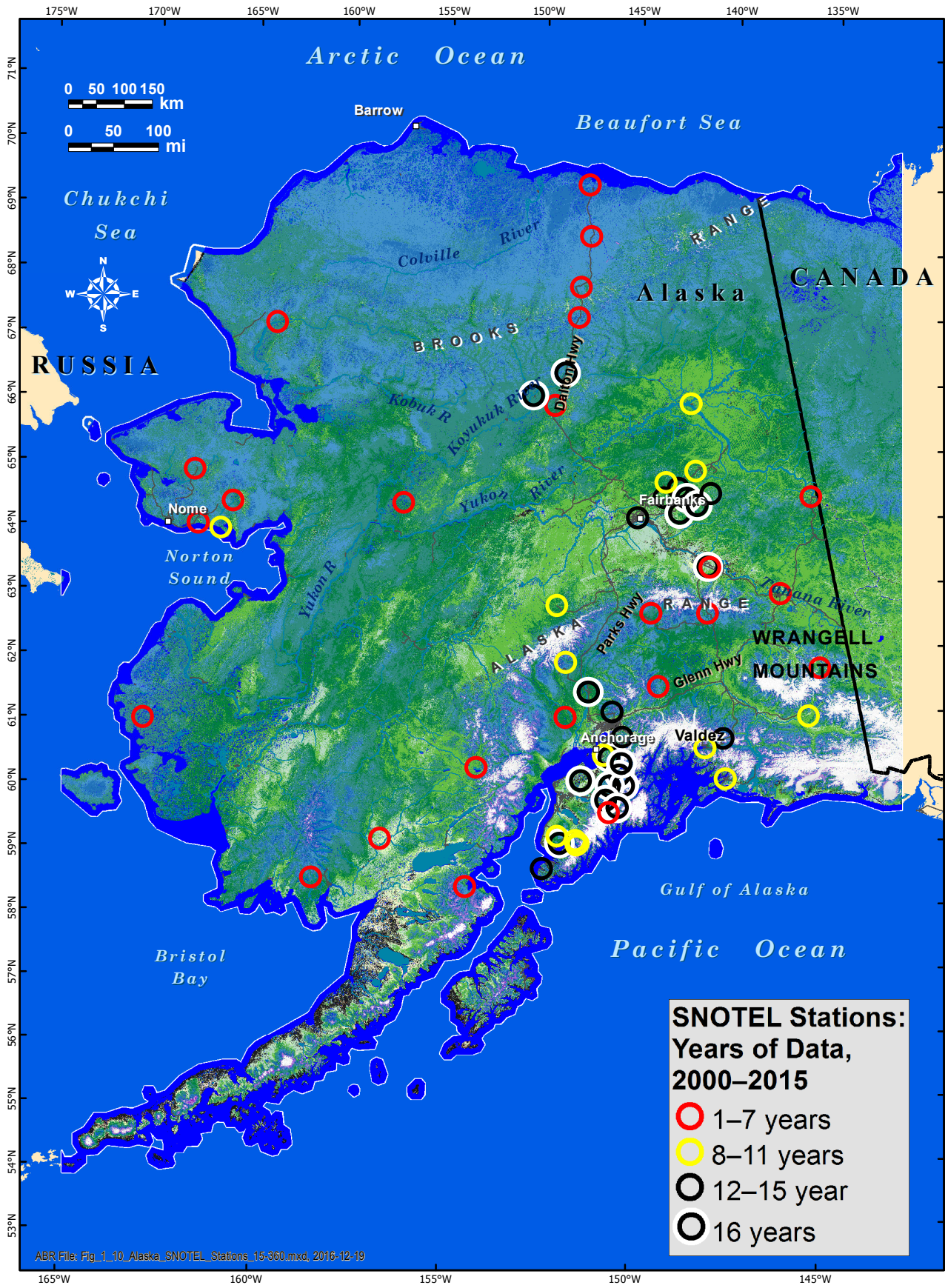



Figure 1.10 Map of Snowpack Telemetry (SNOTEL) sites and count of years with snow persistence data, 2000–2015, Alaska.

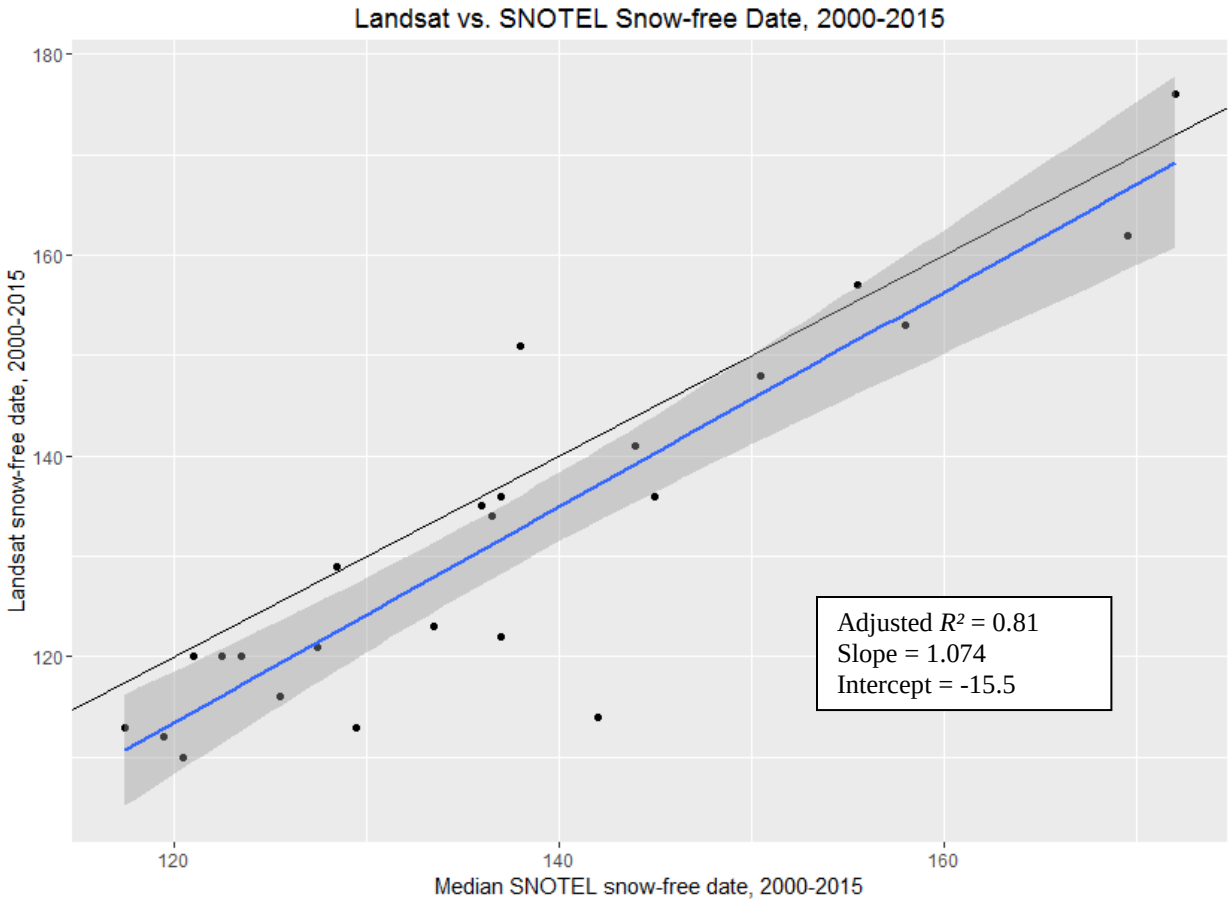



Figure 1.11. Climatogical snow-free date from Landsat vs. median first snow-free date from SNOTEL, 2000–2015, Alaska. The blue line is a linear fit, with the 95% confidence interval in dark gray. The black line is the 1:1 line.

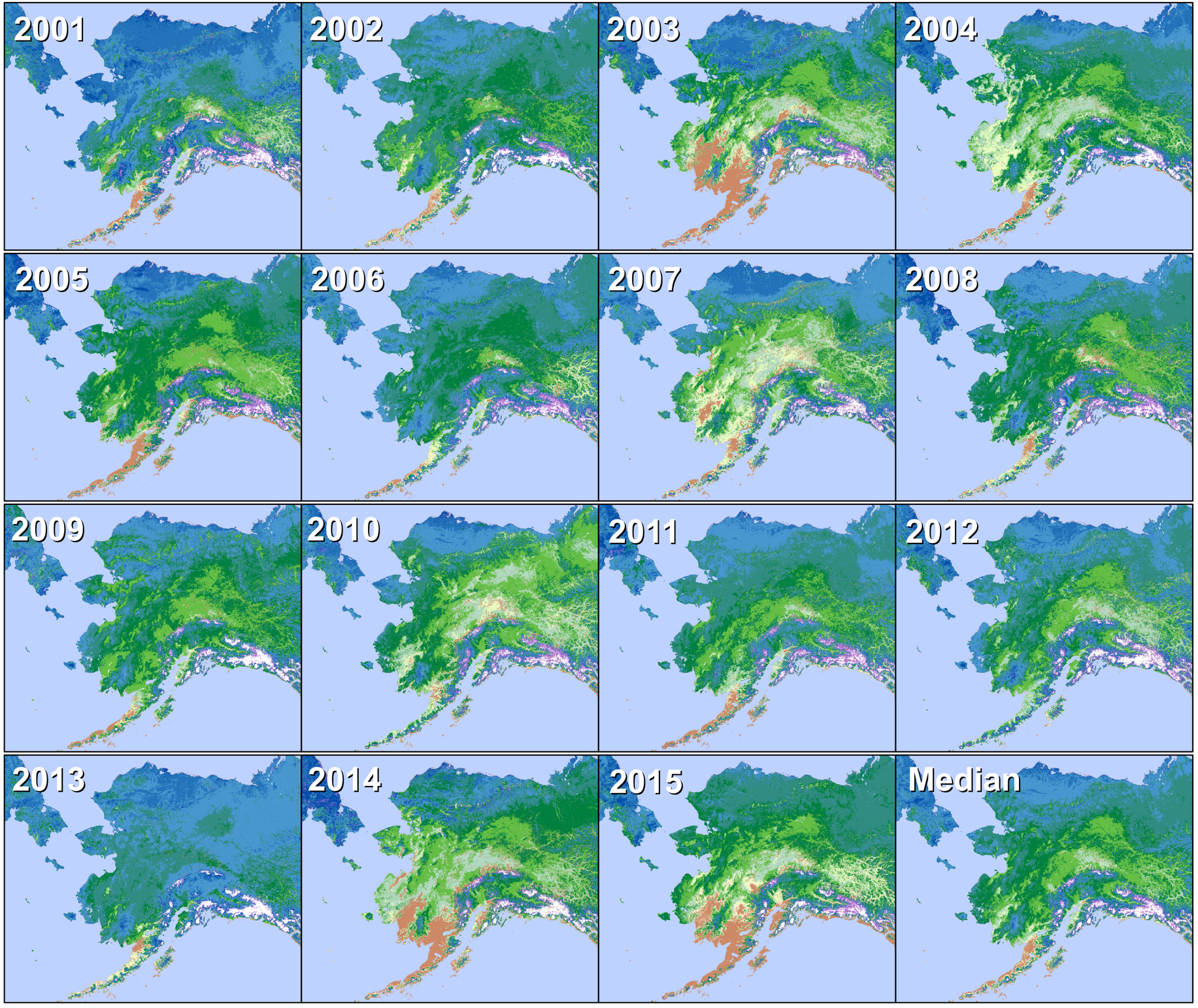



**Figure 1.12. Longest continuous snow segment (CSS) end day, MODIS snow metric, 2001–2015, Alaska.**

ABR File: Fig_1_12_MODIS_Snow_Metrics_LastDayLongCSS_15-360.mxd, 2017-01-11

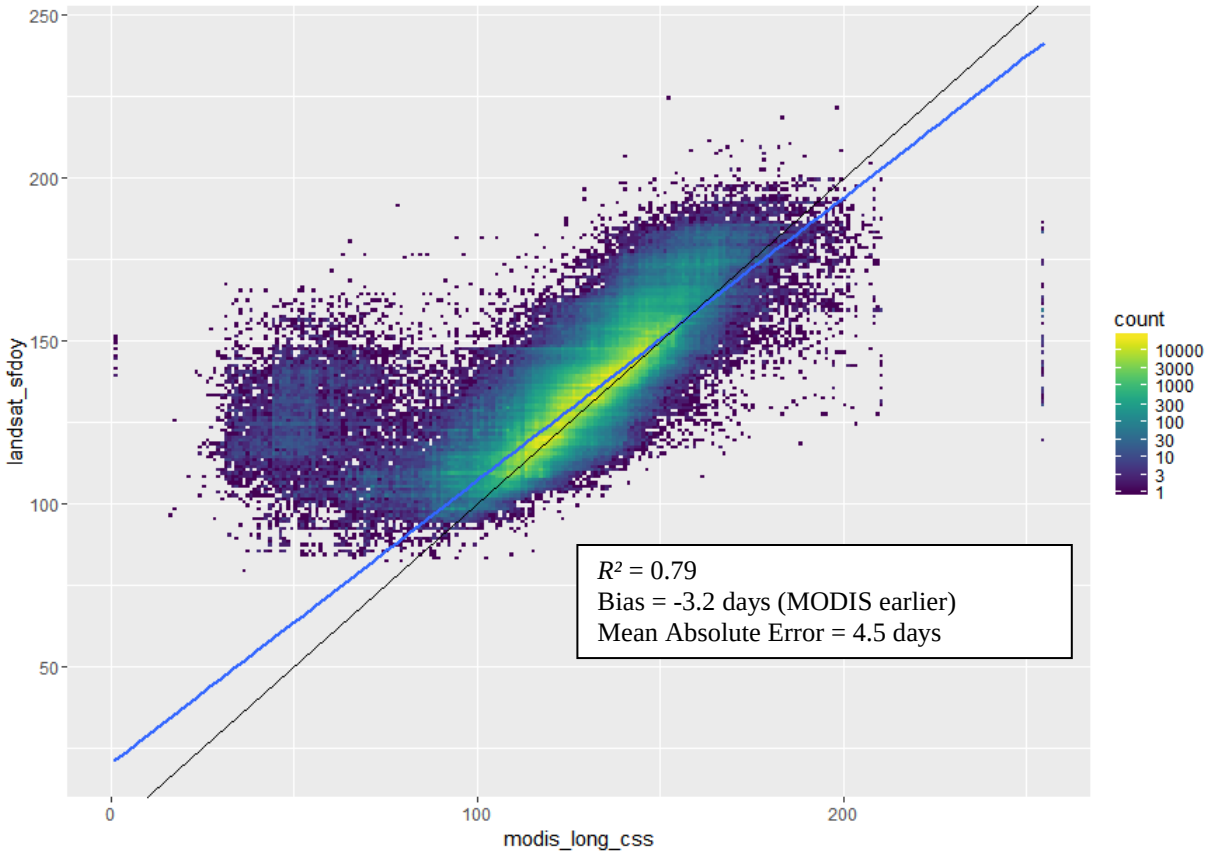
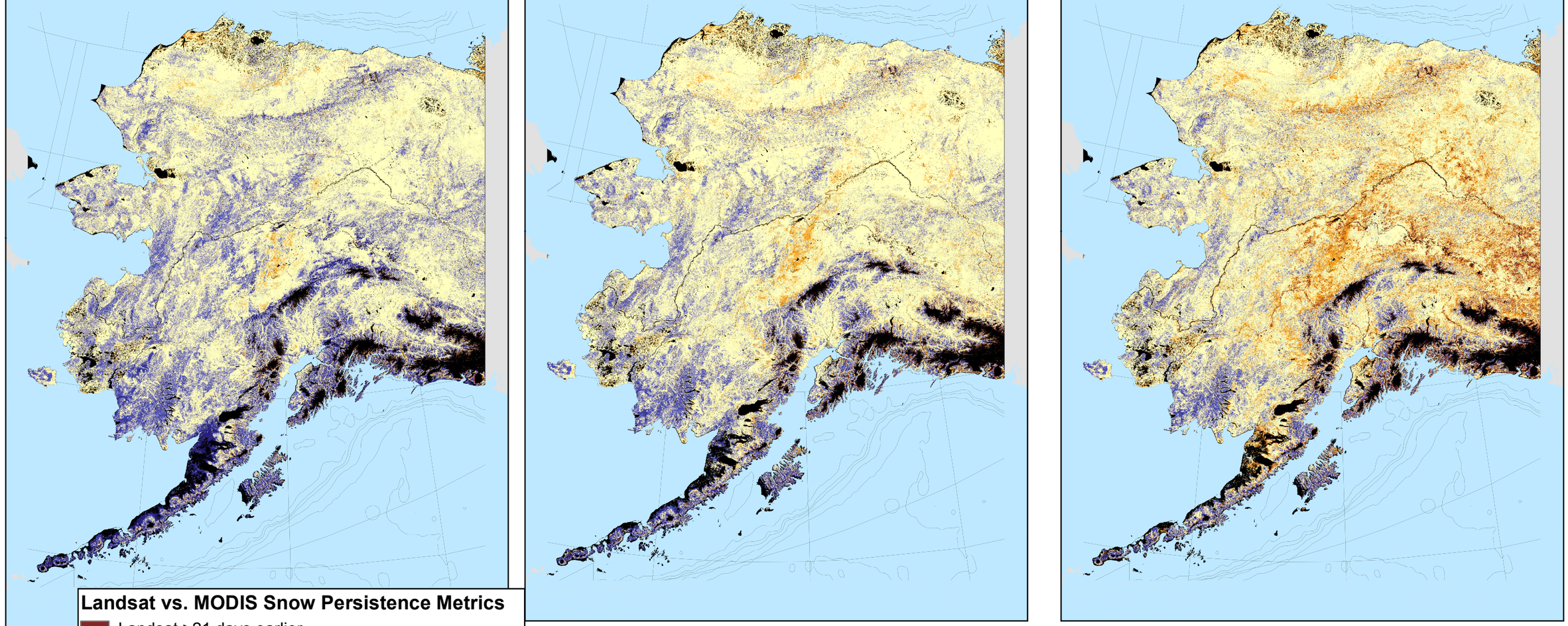



Figure 1.13. Climatogical snow-free date from Landsat (aggregated to 500 m) vs. Median MODIS last day of longest continuous snow segment metric, 2001–2015, Alaska.

Aggregated Landsat vs. Median MODIS Longest CSS End Day, 2001–2015

Aggregated Landsat vs. Median MODIS Combined (Longest CSS End Day, Last Snow Day), 2001–2015

Aggregated Landsat vs. Median MODIS Last Snow Day, 2001–2015



**Landsat vs. MODIS Snow Persistence Metrics**

- Landsat >21 days earlier
- Landsat 15–21 days earlier
- Landsat 8–14 days earlier
- Landsat 5–7 days earlier
- Landsat within 4 days
- Landsat 5–7 days later
- Landsat 8–14 days later
- Landsat 15–21 days later
- Landsat >21 days later
- >50% of Landsat pixels water or lack a snow-free date

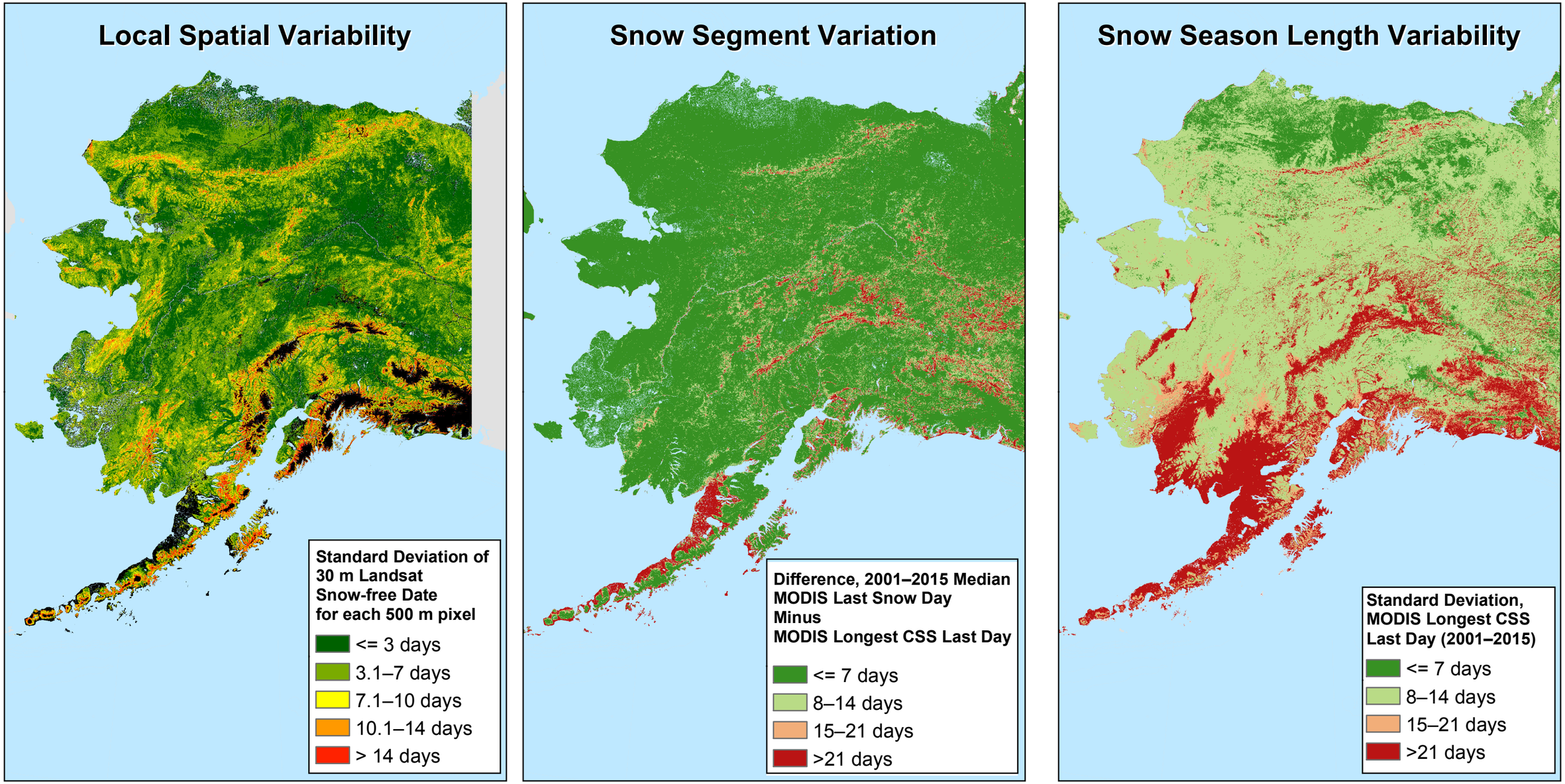
N W E S

0 100 200 300 400 Miles

0 200 400 600 Kilometers

**Figure 1.14. Difference between Landsat snow-free date (aggregated to 500 m pixels) and median MODIS snow persistence metrics (2001–2015), Alaska. MODIS metrics are Longest Continuous Snow Segment (CSS) Last Day and Last Snow Day.**

ABR file: Fig_1_14_Landsat_MODIS_SnowPersistence_Diff_15-360.mxd; 20 Dec 2016




**Left panel:** Local variability of snow persistence was assessed by calculating the standard deviation of the 30-m snow-free date within each 510 m pixel. This local spatial variability shows areas where snow is highly heterogeneous at the scale of MODIS pixels (500 m) and where the information from the 30 m Landsat scale is most valuable.

**Middle panel:** The difference between the 2001–2015 median values of two MODIS snow metrics: longest CSS end day and last snow day. The difference is generally low where the snow regime is characterized by a continuous period of winter snow directly followed by snow-free conditions for the spring and summer, and high in areas where multiple periods of snow cover tend to occur during the late winter, spring and summer.

**Right panel:** The interannual variability of snow persistence was evaluated by calculating the standard deviation of the MODIS longest CSS end day metric for 2000–2015. This measure of the snow season length does not consider snow onset date, but is a useful metric of variability in the persistence of snow in spring.

**Figure 1.15. Metrics of snow regime variability based on Landsat and MODIS snow persistence mapping, Alaska.**

ABR file: Fig_1_15_Snow_Regime_Variability_Metrics_15-360.mxd; 27 Jan 2017

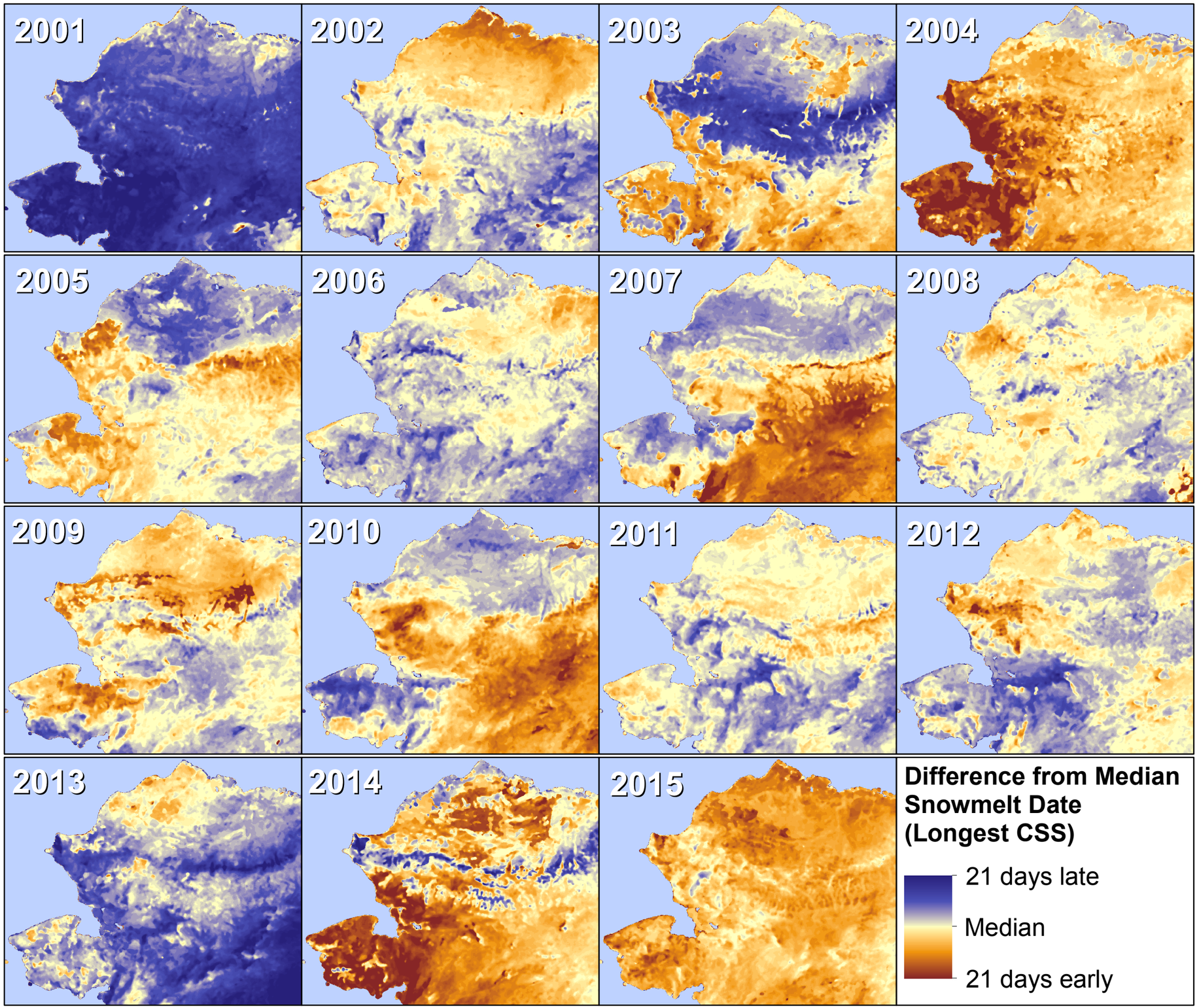



**Figure 1.16. Smoothed annual anomaly in MODIS last day of longest continuous snow segment, Northwestern Alaska, 2001–2015.**

ABR File: Fig_1_16_Smoothed_MODIS_Anomoly_15-360.mxd, 2017-01-27

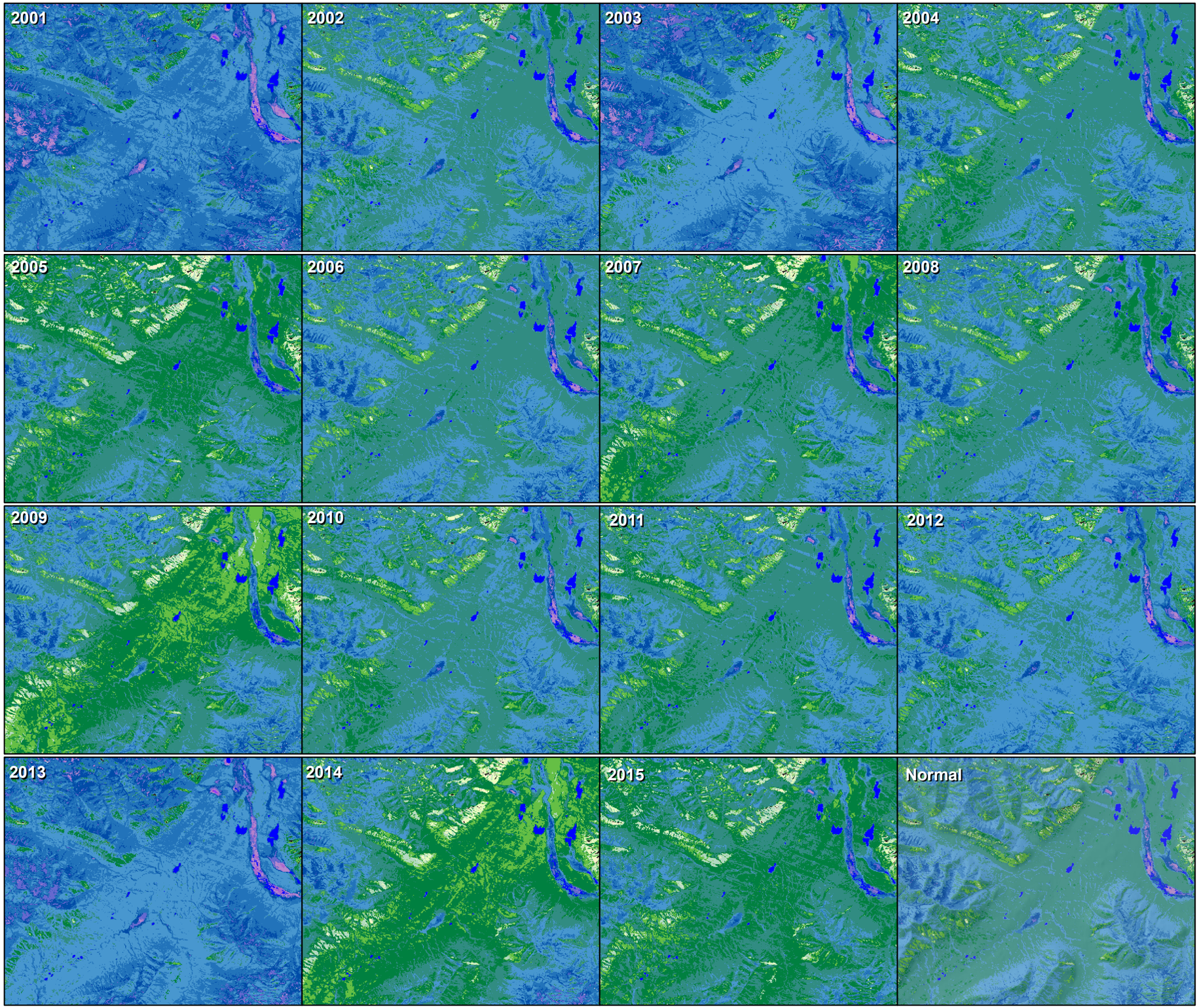



**Figure 1.17. Annual snow persistence map at 30 m resolution based on MODIS and Landsat snow persistence metrics, Anaktuvuk Pass, Alaska, 2001–2015.**

**Estimated Date of Snowmelt, 30 m**

- No Pattern, Usually or Always Snow-free
- March 1–10
- March 11–20
- March 21–31
- April 1–10
- April 11–20
- April 21–30
- May 1–10
- May 11–20
- May 21–31
- June 1–10
- June 11–20
- June 21–30
- July 1–15
- July 16–31
- August 1–15
- August 16–31
- No Pattern, Usually or Always Snow
- Water

0 2 4 6 8 10 Kilometers

0 1 2 3 4 5 6 Miles

N W E S

ABR File: Fig_1_17_Anaktuvuk_SnowFreeDate_by_year_15-360.mxd, 2016-12-19

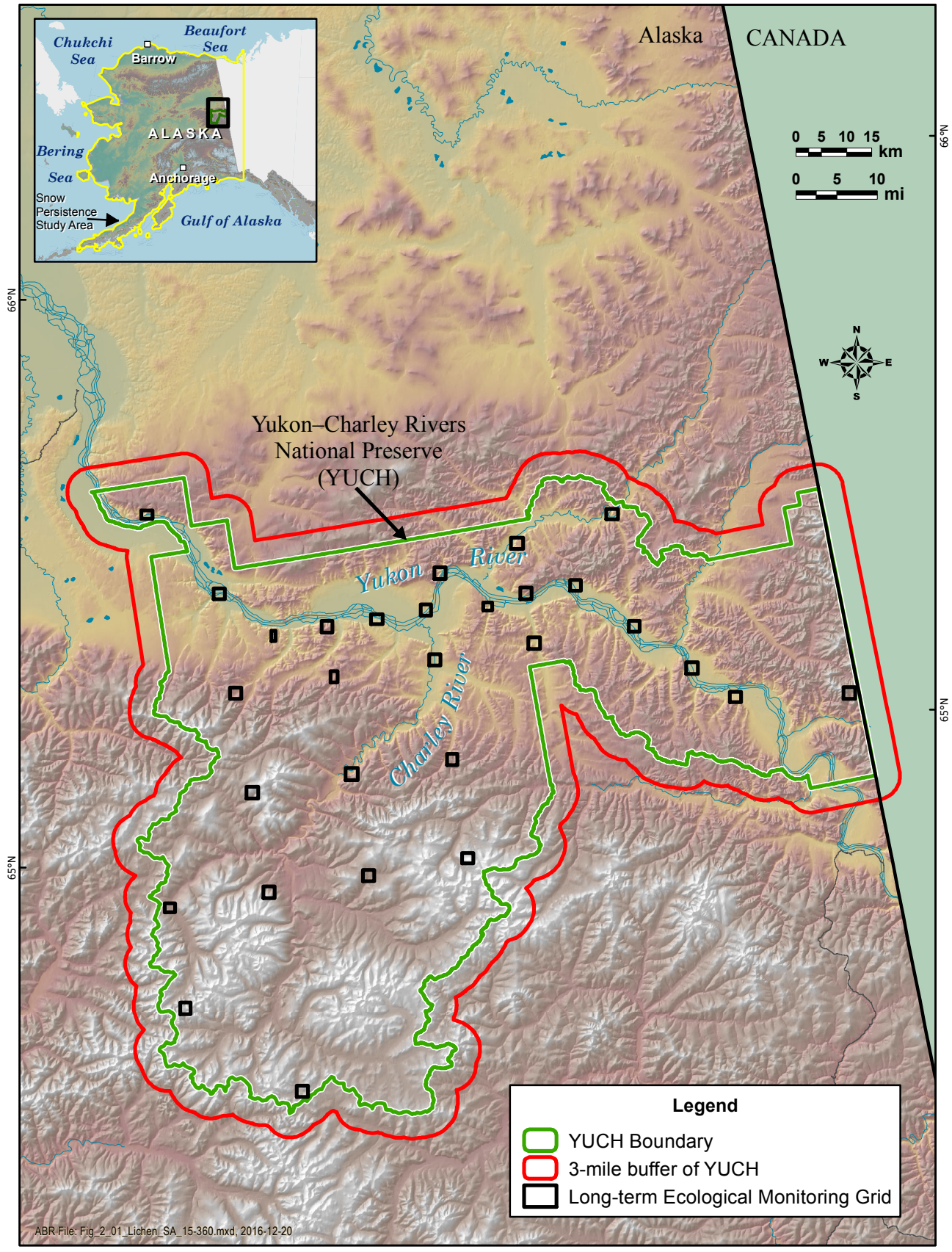



Figure 2.1 Lichen mapping study area, east-central Alaska.

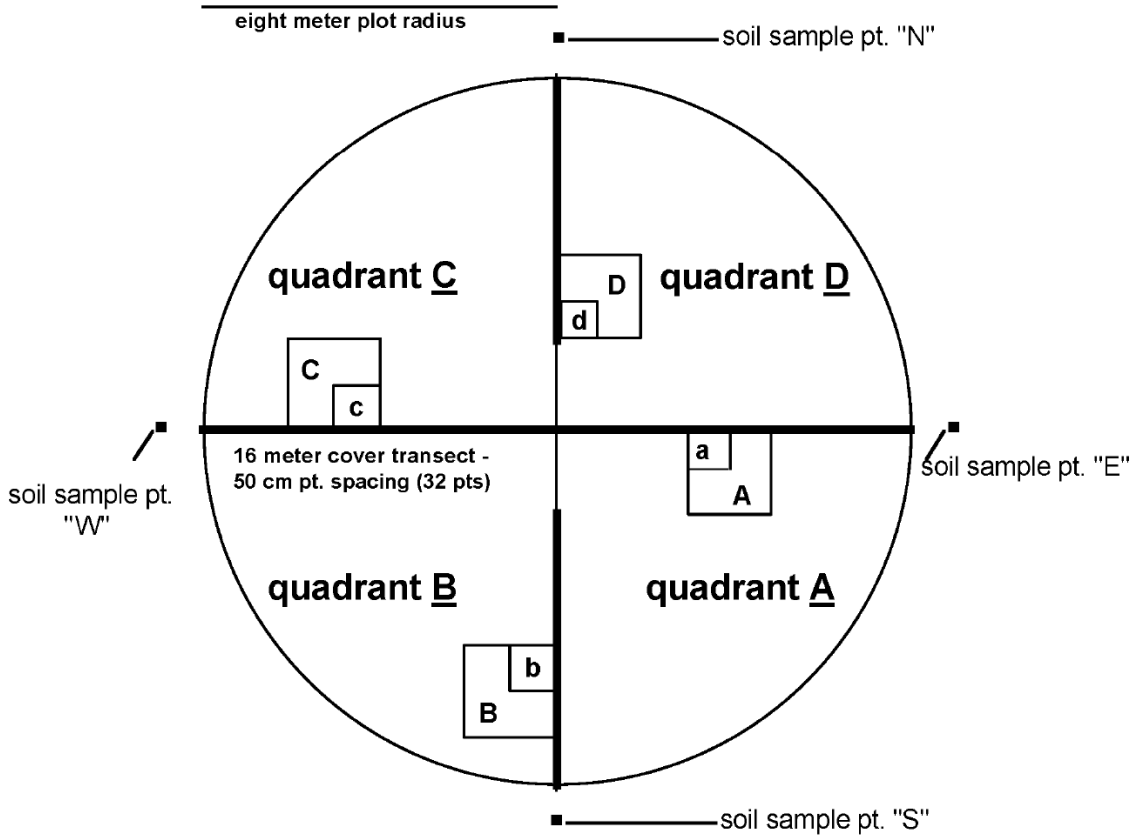



Figure 2.2. Diagram showing the layout of a vegetation monitoring plot, including transects and quadrat placements, for Yukon–Charley Rivers National Preserve, Alaska (from Roland et al. 2004). These plots are 16 m in diameter and encompass about 200 m².

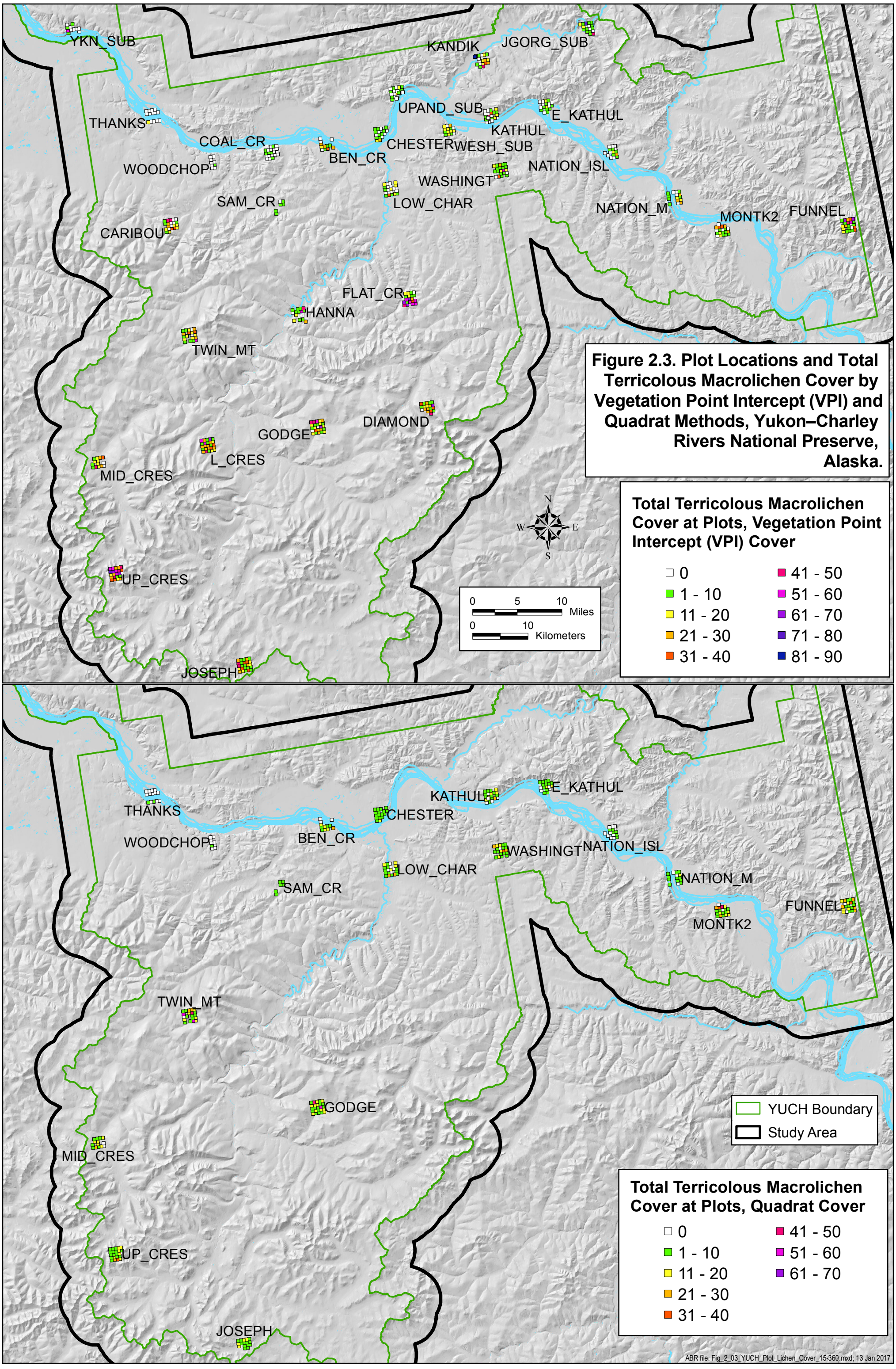



**Figure 2.3. Plot Locations and Total Terricolous Macrolichen Cover by Vegetation Point Intercept (VPI) and Quadrat Methods, Yukon–Charley Rivers National Preserve, Alaska.**

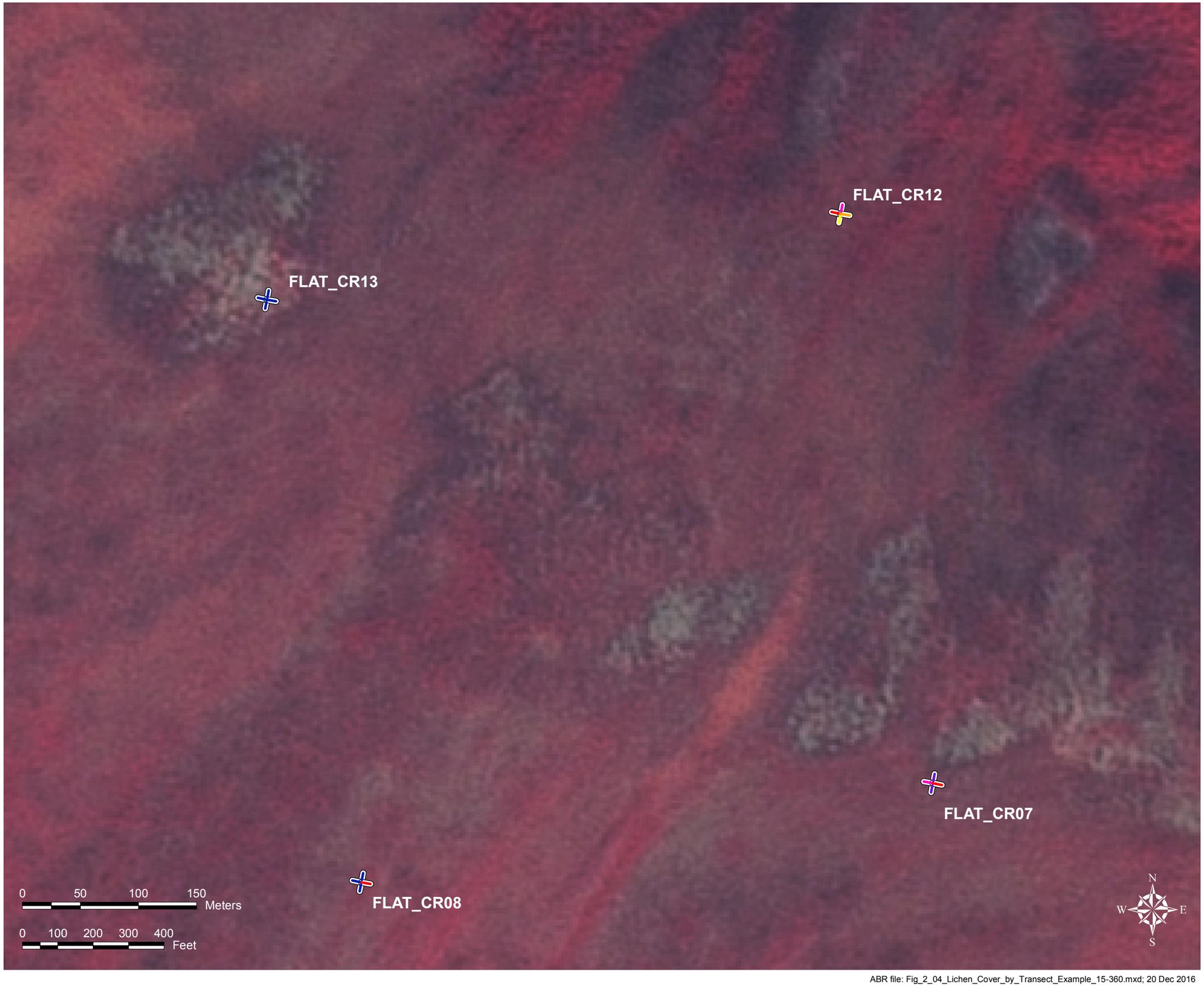
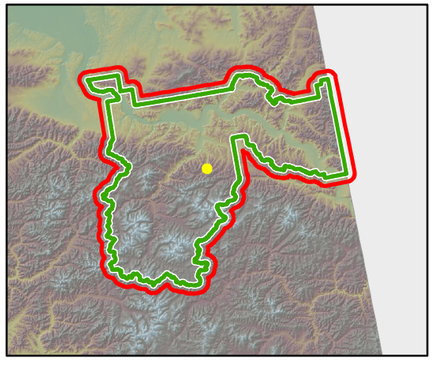



**Figure 2.4. Total terricolous macrolichen cover on vegetation sampling transects by Vegetation Point Intercept method, for 4 plots on the Flat Creek grid, Yukon–Charley Rivers National Preserve, Alaska.**

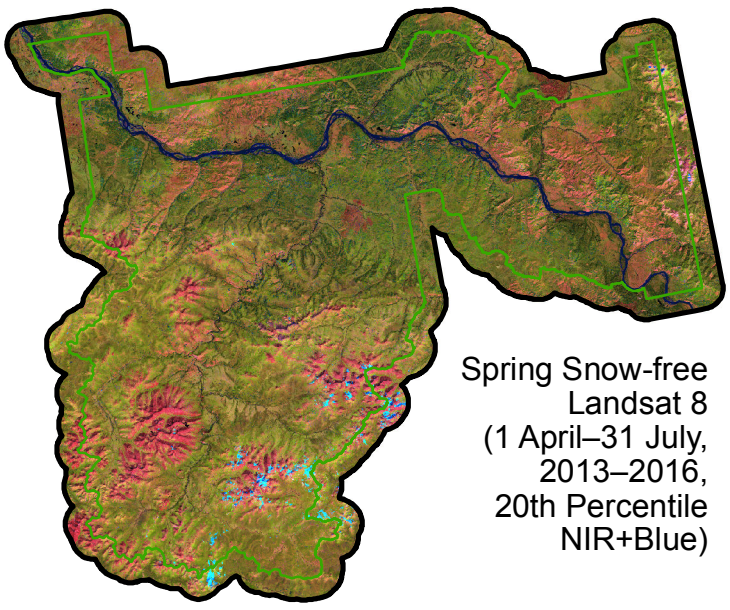
## Total Terricolous Macrolichen Cover (%)

- 0
- 1 - 5
- 6 - 10
- 11 - 15
- 16 - 20
- 21 - 30
- 31 - 40
- 41 - 50
- 51 - 100

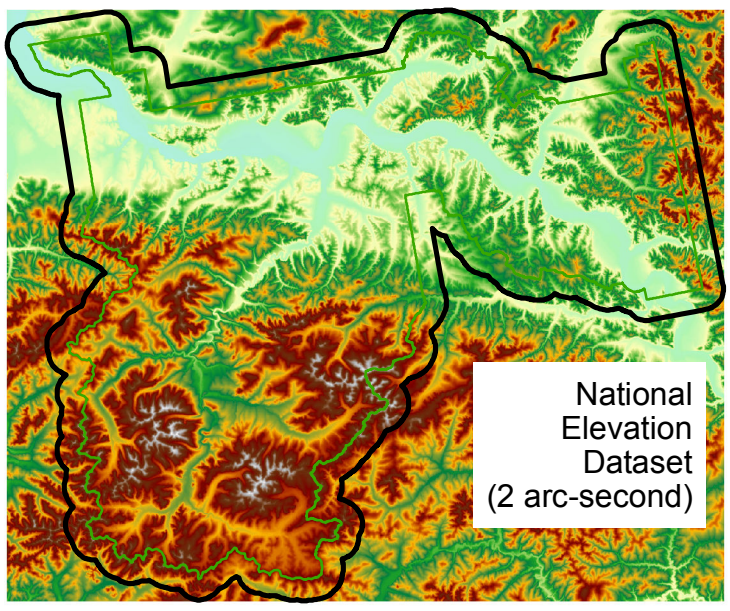


ABR file: Fig_2_04_Lichen_Cover_by_Transect_Example_15-360.mxd; 20 Dec 2016

**Figure 2.5**
**Selected Spectral and Environmental Predictors for Cover Modeling, Yukon–Charley Rivers National Preserve, Alaska.**



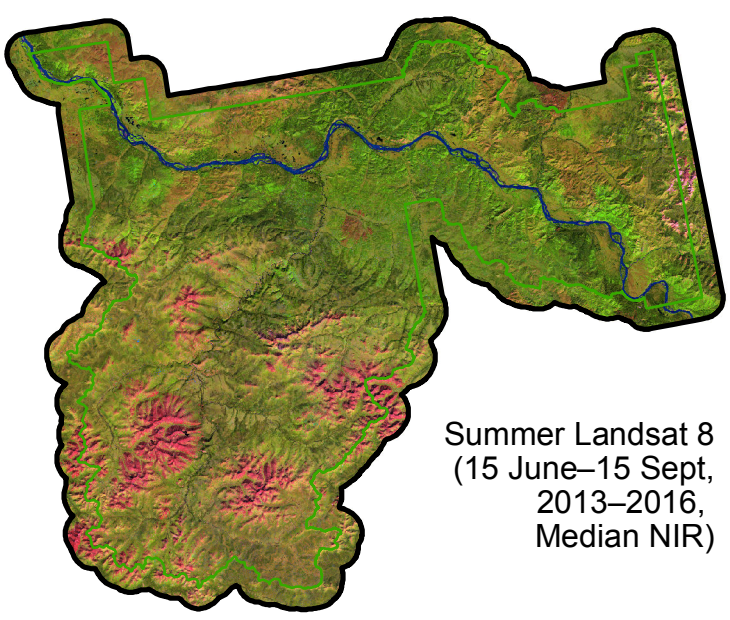
Spring Snow-free Landsat 8 (1 April–31 July, 2013–2016, 20th Percentile NIR+Blue)



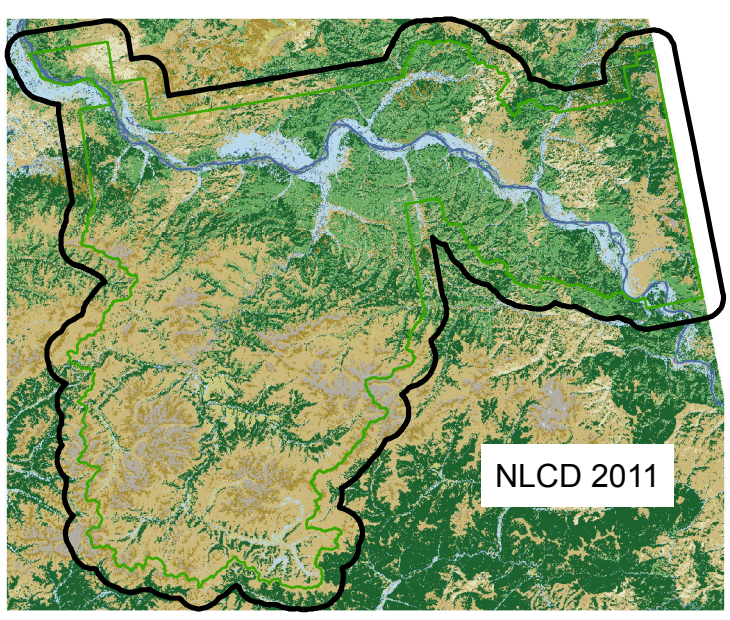
National Elevation Dataset (2 arc-second)

Elevation (m)
1,947 m
160 m

YUCH Boundary
Study Area



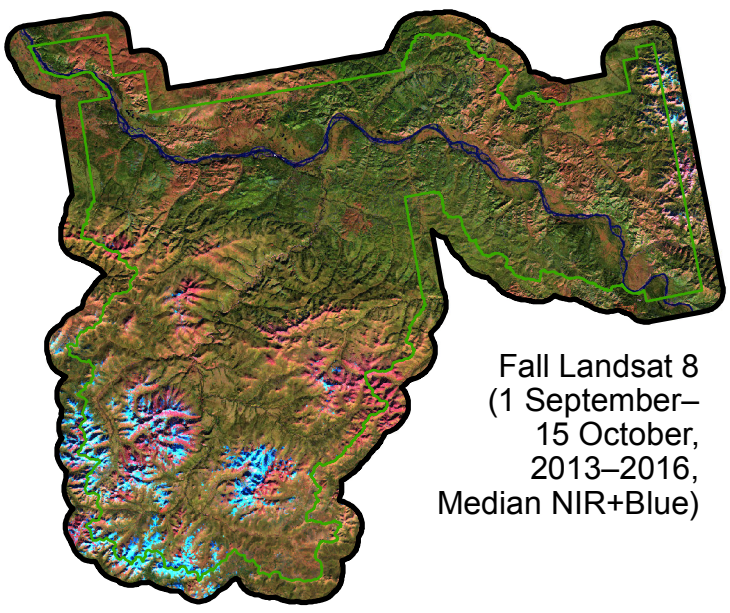
Summer Landsat 8 (15 June–15 Sept, 2013–2016, Median NIR)



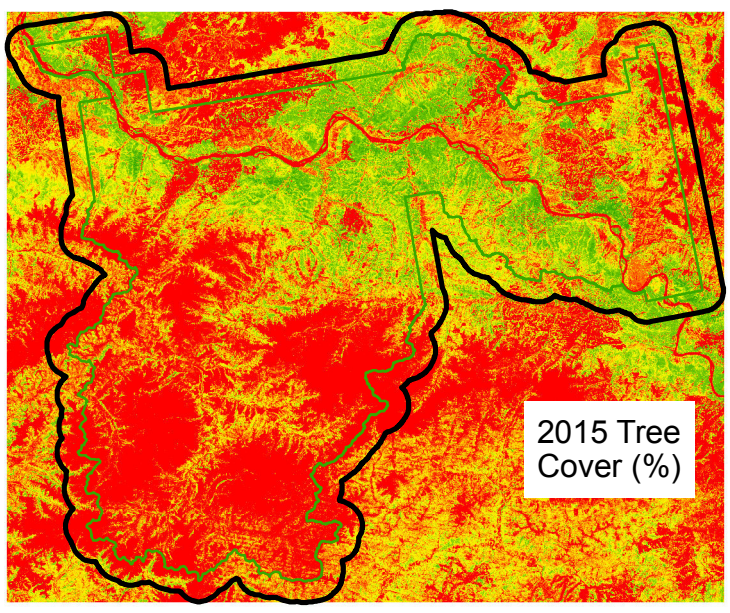
NLCD 2011

NLCD Land Cover Classification Legend
- 11 Open Water
- 12 Perennial Ice/ Snow
- 21 Developed, Open Space
- 22 Developed, Low Intensity
- 23 Developed, Medium Intensity
- 24 Developed, High Intensity
- 31 Barren Land (Rock/Sand/Clay)
- 41 Deciduous Forest
- 42 Evergreen Forest
- 43 Mixed Forest
- 51 Dwarf Scrub*
- 52 Shrub/Scrub
- 71 Grassland/Herbaceous
- 72 Sedge/Herbaceous*
- 73 Lichens*
- 74 Moss*
- 81 Pasture/Hay
- 82 Cultivated Crops
- 90 Woody Wetlands
- 95 Emergent Herbaceous Wetlands

* Alaska only

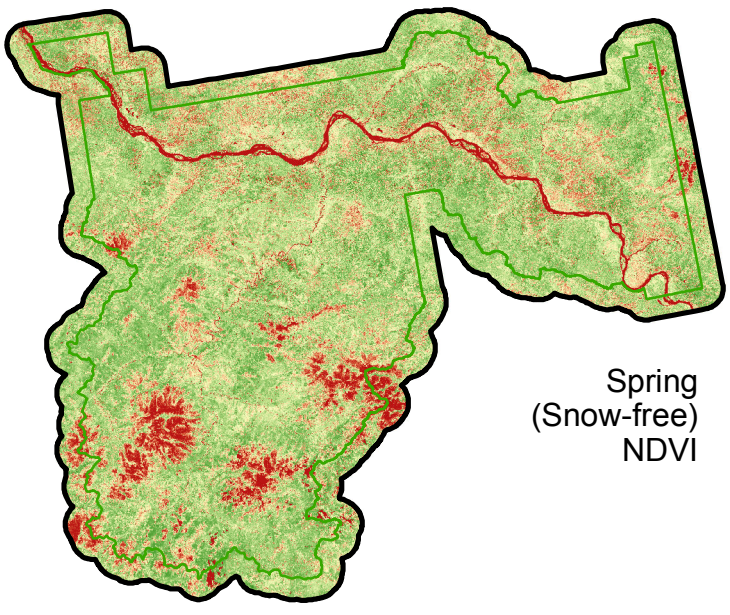


Fall Landsat 8 (1 September–15 October, 2013–2016, Median NIR+Blue)

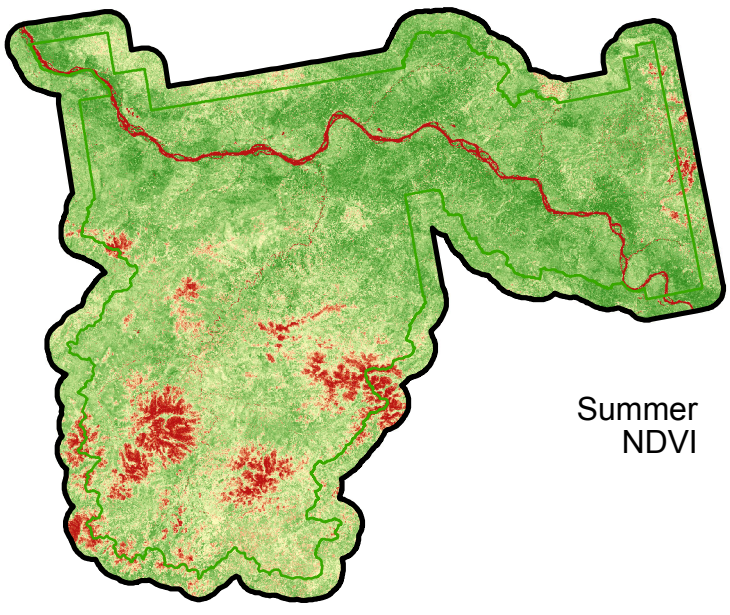


2015 Tree Cover (%)

Tree Cover
%
100
0



Spring (Snow-free) NDVI



Summer NDVI

NDVI
0.900
0.550
0.200

N
W
E
S

Approximate Scale = 1,742,000

0 15 30 45 Miles

0 25 50 Kilometers

ABR file: Fig_2_05_Predictors_Lichen_Cover_Models_30m_15-360.mxd; 20 Dec 2016

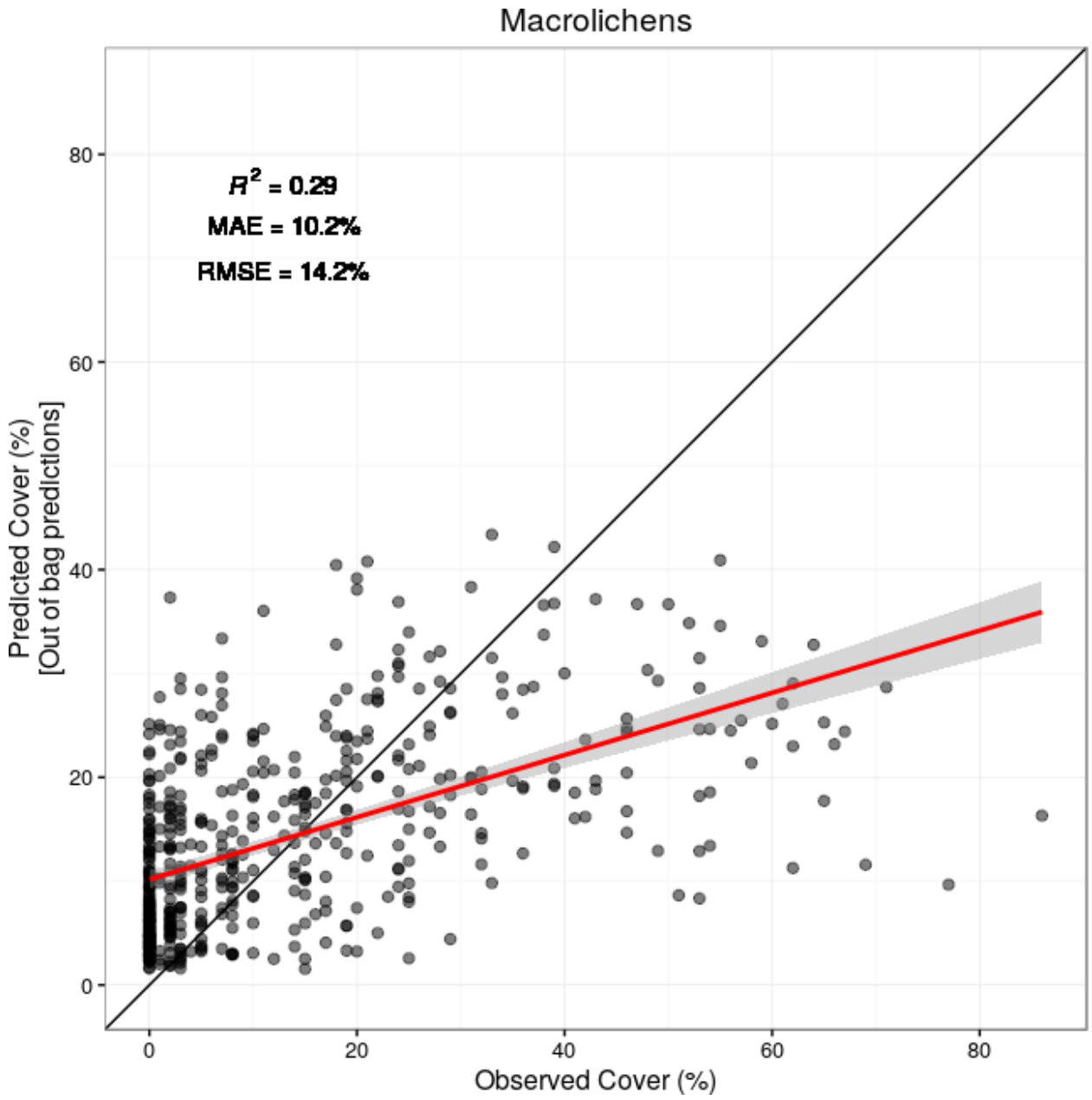



Figure 2.6. Observed vs. out-of-bag predictions of vegetation point intercept total terricolous macrolichen cover, 30 m resolution, Yukon–Charley Rivers National Preserve, Alaska. Linear fit line is red, and 1:1 line is black.

**Figure 2.7. Map of total terricolous macrolichen cover from vegetation point intercept plots, 30 m resolution, Yukon–Charley Rivers National Preserve, Alaska.**

Model trained with plot averaged vegetation point intercept (VPI) data using 30 m predictors.

Total Terricolous Macrolichen Cover (%)

- 0
- 1 - 5
- 6 - 10
- 11 - 15
- 16 - 20
- 21 - 30
- 31 - 40
- 41 - 50
- 51 - 70

0 10 20 30 Kilometers

0 5 10 15 20 Miles

N W E S

ABR file: Fig_2_07_Lichen_Cover_VPI_30m_15-360.mxd; 20 Dec 2016

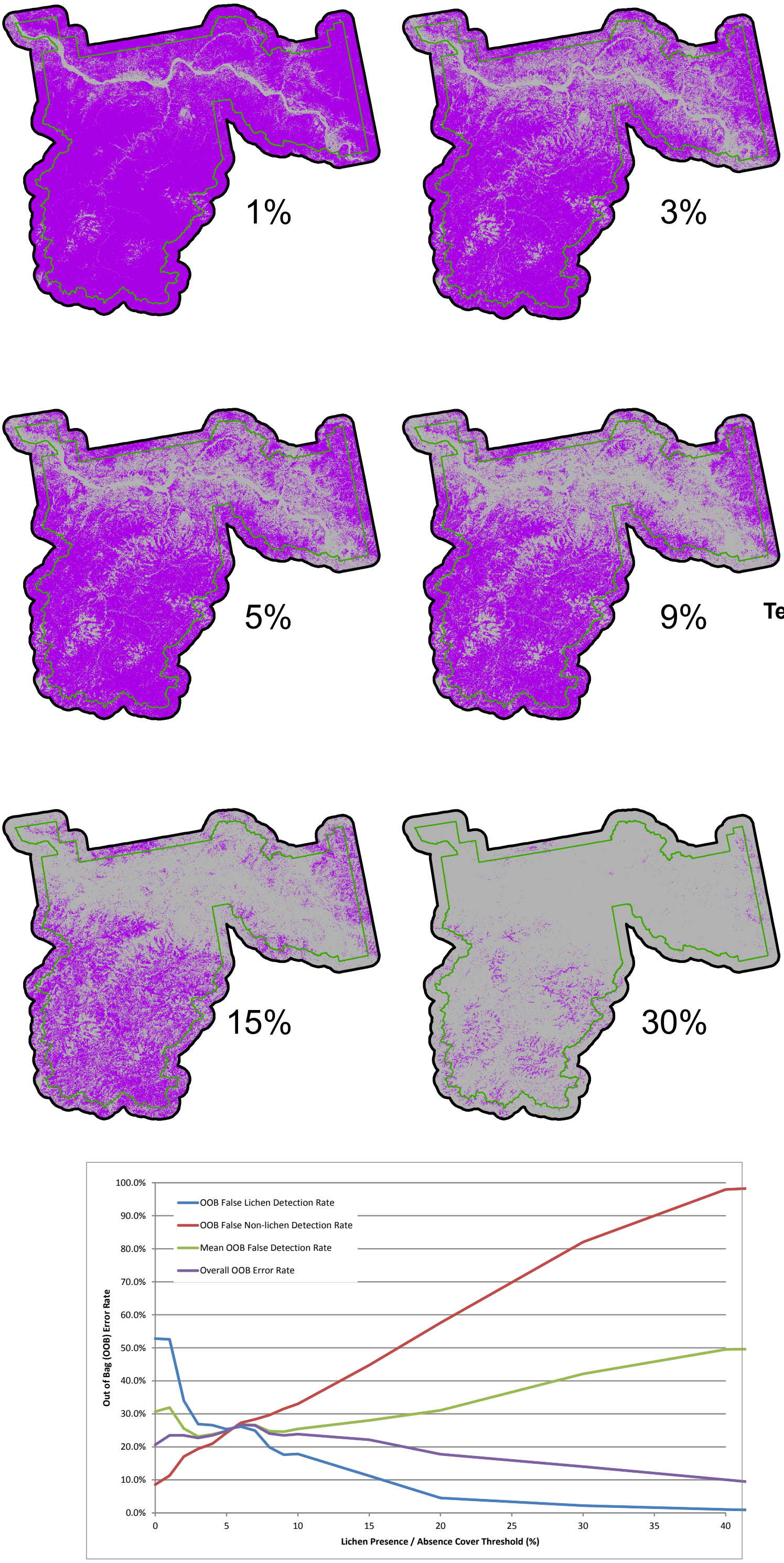
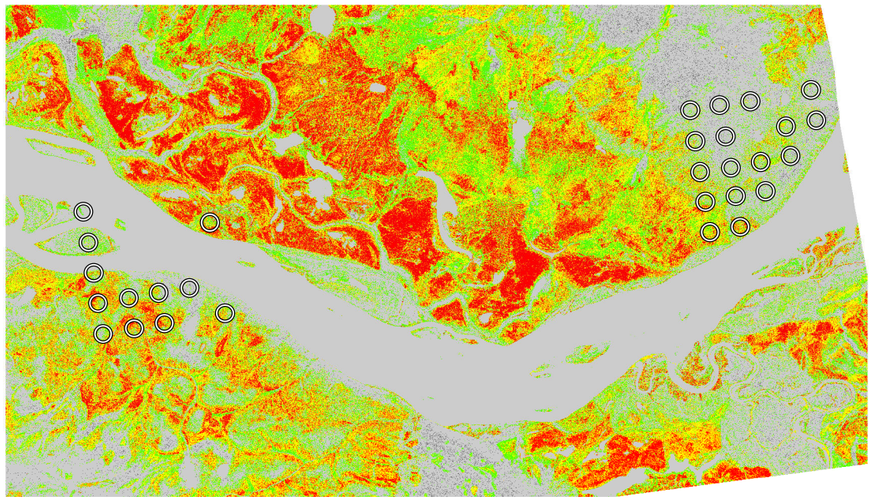
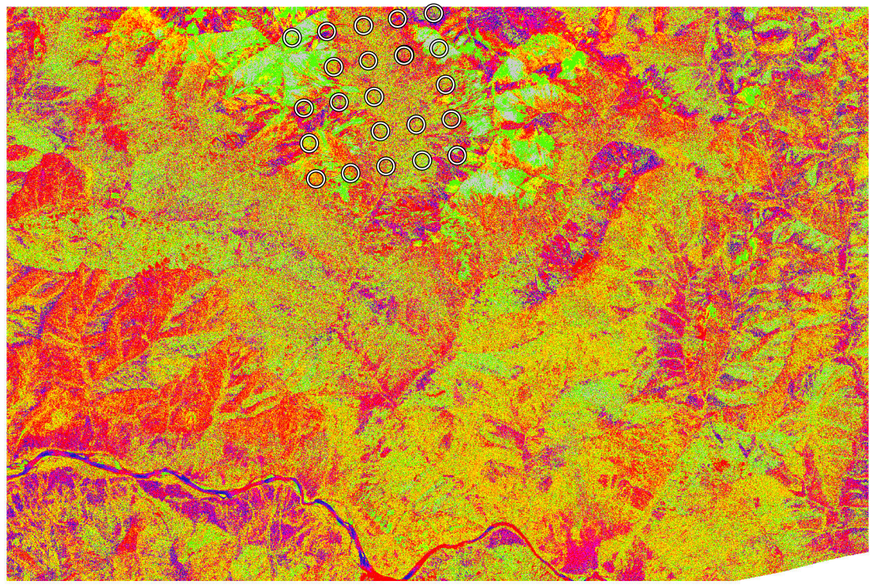



**Figure 2.8. Maps of terricolous macrolichen presence and absence at different thresholds of total lichen cover, 30 m resolution, Yukon–Charley Rivers National Preserve, Alaska.**

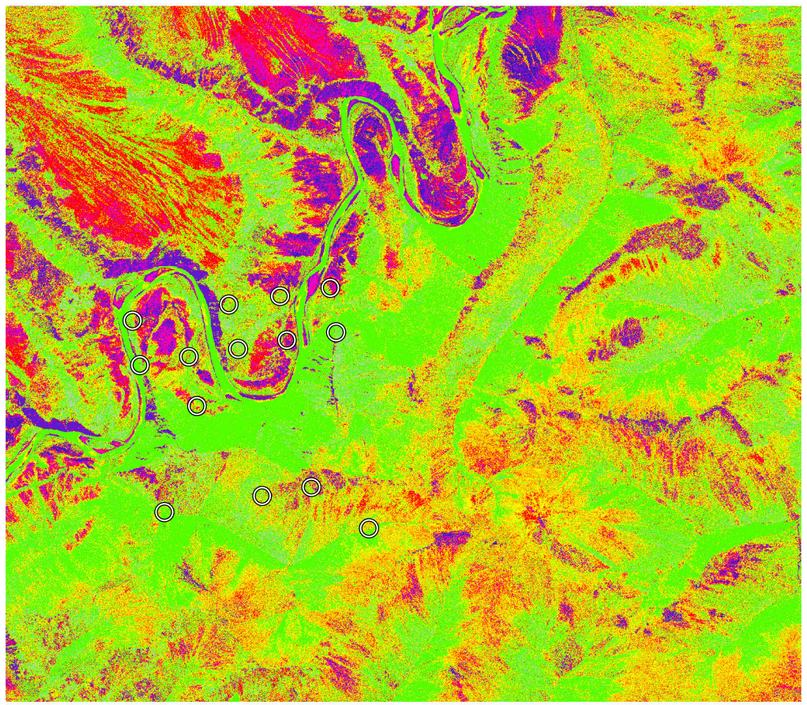
## Ben Creek and Chester Creek



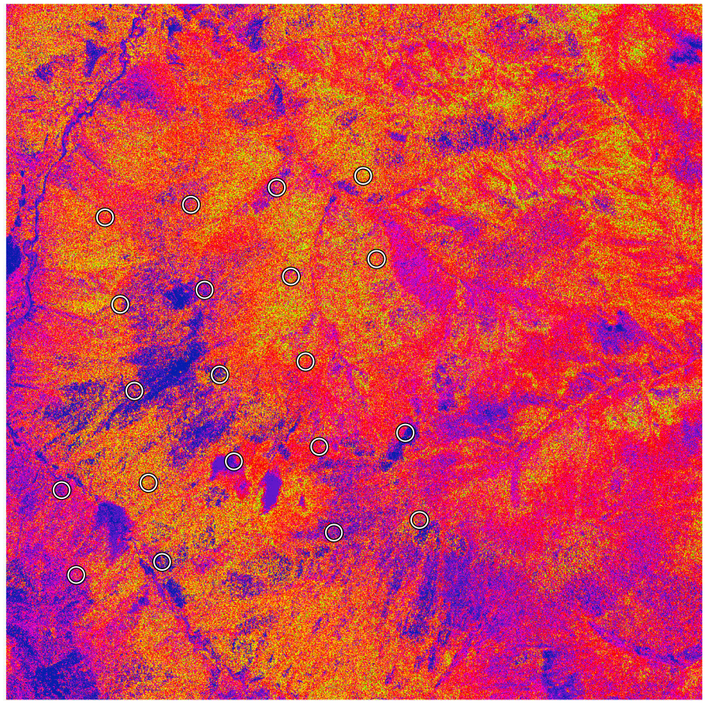
## Funnel Creek



## Hanna Creek

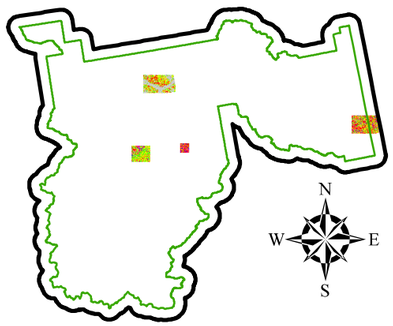


## Flat Creek



ABR file: Fig_2_09_Lichen_Cover_VPI_2m_15-360.mxd; 20 Dec 2016

**Figure 2.9. Maps of total terricolous macrolichen cover from vegetation point intercept transects, 2 m resolution, Yukon–Charley Rivers National Preserve, Alaska.**




**Total Terricolous Macrolichen Cover (%)**

- 0
- 1 - 5
- 6 - 10
- 11 - 15
- 16 - 20
- 21 - 30
- 31 - 40
- 41 - 50
- 51 - 70
- Vegetation Plots

Models trained with transect averaged vegetation point intercept (VPI) data using 2 m predictors.

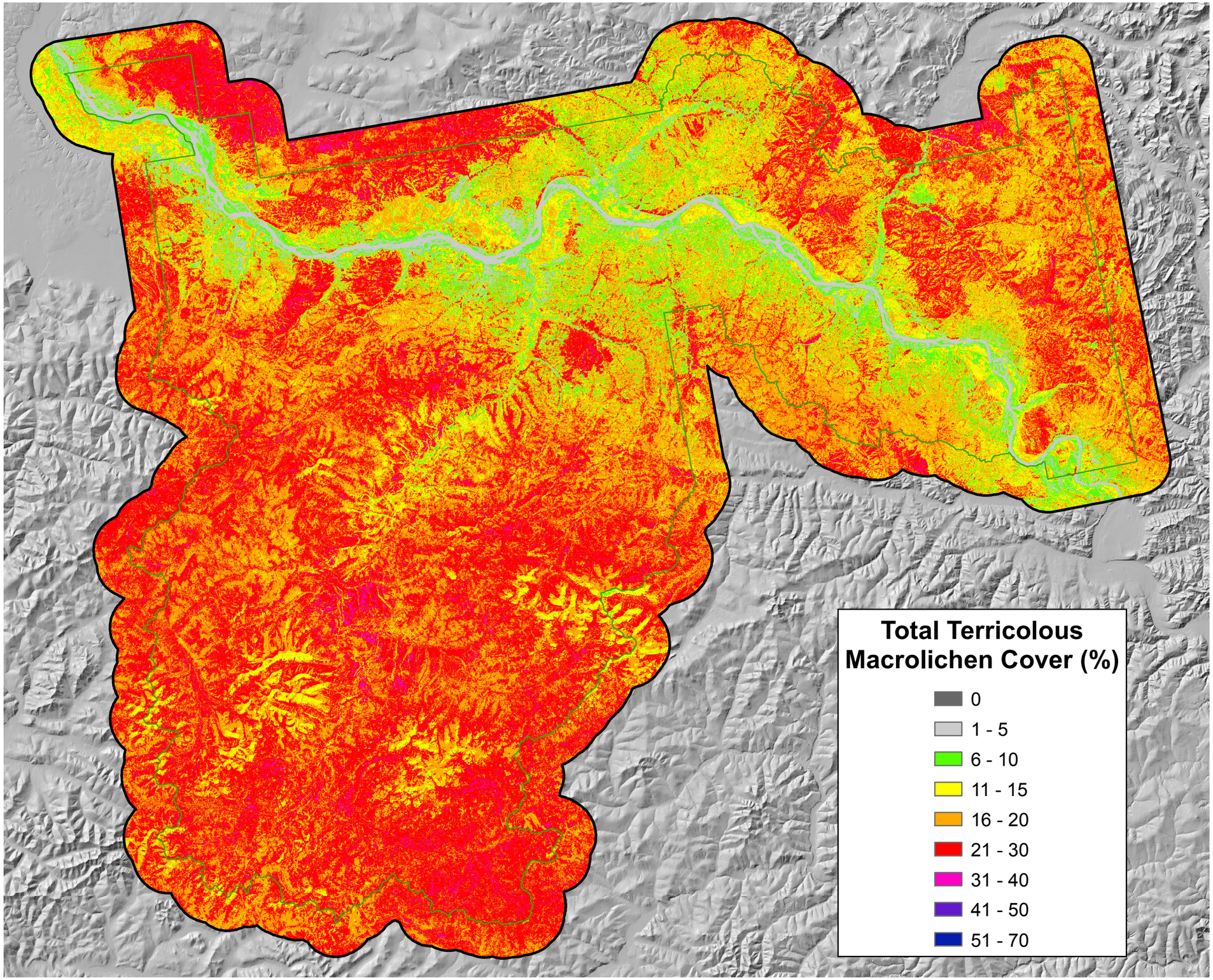



**Figure 2.10. Map of total terricolous macrolichen cover at 30 m resolution, trained from 2 m resolution total lichen cover maps, Yukon–Charley Rivers National Preserve, Alaska.**

Model trained with aggregated 2 m resoluton cover models, using 30 m predictors.

ABR file: Fig_2_10_Lichen_Cover_30m_from_2m_15-360.mxd; 20 Dec 2016